Investigation of Peptides That Exhibit Affinity

Towards Advanced Materials

by

Hyun Seok Kim

A thesis

presented to the University of Waterloo

in fulfillment of the

thesis requirement for the degree of

Master of Science

in

Chemistry

Waterloo, Ontario, Canada, 2017

Author's Declaration

I hereby declare that I am the sole author of this thesis. This is the true copy of the thesis, including any required final revisions, as accepted by my examiners.

I understand that this thesis may be made available to the public.

Abstract

A number of commercially employed polymers are refractory to surface modification and may require harsh conditions ranging from corona discharge to halogenation to assemble a functional surface. We are exploring combinatorial peptide screening using phage display to identify peptides capable of non-covalent binding to advanced polymeric materials to discover mild yet useful surface modification agents. Through the application of phage display techniques, identification of polymer-binding peptides ("adhesons") are the focus of this research. Our studies in this area, including the ability to fabricate phage fibers and membranes, will be presented. Results in this area should contribute to our basic understanding of the interactions between polymeric surfaces and biomolecules, but also lead to potential applications in the area of advanced functional materials.

Acknowledgements

I would like to personally acknowledge and thank Dr. John Honek for everything that he has done to further develop me as a student, and most importantly, as a biochemist along with the opportunity to take me on this project.

I would also like to acknowledge and thank Nina Heinig from Watlab for the assistance and training me on the environmental scanning electron microscope. I would also like to acknowledge and thank Boyd Panton of the Department of Mechanical and Mechatronics Engineering for training me on the uniaxial tensile tester. I would also like to thank the members of the Honek laboratory for their general assistance in the lab.

Of course, I would also like to thank the Natural Sciences and Engineering Research Council of Canada and Imperial Oil for their funding as this project would have been impossible without the two groups.

Last but not least, I would also like to thank my family for supporting me during my program all the way from South Korea.

Table of Contents

List of Figures

List of Tables

List of Abbreviations

AFM	Atomic force microscopy
ATP	Adenosine triphosphate
ATR	Attenuated total reflectance
CNF	Carbon nanofiber
CNT	Carbon nanotube
DFT	Density functional theory
DNA	Deoxyribonucleic acid
E. coli	*Escherichia coli*
EDX	Energy dispersive x-ray spectroscopy
ELISA	Enzyme-linked immunosorbent assay
ESEM	Environmental scanning electron microscopy
FT-IR	Fourier transform infrared spectroscopy
HDPE	High density polyethylene
HOPG	Highly ordered pyrolytic graphite
LLDPE	Linear-low density polyethylene
MoRE	Molecular recognition elements
PE	Polyethylene
PS	Polystyrene
RFDNA	Replicative form DNA
RNA	Ribonucleic acid
SELEX	Systematic evolution of ligands by exponential enrichment
TEM	Transmission electron microscopy

Chapter 1: Introduction

1.1 Molecular Recognition

Molecular recognition plays a critical role in the fields of biochemistry and materials science as it allows for the design and assembly of novel materials from the combination of two or more different types of synthetic or biological materials. Molecular recognition is the specific interaction between two molecular systems through non-covalent interactions which occur at the specific interface of the two individual systems[1]. (Bio)materials can exhibit unique properties due to their formation from a complex resulting from the interaction of two or more molecular recognition elements (MoRE). Biological complexes can also form from the combination of two or more MoREs after the individual components fold into a more ordered structure. Antibody-antigen complexes can form from the combination of various non-covalent and covalent interactions such as hydrogen bonds, $\pi - \pi$ interactions, metal coordination and van der Waals interactions at the interface of the paratopes and epitopes of the antibody and antigen respectively (Figure 1).

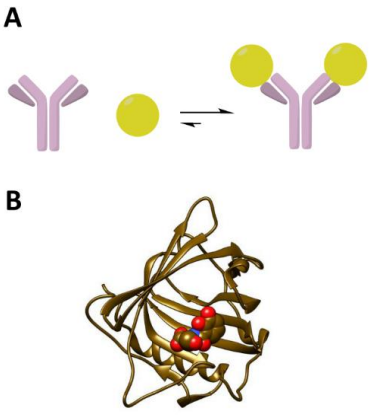

Figure 1: Examples of biological molecular recognition. A: antibody (light purple)-antigen (yellow) complex formation B: lipocalin protein (ribbon) that is complexed with an enterobactin molecule (spheres) PDB:3CBC[2]

Lipocalins (shown in figure 1B) are a class of protein that transport small molecules as lipocalin-small molecule complexes. These complexes are formed through the molecular recognition of the β-barrel motif of the protein and the small molecule cargo[3]. The lipocalin structure offers an ideal platform for generating novel binding reagents and is found to have an application in biopharmaceuticals as antibody-like replacements[3]. With current knowledge and insights from the formation of biological complexes, biosynthetic materials can also be formed through molecular recognition strategies[4].

1.2 Biomolecules and Materials Science

Current research in the area of bionanomaterials has led to an intense interest in finding biomolecules that exhibit affinity toward various molecular recognition elements ranging from noble metals to polymers. The practice of developing new biomaterials can often take a biomimetic approach and employ engineered biological molecules to discover novel MoRE interactions with non-biological materials[5,6]. Oligonucleotides have been investigated and utilized for selective interactions as they offer unique advantages in the molecular recognition process through their linear sequence and their ability to bind to their complementary sequence partner[7]. Short sequences of deoxyribonucleic acids and ribonucleic acids (DNA/RNA) that are engineered to have a molecular recognition motif are called aptamers[8]. Aptamers can be engineered through a technique called systematic evolution of ligands by exponential enrichment (SELEX) as shown in figure 2[9]. SELEX allows for aptamer-material complexes to assemble which can lead to applications such as biosensing and imaging[10]. It has been shown that DNA and gold nanoparticles can complex upon the introduction of the ligand adenosine triphosphate (ATP), which can lead to the release of the oligonucleotide-fluorophore molecule which was originally bound to its complementary aptamer[11]. The release of the oligonucleotide-fluorophore

molecule fluoresced upon treatment with UV light as soon as the ligand bound to the DNA aptamer. The DNA-gold complex allows it to be employed as a molecular probe for intracellular analytes of interest. This was attributed to the fact that aptamer-gold complex is stable at room temperature and that the stability of the aptamer increases when it is in the cell compared to the free aptamer[10,11]. Secondly, DNA-single-walled carbon nanotube (SWCNT) biosensors were constructed which greatly altered their conductance upon thrombin binding to their recognition DNA [8].

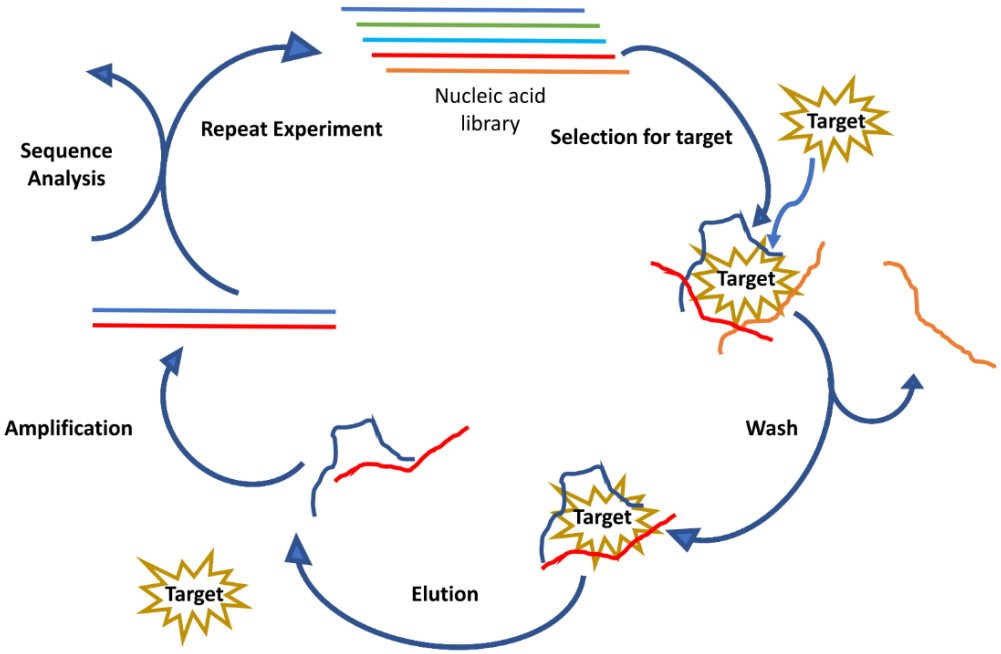

Figure 2: Overview of the process of systematic evolution of ligands by exponential enrichment (SELEX)[144].

While nucleic acids are very useful as the biological component in a functional material due to their increased stability compared to antibodies or large proteins[8], they are limited in the

number of functional groups present in their structure, which can reduce binding versatility. In addition to the limited number of functional groups, adding new functional groups onto DNA/RNA may pose additional challenges. Peptides on the other hand are versatile and considered more favourable for certain types of molecular recognition tasks due to the availability of diverse functional groups present in the side chains of the amino acids as shown in figure 3.

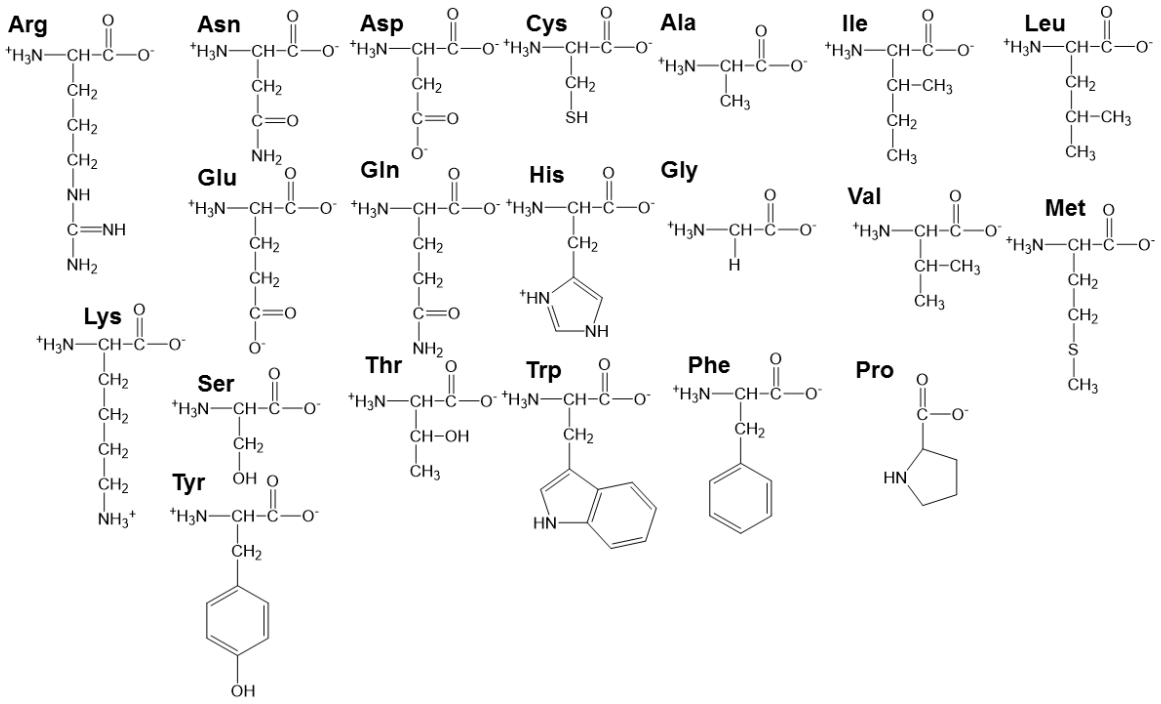

Figure 3: All 20 amino acids showing the diversity of side chain groups.

Peptides also allow for the development of binding motifs to a range of materials, and these binding sequences are composed of sequential combinations of the twenty natural amino acids. The applications of peptides in the biological sciences were initially focused on the areas of therapeutics and biotechnology. For example, an analogue of the glucagon peptide has been developed that is employed for the emergency treatment of hypoglycemia[12]. It was also

discovered that peptides could be used to assemble a fusion protein of peptide-elastin-like protein to prolong the release time of the glucagon analogue. The elastin-like protein can form a drug depot, which allows for the deposition of the drug/peptide to occur at physiological temperature and which increases the half-life of the peptide drug[13]. Peptides have also been employed in the area of materials science. An example is that of their application to amyloid fiber –based biomaterials. Amyloid fiber is a highly ordered protein structure that is misfolded and is implicated in the physiology of prion disease and Alzheimer's disease[14]. It was also determined that amyloid fibre is an excellent candidate for materials applications such as in liquid crystals, wires, and gels due to its mechanical properties and stability[4]. The designed amphiphilic nanofibre, composed of ten amino acids, was shown to exhibit high affinity towards a chemically synthesized heptameric peptide. The heptameric peptide was able to discriminate among various amino acid arrangements in the assembled nanofibre[4]. In order to isolate a peptide that exhibits affinity to a target of interest, rational design of peptides could be used if substantial information about the target of interest is known. However, it would be impractical to employ this approach to targets having little structural information. In addition, the design of a peptide that binds to a specific target based on first principles is a difficult challenge as our fundamental understanding of protein-folding and surface binding energies associated with the protein/peptide-target interactions is still in its infancy[15]. The preferred approach in these circumstances is to use a randomly generated library of peptides that are displayed on a surface of bacterial cells (also known as cell surface display) or bacteriophage (also known as phage display) to screen for peptides showing affinity to a specific molecular target [15]. In the current work, intense interest is focused on the identification of peptides that exhibit affinity towards nanostructures and synthetic materials through application of phage display techniques.

1.3 Noble Metal Binding Peptides

Noble metals, such as ruthenium (Ru), rhodium (Rh), palladium (Pd), silver (Ag), osmium (Os), iridium (Ir), platinum (Pt), and gold (Au), are a group of metals that are resistant to oxidation by air, acid and corrosion. Noble metals are of high interest in materials science due to their unique optical and electronic properties that arise from the large enhancement of the surface electric field on the metal nanostructures[16–18]. At nanoscale dimensions, the physicochemical properties of noble metal based materials are dependent on their size and shape which can be used to tailor the functionalities of these noble metal-based nanostructures[17]. Peptides exhibiting affinity towards noble metal nanostructures have been identified and can be utilized to attach additional functionalities to their surfaces as well as control their syntheses. Additionally, these interactions can be employed to further understand the atomistic level nature of interactions between biomolecules and metal nanostructures. As shown in Table 1, various noble metal binding peptides have been identified

Table 1: Peptide sequences identified as having affinity to noble metal surfaces.

Metals	Peptide Sequence	Peptide Length
Au[19–22]	MHGKTQATSGTIQS	14
	TGTSVLIATPYV	12
	AYSSGAPPMPPF	12
	WAGAKRLVLRRE	12
	WALRRSIRRQSY	12
Ag[23,24]	NPSSLFRYLPSD	12
	KIEELKQKIEQLKQENQQLEEENSQLEYGC	30
	ENQSLESKISQLKRKNEELKQEISQLEYGC	30
Pt[15,25–27]	PTSTGQA	7
	DRTSTWR	7
	QSVTSTK	7
	SSSHLNK	7
	TLTTLTN	7
	SSFPQPN	7

It has been determined by Brown and co-workers that dodecamer peptides having affinity to gold powder can be isolated utilizing phage display techniques and that these peptides can also mediate the growth of colloidal gold crystals (figure 4)[19,28].

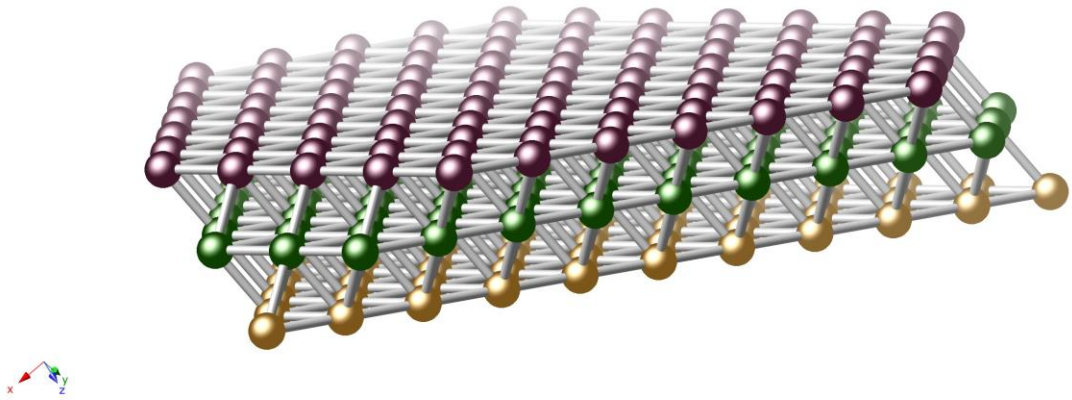

Figure 4: Crystal structure of gold showing three layers of gold atoms. Drawn using CrystalMaker Inc. (version 9.2) software based on the crystal structure data from Swanson H E, Tatge E (1953) Standard X-ray diffraction powder patterns. National Bureau of Standards (U.S.), Circular 359:1-1

The identified gold-binding peptides were found to be able to recognize the six-fold symmetry of the gold surface. The researchers observed that the deposition of Au onto the gold surface was not stopped until the surface was covered, indicating the effectiveness of the interaction between the peptide and the gold surface[28]. The ability of peptides to control the morphology and the extent of metal deposition was further described by Kim and colleagues when they observed that Au surface morphology could be modulated by the choice of peptide employed[29]. Peptides can also direct the assembly of chiral nanoparticles in which the resulting superstructure (peptide + gold nanoparticle) could be engineered to produce a helical shape wherein the gold atoms are bound to the peptide at the exterior face[30,31].

In addition to gold, silver is also of interest in materials science. Similar to gold nanostructures, assembly of silver nanostructures that are 60 nm to 150 nm in dimension can also be synthesized by various peptides that induce the nucleation and deposition of silver[23]. It has been reported that various silver-binding peptides are able to initiate the assembly of silver nanoparticles during the chemical reduction of $AgNO_3$, a consequence of the presence of lysine and glutamate/glutamine residues found in the peptide sequence[24]. Peptide-controlled metal deposition has been considered to be a more ecofriendly and green approach to the control of metal surfaces[32]. The formation of silver nanoparticles by peptides can be applicable to the formation of Ag-based antibacterial coatings. Platinum is another key metal that is extensively employed in catalysis. The surface morphology of a platinum catalyst is critical to its catalytic properties. Several peptides have been identified that not only have affinities to specific facets of a platinum crystal, but are also capable of directing the growth of platinum cubic and tetrahedral crystals[27].

1.4 Carbon-Based Nanostructure Binding Peptides

The carbon nanotube (CNT) is an allotrope of carbon that has potential applications in sensor design, drug delivery and energy storage[33,34]. At an atomic level, CNTs can be viewed as a rolled-up sheet of graphene to form a single-walled CNT (figure 5) and it can also be multi-walled when additional graphene sheets are rolled onto the single-walled CNT[35].

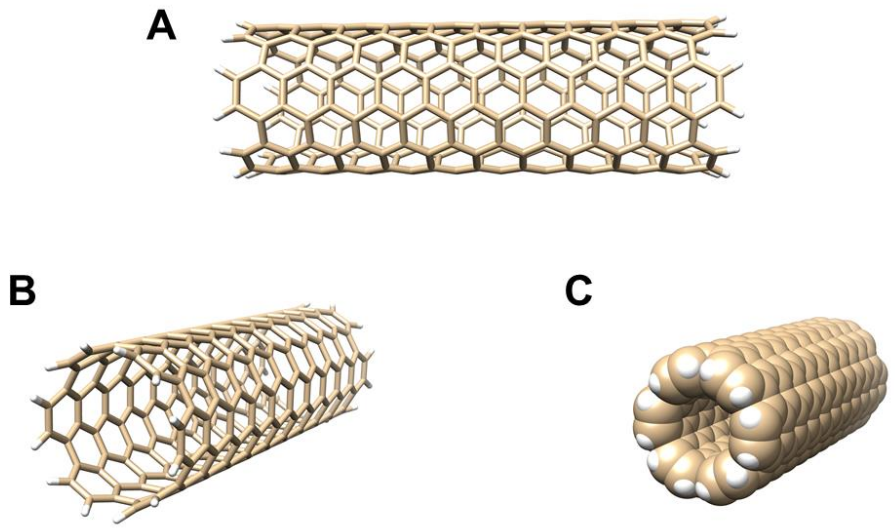

Figure 5: Structure of carbon nanotube with chiral indices n = 6 and m = 6, and number of unit cells = 10. **A** and **B** are shown in different orientation and **C** is a space-filling model of CNT.

The electrical properties of CNT are heavily dependent on its structure as it can either be semi-conductive or metallic[35]. The techniques of CNT production often lead to a mixture of CNTs that have heterogeneous dimensions[35]. The Honek laboratory has reported the isolation of peptides (Figure 6) exhibiting affinity towards single-walled CNT, which may lead to a potential solution to the problems of hydrophobicity of the nanotube that can pose problems for its future use in various applications[34,35].

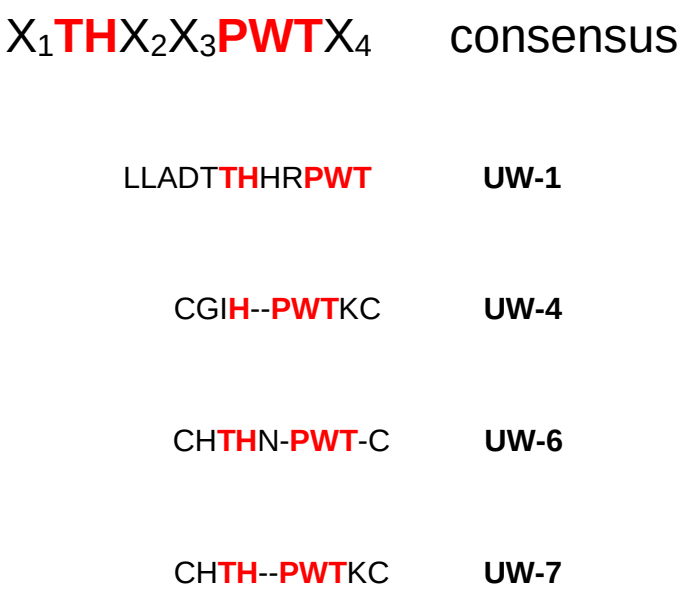

Figure 6: Consensus sequence of single walled CNT binding peptide where X_1 is G or H, X_2 is H or A or null, X_3 is null or R, and X_4 is null or K.[34]

Utilizing a combination of circular dichroism (CD), fluorescence and nuclear magnetic spectroscopy, the free peptide of UW-1 in Figure 4 was analyzed and exhibited a β-sheet-like structure at low pH. It was interesting to note that the conformation of the peptide in the absence of singled-walled CNTs was a random coil but upon the addition of single-walled CNTs, a β-hairpin structure was formed whereas the addition of multi-walled CNTs or single-walled nanohorns did not change the conformation of the peptide[34]. Analysis of the results from molecular modeling of UW-1 and UW-4 indicated that the two peptides are in β-turn like structures that allow for the binding of the single-walled CNT to occur. Specifically, for both UW-1 and UW-4, each structure showed a special clustering of aromatic and hydrophobic residues that lead to the formation of the β-turn structure as that appears to promote both

hydrophobic and $\pi - \pi$ stacking interactions at the interface between the single-walled CNT and the peptide.

Graphite is an allotrope of carbon and has a layered, planar structure (figure 7).

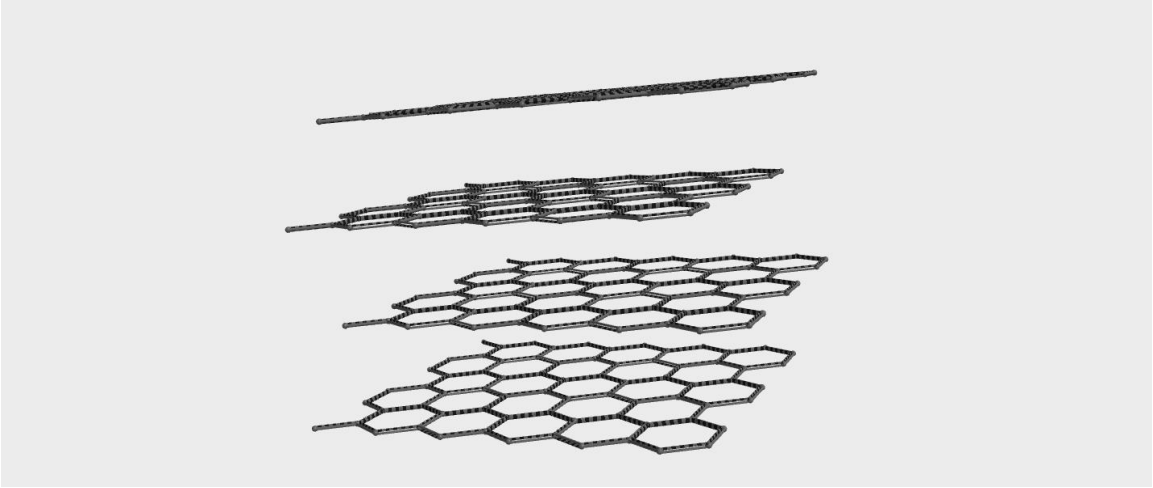

Figure 7: Structure of graphite (Drawn using Spartan 16 (Wavefunction, Inc.) software.)

The individual layers are called graphene. Alpha (hexagonal) and beta (rhombohedral) graphite have very similar physical properties, except that the graphene layers stack somewhat differently[36]. Several reports have appeared that successfully identify peptide sequences having very good affinity to graphite surfaces, such as highly ordered pyrolytic graphite (HOPG), using the techniques of phage display. Phage display was utilized to identify a graphite binding peptide, termed GrBP5, having the sequence IMVTESSDYSSY[37]. Mutations of the two aromatic residues at the C-terminus significantly modified the binding characteristics of GrBP5. The tyrosine (Y) residues replaced by alanines (A) largely eliminated the ability for the peptide to bind to graphite, while replacing the tyrosines with phenylalanine (F), or tryptophan (W) modified GrBP5's affinity to graphite from strong to moderate to weak binding, respectively.

Mutation of the N- terminus from hydrophobic to hydrophilic eliminated the amphiphilic character of the peptide, and disrupted intermolecular interactions with the graphite surface, and also prevented the peptides from forming defined nanoarchitectures[37].

A preliminary atomistic view of the molecular dynamics involved in the binding process of a high affinity binding peptide (graphite binding peptide 5, GrBP5; IMVTESSDYSSY) to a graphite surface was studied using the CHARMM27 force field[38]. This study provides an important overview of the initial diffusion, preliminary interaction and binding process that may occur between this peptide and the graphite surface. The peptide is composed of several domains: a hydrophobic domain (IMV); a hydrophilic domain (TESSD); and an aromatic domain (YSSY). The molecular dynamics studies indicate that the adsorption process is composed of the diffusion stage, followed by the anchoring and lockdown stages. The authors propose that the hydrophobic domain plays an important part in the diffusion and anchoring stages of the peptide to the graphite surface, and that the initial interaction is likely heavily reliant upon hydrophobic properties. In the adsorption process the aromatic residues of the peptide contribute critical interactions between the peptide and the graphite surface, with the hydrophilic central domain providing flexibility to optimize the aromatic and hydrophobic interactions. The importance of the interaction between the peptide and interfacial water molecules are noted in this molecular dynamics study. Previously reported computational studies on the interaction of benzene with multilayered graphenes using a density-functional tight-binding method have shed some light on the nature of aromatic-aromatic interactions that occur on graphite surfaces[39]. As well, predictions put forth based on molecular dynamics simulations[40] of a peptide (sequence: GAMHLPWHMGTL) obtained by phage display[41] against HOPG were found to be consistent with physical characterization of the peptide bound to HOPG as determined by atomic force

microscopy (AFM), Raman spectroscopy, Fourier-Transform Infrared (FTIR) spectroscopy and attenuated total reflectance (ATR)-FTIR measurements[40]. The 7-mer peptide, EPLQLKM, identified from phage-display biopanning against SLP30 graphite, has been determined to bind preferentially at the graphene edges[42]. Addition work on carbon nanotube, graphene and graphite binding peptide interactions can be reasonably studied by computational techniques employing polarizable force fields in molecular dynamics simulations. These studies indicated that aromatic-aromatic interactions as well as interfacial shape of the carbon allotrope are important factors in these interactions[43].

Graphene has been of increasing interest in terms of its fundamental structure as well as its potential applications in materials science (figure 8).

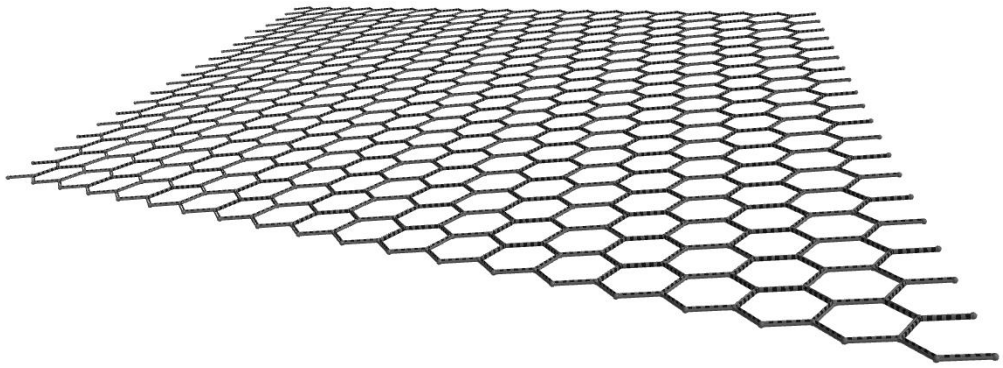

Figure 8: Structure of graphene. (Drawn using Spartan 16 (Wavefunction, Inc.) software.)

Phage display studies have been reported and have led to the identification of peptides, such as the peptide GAMHLPWHMGTL, exhibiting affinity interactions with this carbon allotrope[41] and the study of its interactions with graphene[40]. This peptide sequence was

successfully utilized to immobilize gold nanoparticles onto graphene surfaces and also fabricate an ultrasensitive graphene-based trinitrotoluene (TNT) sensor[41]. Utilizing a bacterial surface display system rather than a phage display strategy, the peptide CGPRTYLPLPWMAALGPC was identified as having strong affinity to graphene[44]. Positively charged residues also play important roles in peptide/protein-graphene interactions. This is clearly the case in a recent study that determined that blood proteins having basic residues bind well to graphene, possibly due to pi-cation interactions[45]. Density functional theory (DFT) calculations at the M06-2X-6-31+G(d,p)//M06-2X-6-31G(d) level of theory have provided additional insight into the interaction of aromatic residues in peptides, such as tryptophan, tyrosine, phenylalanine and histidine with graphene sheets as well as carbon nanotubes[46]. Other computational studies have been reported[47], including molecular mechanics methods utilizing polarizable force fields[48,49]. Molecular dynamics simulations have been undertaken in regards peptide-graphene interactions[50]. Additional studies have further elaborated upon the factors involved in peptide-graphene interactions[51]

A report on the development of an antibody against another carbon allotrope, C60 fullerene, has been reported (figure 9)[52]. With respect to phage display approaches, biopanning was reported using a cyclic 7-mer peptide library (constrained disulfide) against C60 films layered upon silicon surfaces[53]. The peptide having the sequence CNMSTVGRC was found to be selective to the bound C60 molecules.

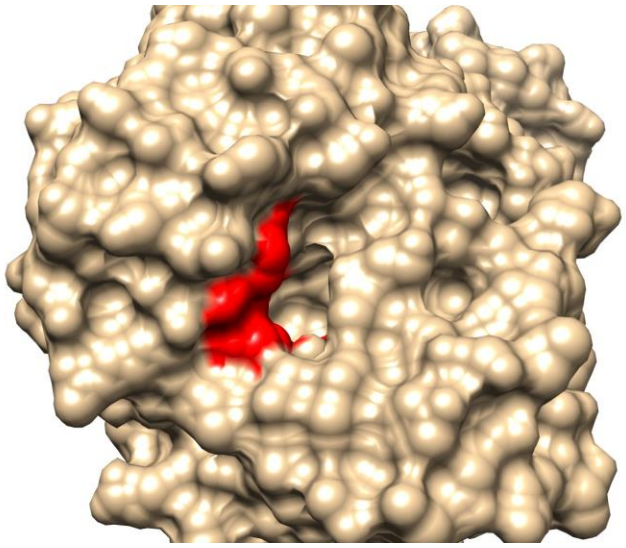

Figure 9: Antibody fragment of a C60 antifullerene antibody [52] (PDB: 1EMT). Residues believed to make stacking interactions with fullerene are shown in red on a Connolly surface representation of the antibody.

Carbon nanofibers (CNF), having diameters of 50-150 nm, are readily synthesized[54]. These materials have been employed in electrochemistry and as electrode materials[54–56]. As well, they have applications in the areas of energy conversion and storage devices[57–59]. Investigations utilizing M13-based phage display identified an M13 having a singe point mutation in its pVII protein compared to wild-type M13. The nearby region in pVII was found to be: ….TIY**R**AM….., where the bold and underlined residue (Arginine) replaced the amino acid glutamine found in the wild-type pVII phage protein[60]. Analysis of binding affinities indicated that the mutant phage bound two orders of magnitude better to CNF than the wild-type phage. A combination of atomic force microscopy (AFM), and transmission electron microscopy (TEM) was employed to confirm that the tips of the M13 phage were selectively bound to the CNF materials. No evidence for alternate binding modes to CNF was detected. The CNF-binding phage was also selective as little to no interactions were observed between this phage and other

carbon-based nanomaterials such as single-walled and multiwalled carbon nanotubes, graphite, or reduced graphene oxide. It was suggested by the authors, and based on further studies utilizing circular dichroism (CD), scanning electron microscopy (SEM) and FT-IR, that the presence of the arginine might have altered the conformation of the pVII protein on the phage, which might have led to more exposed hydrophobic or pi-pi interactions (possibly through the adjacent tyrosine side chain or through a nearby phenylalanine residue) between the CNF and the phage surface. The authors expect that phage having CNF affinities could be utilized to prepare new CNF biocomposites and expect to be able to construct unique nanoparticle scaffolds in the future.

The carbon allotropes graphite and graphene are sp^2-hybridized having carbon atoms arranged into planar hexagonal rings. On the other hand, the carbon atoms composing diamond are sp^3-hybridized and organized as two interpenetrating face-centered cubic lattices (figure 10)[44].

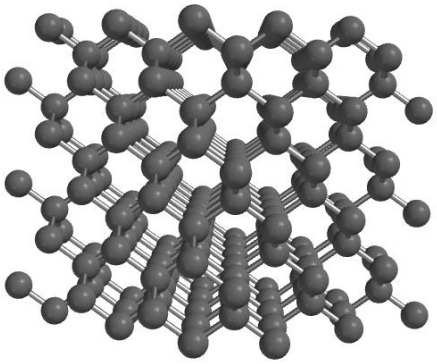

Figure 10: Structure of carbon atoms composing diamond. (Drawn using Spartan 16 (Wavefunction, Inc.) software.)

Peptides such as CGPRTYLPLPWMAALGPC and CGPDSARGFKKPGKRGPC, identified as having the capability to interact with sp2 carbon frameworks such graphene and graphite, also have been found to exhibit some affinity to the sp3 framework of diamond[44]. Phage display screening identified several peptides having diamond-binding properties, and additional structure-activity studies have led to improved affinity interactions[61,62]. Surprisingly, biopanning screen using a 12-mer phage library resulted in the identification of an extremely long peptide, HFYPGANRSTTQGGGSANLHQTAASAKNSAPQKSENRKVPFYSHSRTRENNRSIYTA, and exhibited an affinity of approximately 63 nM to diamond-like surfaces[61]. Although an unusual entity present in phage display systems, it was interesting that such an unusual peptide was isolated and identified in such a biopanning screen. Linking several copies of this peptide improved affinity interactions[62]. A recent report has appeared that has identified several short peptides from phage display techniques, such as GVGGLTTVNYSR, NVVRNVFPALDH, ISYQTRHTFPTI, HKPPRQKPKAQQ, and NVDYNRKDRIDR, which exhibit diamond-binding properties[63].

1.5 Polymer Binding Peptides

In addition to noble metal nanostructures and carbon nanostructures, polymers and biopolymers are of intense interest in materials science and have wide applicability. There have been several studies that have identified peptides having specific affinities toward many (bio)polymers. These peptides have been identified using techniques such as peptide display systems (described in chapter 2). Several of the most interesting examples in this area are presented in Table 2[64–75].

Table 2: Peptide sequences and its corresponding polymers

Target	Peptide	Peptide Length
Silk[75]	SYTFHWHQSWSS	12
	QSWSWHWTSHVT	12
Lignin[64]	HFPSPIFQRHSH	12
Cellulose[68]	WHWTYYW	7
Chitin[67,69]	SRTTRTR	7
	GEVGEQEKARVG	12
	EGKGVEAVGDGR	12
poly (methyl methacrylate)[70]	ELWRPTR	7
	HKPDANR	7
Polystyrene[65,71,72]	HWGMWSY	7
	WHWNAPWWNGVY	12
	FHWTWQFPYTST	12
	GAMHLPWHMGTL	12
	HWNIWWQHHPSP	12
	HFFKWHTRTNDQ	12
	HFFRWHPSAHLG	12
	HFAYWWNGVRGP	12
	GSFYDSILFYCMTCR	15
	GETRAPL	7
	FPGRPSP	7
Polypyrrole[66]	THRTSTLDYFVI	12
Poly (phenylene vinylene)[74]	HTDWRLGTWHHS (linear)	12
	ELWSIDTSAHRK (hyperbranched)	12

Cellulose, a polysaccharide consisting of a linear chain of several hundred to many thousands of β(1→4) linked D-glucose units, has been investigated for its use in biomaterials science due to its high abundance in plant biomass and its potential source for biofuels production and for cellulose-based fibre synthesis [76–78]. Enzymatic hydrolysis via the bacterial cellulase complex has been investigated as an alternative to chemical hydrolysis due to environmental pollution arising from the chemicals used in the degradation process and to the poor yields of the desired products from these chemical hydrolytic approaches[79]. In the cellulosome complex, cellulose-binding modules allow for cellulose binding and targeted enzymatic hydrolysis[80]. As the structural requirements of the binding modules are not completely understood, phage display (phage display will be explained in detail in chapter 2) has been utilized to identify peptides that exhibit cellulose affinity[81]. The identified peptides have been determined to be rich in tryptophan and tyrosine residues, showing that the cellulose binding modules require tryptophan and tyrosine for their interaction with the glucose residues of the cellulose polymer.

Typically, the degradation of lignocellulose biomass to produce biofuels is found to be a challenging process due to the presence of lignin that is also present in plant cell walls[82]. Lignin is a complex heteroaromatic polymer that inhibits the enzymatic hydrolysis of lignocellulose and it is of intense interest to be able to selectively remove lignin during this process while keeping the integrity of the biomass source in biofuels production[83–85]. A series of 12-mer peptides having an affinity towards lignin was identified and determined to have an amino acid consensus sequence of HFPSP. It was observed that changing the phenylalanine residue in the peptide to isoleucine altered the lignin selectivity of these peptides[64].

Synthetic polymers have also been investigated for their ability to bind peptides, which may provide attachments to the polymer for the assembly of novel functionalized polymeric materials. Synthetic polymers such as polystyrene (PS) have been investigated for its ability to non-covalently bind peptides to its surface[65,71,86,87]. It is important to note that the tacticity of the PS is important in the recognition event as peptides have been shown to be able to recognize the stereoregularity of PS. These findings show the capability of peptides to recognize the specific structure of a molecular target[65]. Interesting potential applications of these types of PS-binding peptides to the improvement of biochemical assays was investigated by Kogot and coworkers. It was shown that the affinity peptide, when fused to a second unrelated peptide, can acted as a capture agent to PS-coated microplate reader wells[73]. Through the use of enzyme-linked immunosorbent assays (details of this assay will be discussed in chapter 3), it was determined that the PS-fused peptide conjugates exhibited lower detection limits for horseradish peroxidase conjugated antigen based assays for the pathogen *Bacillus anthracis* than the free peptide, as the free peptide would not exhibit affinity to the PS coating and subsequently be washed out in the assay procedure[73]. PS-binding peptides were shown to be rich in aromatic side chains and it is thought that interactions such as the $\pi - \pi$ interaction between aromatic side chains of the peptide and the aromatic groups of the styrene units of PS greatly contribute to the affinity interaction.

1.6 Polyethylene Polymers

Polyethylene (PE) is a polymer that is derived from the polymerization of ethylene. One of the products, polyethylene resin, is a semicrystalline polymer that is found in plastic bottles and construction materials[88]. The general structure of PE is shown in figure 11 and a model representation of PE is shown in figure 12.

$(CH_2\text{-}CH_2)_n$

$[(CH_2CH_2)_x\text{-}(CH_2CH\text{-}(CH_2)_n\text{-}CH_3)]_m$

Figure 11: General chemical structure of PE. The structure at the bottom is the structure of PE with an α-olefin as the branching molecule.

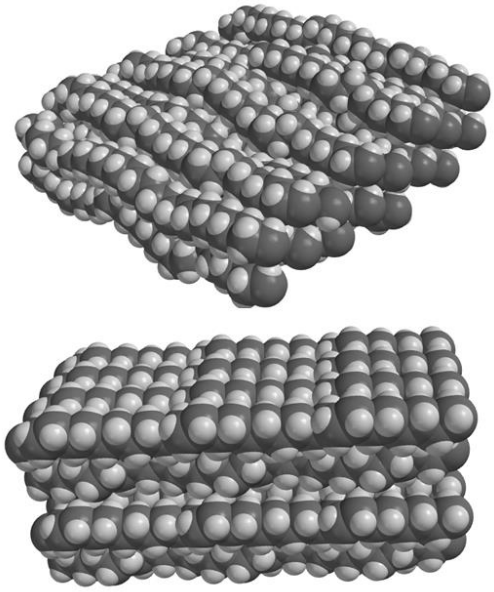

Figure 12: Model representation of PE in two different orientations. (Drawn using Spartan 16 (Wavefunction, Inc.) software.)

The branches on the PE resin in terms of its chemical structure are formed from alkyl substituents found on the α-olefin comonomer and the overall composition of PE can vary depending on the length of the α-olefin[89]. Branching of polyethylene occurs from the α-olefin or

ethylene and the degree of branching depends on the mechanism of polymerization and the comonomer[90]. PE is classified into various types based on its density and its internal branching as shown in Table 3.

Table 3: Different types of PE, their applications, and density[90]

Polyethylene types	Application	Density (g/cm^3)
High Density PE	Construction materials	0.941-0.965
Medium Density PE	Pipes	0.926-0.940
Linear-low Density PE	Food and retail packaging	0.915-0.930
Low Density PE	Food packaging	0.915-0.935
Very low Density PE	Food packaging	0.855-0.885

1.7 Industrial Synthesis of PE

Industrial syntheses of PE resins involve the usage of catalysts such as Ziegler-Natta catalysts, single site catalysts and chromium catalysts as shown in figure 13[90].

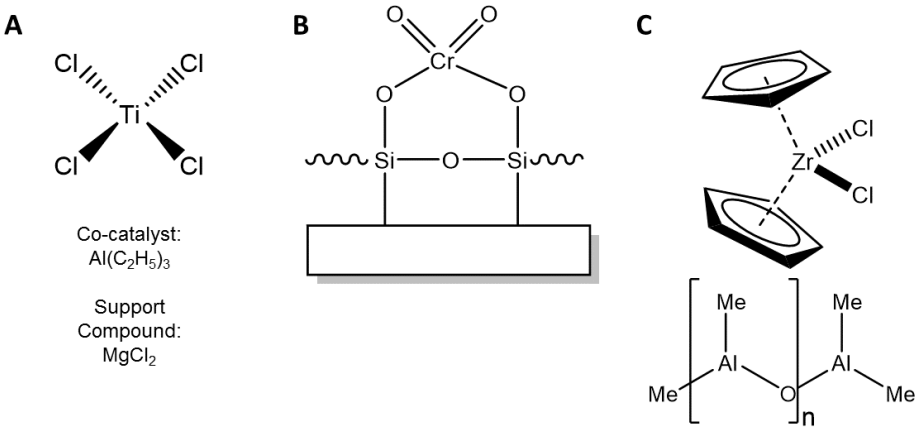

Figure 13: Catalysts used in industrial PE synthesis. A: Ziegler-Natta system B: Chromium (Phillips) Catalyst on a silica support C: Metallocene-based catalyst with methyl aluminoxane as co-catalyst

Ziegler-Natta catalysts are a combination of two individual catalysts that are composed of a transition metal compound (typically titanium tetrachloride) that serves as a main catalyst in the polymerization and an organometallic compound that serves as a co-catalyst/activator[91]. Support compounds such as $MgCl_2$ are also added in the reaction to control particle size and morphology of the catalyst. Ziegler-Natta catalysts are typically used to produce linear-low density PE, medium density PE, high density PE, and very low density PE depending on the amount of pressure that is applied in the reactor[90]. High pressure leads to a heavily branched PE whereas low pressure leads to a linear PE[90]. The chromium catalyst system (also known as the Phillips catalyst) is composed of chromium oxide that is fixed to silica, which is the only active catalyst in the polymerization process in contrast to the Ziegler-Natta system[90]. Chromium catalysts can also be used to produce high density PE and linear-low density PE[90]. Single site catalysts are homogeneous catalysts that also use co-catalyst compounds such as methylaluminoxane (MAO) albeit it is not well characterized in contrast to the Ziegler-Natta system[90,92]. Metallocene-based catalyst systems such as zirconocene dichloride, ferrocene and dimethyl titanocenes are well known single site catalysts that are used in the commercial synthesis of PEs[90]. Single site catalysts differ from Ziegler-Natta catalysts as single site catalysts have one type of active center that produces PEs with very narrow molecular weight distributions[90]. Ziegler-Natta catalysts have multiple active sites that catalyze the polymerization of ethylenes, leading to the production of PEs with a broader molecular weight distribution[90].

1.8 Surface Modification of PE

Although PE polymers have excellent bulk physical and chemical properties, the polymer is very inert to further chemical reaction. Since the interaction of any polymer with its partner of choice occurs at the surface, modification and functionalization of the PE surface is being

studied as it will allow for an inexpensive polymer to gain novel functionalities that may increase the value and the applications of these polymers[93]. There are several approaches that have been reported to be successful in functionalizing the PE surface. PE can be treated with oxidising flame as this oxidizes the surface of PE which then generates various functional groups ranging from hydroxyl groups to carboxyl groups[93]. Flame treatment is used to treat bulk materials to enhance the ink permeability on the surface for purposes of dyeing. Another approach is to halogenate the PE surface through the irradiation of the surface with bromine vapour followed by irradiation of the surface for thirty second irradiation cycles using a mercury vapour lamp. Oxidation of the PE surface can also be done through a corona discharge treatment. The corona discharge treatment as shown in figure 14 at first generates a plasma (corona) through the ionization of the air as voltage is applied on the electrode. The PE film, after being reacted with the corona discharge, forms radicals which lead to the reaction of atmospheric oxygen with the PE radical to generate oxidized surface groups[93].

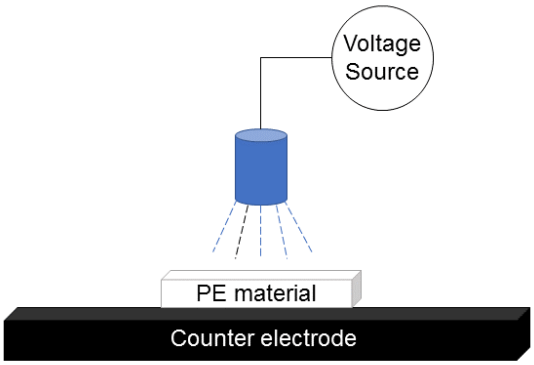

Figure 14: Schematic of Corona Discharge

Functionalization of PE through corona discharge treatment is dependent on the voltage of the corona discharge, the subsequent reaction time and temperature. The corona discharge treatment is mainly used in the plastics industry to improve the adhesion of polyolefin films and materials. While the synthetic methods are useful and are still used, it can damage the surface integrity of the PE itself due to the condition of the materials used in the modification. For example, very high corona discharge voltages can lead to surface degradation and induce the polymerization of the reactive group containing molecule[93]. It has also been observed that excessive bromination can damage the surface and undo the surface bromination itself [93]. The motivation to find a biomolecule, specifically peptide-based, that exhibits affinity towards PE would arise from the fact that surface modification of PE through a mild molecular recognition of the peptide and PE could preserve the integrity of the PE surface in contrast to the synthetic methods described above. The hypothesis of the thesis is to determine and isolate peptides (herein defined as adhesons) that exhibit affinity towards advanced materials and as a starting point, polyethylene resins will be used as the target for screening phage libraries.

Chapter 2: Phage Display

2.1 M13 Bacteriophage and Phage Display

Phage display is a combinatorial technique used in biochemistry and molecular biology and introduced by George P. Smith in 1985[94,95]. Phage display is an *in vitro* selection and screening method in which a combinatorial library of random peptides is expressed as a fusion protein in a coat or tip protein of filamentous bacteriophages such as M13 as shown in figure 15[95].

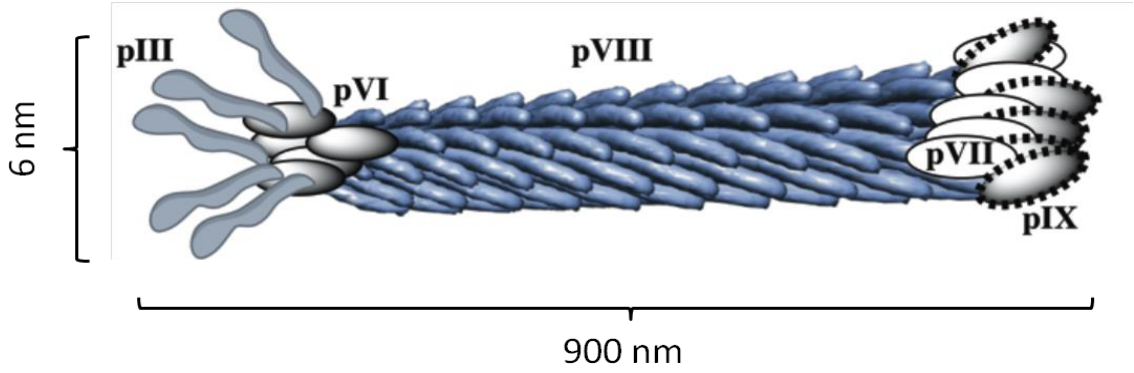

Figure 15: M13 bacteriophage structure labeled with five coat proteins and its dimensions

The M13 bacteriophage is a filamentous phage that is 6 nm by 900 nm in dimensions and in contrast to the archetypal bacteriophage set of viruses can reproduce without killing the host cell to form plaques from the diminished growth of the host cell[96]. As M13 binds to the F-pilus complex found on the surface of the *Escherichia coli* host, M13 extrudes its single-stranded DNA (ssDNA) into the cytoplasm of the host cell. Following the entry of the DNA, a new strand of DNA that is a base complement to the ssDNA is replicated to form a replicative form (RF) DNA which is double-stranded. The RFDNA then serves as a template to synthesize phage proteins that are required to make up a whole particle and replicate more of the ssDNA genome.

Later in the life cycle of M13, dimers of DNA-binding protein pV bind to the ssDNA and transport the DNA to the phage-encoded transport complex where the assembly of the phage particle occurs. As pVIII coat proteins replace pV proteins, other minor coat proteins are attached to the phage unit and then the intact phage is released into the medium. Phage display allows for the detection of desired peptides from an extensive collection of phage variants. Ever since its foundation[94,97], phage display has led to a significant application in a wide range of scientific fields[98–104]. Upon the discovery of phage display, application to the areas of protein and antibody engineering along with its use in the study of protein-ligand interactions has resulted[97]. For example, phage display has been utilized to select for a recombinant antibody of interest that bound to antigens present on a surface of malignant cells[96]. Recent advances in both biochemistry and materials science have led to the use of phage display to screen for peptides exhibiting affinity towards non-biological targets[105–109]. Peptide libraries of phage are constructed through the insertion of randomized sequences of DNA into the appropriate site of a gene that encodes for one of the coat proteins of the phage. As shown in figure 15, five coat proteins make up one M13 phage unit, and while all coat proteins are a candidate for peptide display as illustrated in figure 16[96,110], the tip coat protein pIII, and the major coat protein pVIII are most often used in phage display[96].

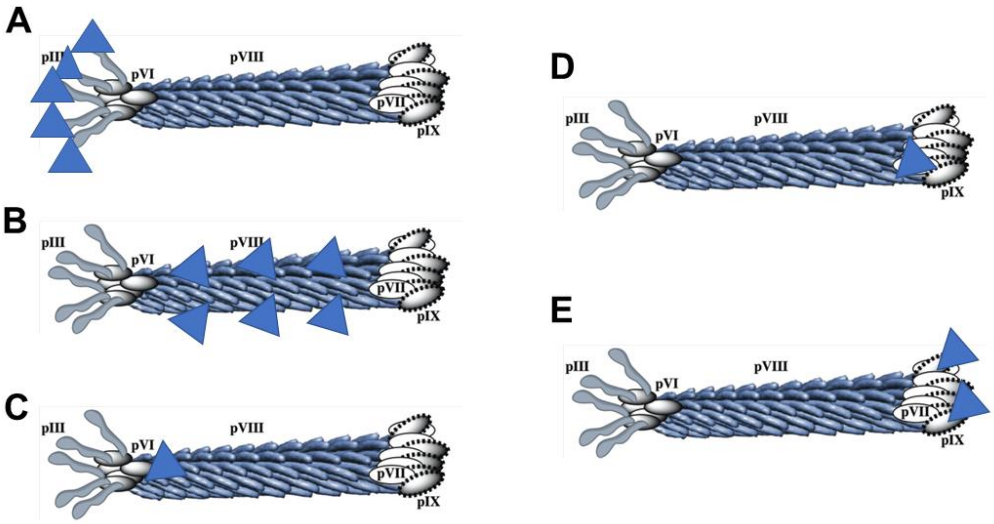

Figure 16: Different examples of displayed peptides on M13 where blue triangles represent peptides displayed on M13. **(A)** Peptides are displayed on pIII. **(B)** Peptides are displayed on pVIII **(C)** Peptide is displayed on pVI **(D)** Peptide is displayed on pVII **(E)** Peptides are displayed on pIX

The tip protein pIII shown in figure 17 mediates the infection of the host cell *Escherichia coli* (*E. coli)* which starts the phage replication[96]. The coat protein pVIII surrounds the genome of M13 as there are approximately 2700 copies per phage.

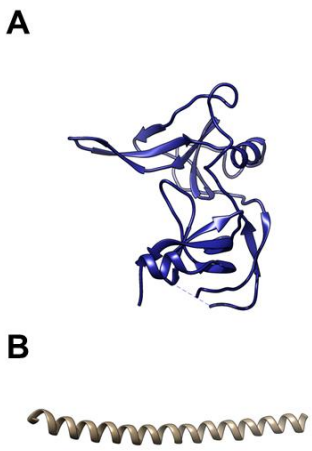

Figure 17: Ribbon structure of (**A**) pIII (PDB: 1G3P[111]) and (**B**) pVIII (PDB:1IFJ[112]) coat proteins.

The advantage of using peptides displayed on the pIII protein is that pIII can tolerate the insertion of larger random peptide sequences into its structure unlike the pVIII display system. The disadvantage of the pIII display system is that the infectivity of the phage clones may be reduced compared to the wild-type phage[113]. The advantage of pVIII is that it is possible to display more than five copies of a peptide per phage particle as there are approximately 2700 copies present of the pVIII protein. The disadvantage of using the pVIII display system is that only small peptides can be present on pVIII as bigger peptides can prevent packaging of the phage particle during its life cycle, hence increasing the instability of M13. While it is possible to generate the library in-lab, three commercially available libraries are often used in phage display. Library of random peptide libraries are established by inserting randomized sequences of DNA into the appropriate site of a gene that encodes for one of the coat proteins of M13 phage. The

libraries of choice have linear 7-mer, linear 12-mer and the disulfide bond-constrained 7-mer peptides attached to the N-terminal of the pIII as shown in figure 18.

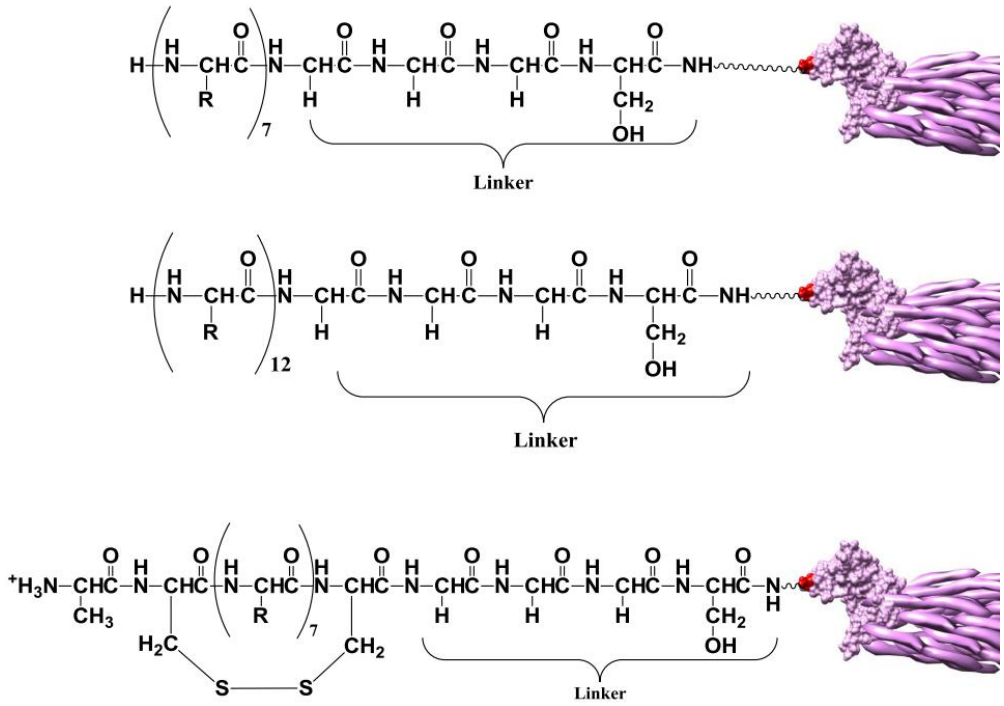

Figure 18: Representation of random peptides in phage display libraries. Only one of the five identical peptides are shown emanating from a single pIII protein. (PDB: 1G3P and 1IFJ)

It is important to note that all three libraries shown in figure 18 contain 10^9 independent phage units in which the linear 7-mer library will display 1.28×10^9 possible sequences from 20 naturally occurring amino acids in each of the positions in the heptameric sequences (20^n where n = 7)[110]. The linear 12-mer library will produce 4.096×10^{15} possible sequences (20^{12}) in which it can only represent 2.44×10^{-5} % of the sequence space given the amount of phage clones $\left[\left(\frac{1.0\times10^9\ clones}{4.096\times10^{15}\ possible\ sequences}\right)\times100\ \% = 2.44\times10^{-5}\ \%\right]$ in a phage panning experiment

compared to 78.0 % [$\left(\frac{1.0\times10^{9} clones}{1.28\times10^{9}\ possible\ sequences}\right)\times100\ \%=78.0\ \%$] of sequence space for the linear 7-mer and disulfide constrained 7-mer library. Due to other limitations on the phage display process such as preferential amino acid sequence use, a somewhat reduced sequence space is available in these display techniques[114–116].

2.2 Materials and Methods

2.2.1 Identification of Phage Adhesons

The general steps in a phage display experiment are shown in figure 19.

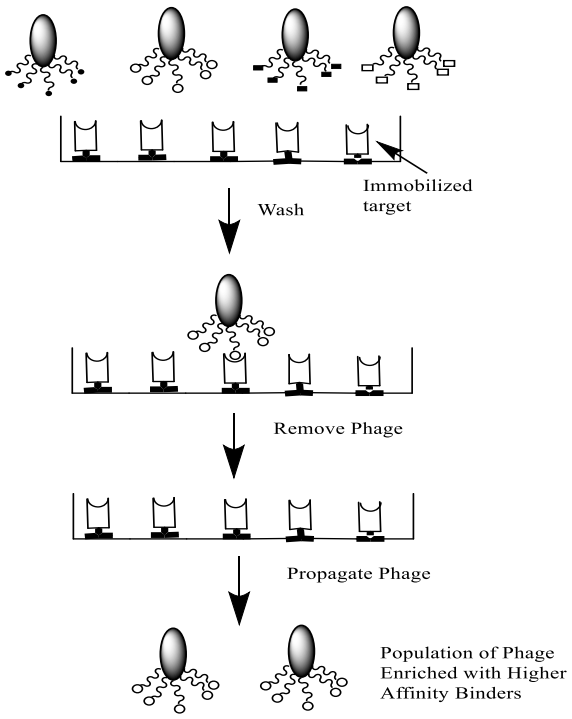

Figure 19: General procedures in phage display

Six resins from Imperial Oil (Sarnia, ON) in the form of pellets of average diameter of 5 mm were washed with Milli-Q™ (MQ) H_2O in a glass vial/plastic Eppendorf tube twice to remove dust particles. The resins as mentioned earlier are the following: Ziegler-Natta catalyzed

HD/LLDPE, chromium catalyzed AD60 and BA46, and metallocene catalyzed 1012KA and 1018KA. The stock library solution (for all three libraries) were diluted to 10^{11} phage forming units (pfu)/mL and incubated in an empty glass vial/Eppendorf tube for 1 hour to remove any potential glass/polypropylene-binding peptides that may interfere with any downstream experiments. After the incubation, 200 µL of the diluted phage solution was transferred to the PE sample contained in a glass vial/Eppendorf tube and incubated for one hour. After incubation, the solution that contained unbound phage was removed and washed five times with Tris-buffered saline (50 mM Tris and 150 mM NaCl pH 7.5) that also contained 0.1 % Tween-20® (Sigma-Aldrich, Oakville, ON.) to remove any nonspecifically bound phage. The resins then were transferred to a new glass vial/Eppendorf tube to reduce any unwanted elution of residual glass/plastic binding phage. Elution of the bound phage was done by adding 200 µL of 2 M glycine-HCl that also contains 1 mg/mL bovine serum albumin (BSA) which was incubated for 10 minutes. From here, the eluted phage solution was transferred to an Eppendorf tube and neutralized with 30 µL of 1 M Tris-HCl pH 9.1. Table 4 and 5 shows some of the differences in the experiment for each resin and the three corresponding libraries used in the biopanning experiment.

Table 4: Number of rounds of biopanning and amplification undertaken for each library

PE resin	Linear 7-mer	Disulfide constrained 7-mer	Linear 12-mer
HDPE-ZN	5th round	4th round	4th round
LLDPE-ZN	5th round	3rd round	NA
AD60	5th round	NA	NA
BA46	5th round	NA	NA
1012HA	5th round	NA	NA
1018KA	5th round	NA	NA

Table 5: Different containers used in biopanning

PE resin	linear 7-mer	Disulfide constrained 7-mer	linear 12-mer
HDPE-ZN	Eppendorf Tube	Glass vial	Glass vial
LLDPE-ZN	Eppendorf Tube	Glass vial	NA
AD60	Eppendorf Tube	NA	NA
BA46	Eppendorf Tube	NA	NA
1012HA	Eppendorf Tube	NA	NA

2.2.2 Amplification of Eluted Phage

To increase the titer of the phage solution, the phage were amplified as followed: With a 5 mL solution of *E. coli* K12 ER2738 culture grown overnight, the culture solution was diluted 100-fold in 20 mL of lysogenic broth (LB) (10 g/L tryptone, 5 g/L NaCl, and 5 g/L yeast extract) and 230 μL of 10^7 plaque forming unit/mL (pfu/mL) phage solution was added to infect the cells and initiate amplification. The phage containing solution then was incubated in a shaker (at 200 rpm) for 4.5 hours at 37 °C. The solution was centrifuged at 12000xg for 10 minutes at 4 °C to sediment the infected cells, and the phage containing supernatant was collected. A 4 mL of 20 % polyethylene glycol 8000 (PEG) / 2.5 M NaCl was used to precipitate the phage containing supernatant, and it was incubated overnight at 4 °C. The phage precipitated solution was centrifuged at 13500xg for 20 minutes at 4 °C, and the sedimented phage was resuspended in 1 mL of TBS. The solution was transferred to an Eppendorf tube and the solution was centrifuged with a benchtop centrifuge for 5 minutes at 3834xg to remove any residual cells. After collecting 1 mL of the supernatant, the solution was precipitated with 200 μL of PEG/NaCl solution and incubated on ice for 1 hour. The precipitated phage solution was centrifuged with a benchtop centrifuge at 13225xg for 20 minutes at 4 °C, and then as the supernatant is removed, the phage pellet was resuspended with 200 μL TBS. From this point the first round of phage display is complete. Biopanning and amplification were repeated until the final rounds as mentioned on table 4 and with each succession round of biopanning, the concentration of Tween®-20 was

increased by 0.1 % except for the linear 12-mer library in which the Tween®-20 was raised to 0.5 % in the fourth round of biopanning/amplification. The general steps for amplifying the eluted phage are shown in figure 20.

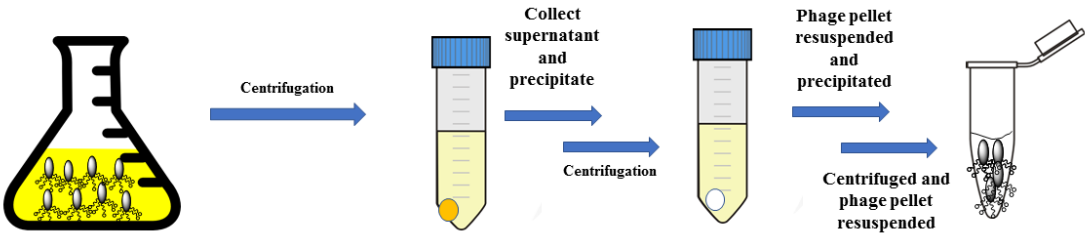

Figure 20: General procedures in amplifying M13 phage

2.2.3 Determination of Phage Titer

To quantify the amount of phage that has been either amplified or eluted and for the extraction of replicative form DNA, a colony of *E. coli* K12 ER2738 was inoculated in 5 mL of LB media, and it was incubated in a shaker (200 rpm) for approximately 6 hours at 37 °C. While growing, eluted/amplified phage stock solution was diluted 10^{-4} to 10^{-5}-fold for eluted phage and 10^{-9} to 10^{-10}-fold for amplified phage. A Soft LB agar solution (3 mL) was added to 200 µL *E. coli* culture. Right away the soft agar solution (3 mL) was added to an LB agar plate containing 210 µmol of isopropyl-β-D-thiogalactoside or IPTG (BioShop Canada, ON) and 98.0 µmol of 5-bromo-4-chloro-3-indolyl-β-D-galactopyranoside or X-Gal (BioShop Canada, ON). A diluted phage solution (10 uL) was spotted on the plate and was let dried in a 37 °C incubator overnight. The blue phage plaques formed from a diminished growth of *E. coli* were then counted. There

should be on average 15 to 70 plaques at 10^{-9th} dilution of the amplified phage stock and 20 to 80 plaques at 10^{-3rd} dilution of the eluted phage solution from the biopanning step of the experiment.

2.2.4 Extraction of M13 DNA for Sequencing

With an overnight culture of *E. coli* K12 ER2738, 20 µL was added to 2 mL LB solution. A single blue plaque of the latest round of the amplified phage was randomly picked and added to the corresponding culture tubes to be grown for 4.5 hours at 37 °C as shown in figure 21.

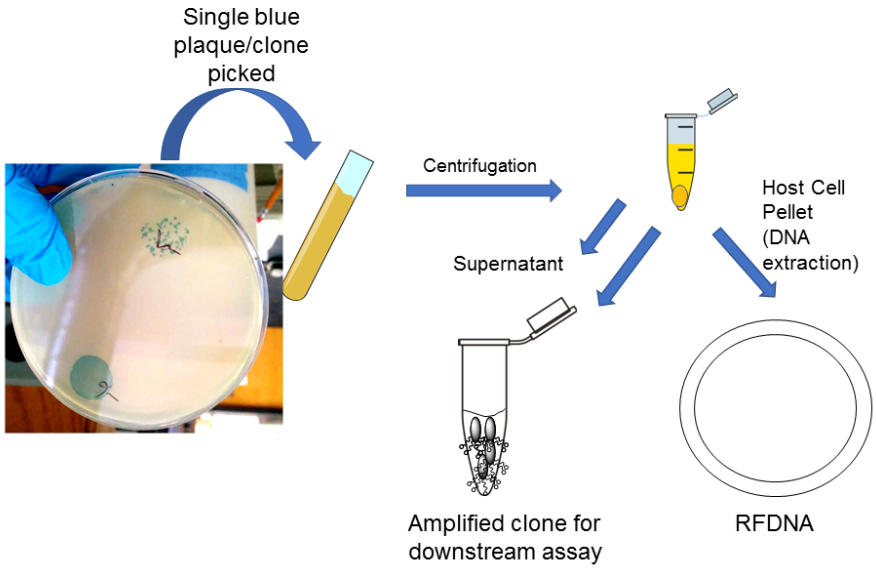

Figure 21: General description for RFDNA extraction

The infected culture was briefly centrifuged at 13225xg to sediment the infected cells that carry the replicative form DNA (RFDNA) of M13. As the RFDNA is double stranded, a plasmid DNA extraction kit (Sigma-Aldrich, Oakville, ON.) was used to extract the RFDNA through the following: The sedimented cells were resuspended with 200 µL of resuspension solution. The solution was vortexed thoroughly until it was homogeneous. The cells are lysed with 200 µL of

lysis solution and then gently inverted 6 to 8 times which leads to the solution becoming clear. The lysed cells were neutralized with 350 µL of neutralization solution which precipitates chromosomal DNA, cell debris, proteins and lipids and keeps the RFDNA in solution. The solution was inverted 5 to 7 times to ensure gentle mixing. The solution was centrifuged with a benchtop centrifuge at 13225xg for 10 minutes at room temperature. A miniprep binding column which washes out everything but the RFDNA were prepared by adding 500 µL of column preparation solution which increases the binding affinity between the RFDNA and membrane on the miniprep binding column. The column was centrifuged at 13225xg for 1 minute at room temperature and discarded the flow-through liquid. The cleared lysate solution (700 µL) was transferred to the column and centrifuged at 13225xg for 1 minute at room temperature and discarded the flow-through solution. The wash solution (750 µL) was added to the column and centrifuged at 13225xg for 1 minute at room temperature. After discarding the flow-through solution, the column was centrifuged at 13225xg for 1 minute at room temperature to remove excess ethanol in the column. The column was transferred to a new collection tube and added 50 µL of MQ H_2O. It was centrifuged at 13225xg for 1 minute to elute the bound RFDNA. Absorbance at 260 nm, 280 nm, and 230 nm was measured using an UV-visible spectrometer to check for the purity of the RFDNA. Agarose gel electrophoresis (Method is described in 2.2.5) was run on the DNA sample to check for the purity of the extracted DNA sample. As the gene for the adheson is encoded in the genome of M13, the DNA samples were sent to Mobix laboratory of McMaster University for sequencing. The resulting sequences (circled in appendix A) are then converted to their reverse complement sequences and then they are translated to their corresponding amino acids.

2.2.5 Preparation of Agarose Gels for Electrophoresis

To prepare a 0.8 % agarose gel, 0.32 g of agarose (BioShop Canada, Burlington, ON.) was weighed out and dissolved in 40 mL of TBE buffer (90 mM Tris, 90 mM boric acid, and 2 mM ethylenediaminetetraacetic acid (EDTA) at pH 8) by microwaving the solution until it became transparent. SYBR Safe DNA gel stain (1.5 µL) (ThermoFisher Scientific catalog number S33102, lot 1105019), solution was added when it was cool enough to touch and the solution was poured into a casting chamber to solidify it into a gel with a well comb (well comb creates the wells in which the DNA solution can be added to) as it cools down further. The gel was transferred to an electrophoresis chamber and the TBE buffer solution was poured until it filled about 80% of the chamber. A DNA standard marker (5 µL) which shows the corresponding DNA and its absolute number of base-pair along with the RFDNA (10 µL) which contained 2 µL of 6X loading dye was added to the wells made from the well comb and ran it for 60 to 90 minutes at 50 V. Figure 22 shows a general result of RFDNAs that were electrophoresed.

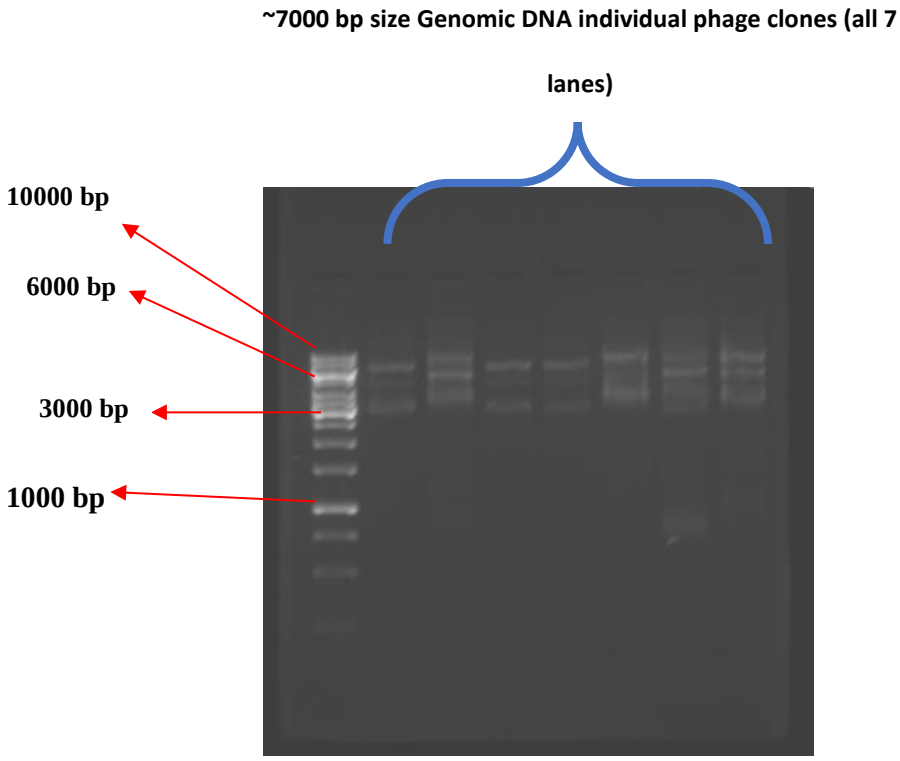

Figure 22:Agarose gel electrophoresis of phage panned against (BA46) chromium catalyzed PE resin. DNA was prepared using Genscript Quickclean II plasmid miniprep kit. Leftmost lane is the DNA standard marker. The multiple bands shown in the gel represent different conformation of the DNA.

2.3 Results of Biopanning / Amplification Experiments

The panning and amplification steps with the linear 7-mer libraries on four different type of polyethylene resins have been accomplished up to the 4th round of panning for HDPE and LLDPE. 5th round of panning for chromium catalyzed BA46 and metallocene catalyzed 1018KA was accomplished. For the disulfide constrained 7-mer library, the experiment was done against HDPE and LLDPE up to the 4th and 3rd round respectively. The linear 12-mer library was panned and amplified against just HDPE up to the 4th round. The concentration in the final rounds of

eluted phage was on average 10^5 to 10^6 $\frac{\text{pfu}}{\text{mL}}$, and the amplified phage was on average 10^{13} to 10^{14} $\frac{\text{pfu}}{\text{mL}}$.

2.4 Adheson Sequences Obtained by Biopanning

Table 6: Resulting phage adheson sequences from screening the linear 7-mer library

Type of PE	Sequence	Frequency of appearing sequences
Ziegler-Natta catalyzed HDPE	TDVALQQ	1/7
	YLRVGGH	1/7
	WRFDIYH	1/7
	YLKFNVT	4/7
Ziegler-Natta catalyzed LLDPE	RYWSSDS	1/5
	KPTLFIN	1/5
	DLHAYFK	1/5
	FNISVQH	1/5
	YLKFNVT	1/5
Chromium catalyzed BA46	PKHGEVG	2/6
	HMGLNYN	1/6
	DRTNATV	3/6
Exceed 1018KA	PPSSMMG	1/4
	KTEGPVL	1/4
	PGSGIEW	1/4
	SNTNTWS	1/4

Table 7: Resulting phage adheson sequences from screening the disulfide constrained 7-mer library

Type of PE	Sequence	Frequency of appearing sequences
Ziegler-Natta catalyzed HDPE	EKNIMWD	2/4
	QKNHRGN	1/4
	AHHWGTP	1/4
Ziegler-Natta catalyzed LLDPE	YPEVRAT	1/2
	WPVVINK	1/2

Table 8: Resulting phage adheson sequences from screening the linear 12-mer library

Type of PE	Sequence	Frequency of appearing sequences
Ziegler-Natta catalyzed HDPE	NSIQVSSWSPSV	1/16
	HTDNAPRMYDFQ	6/16
	RLVPQYLPASPS	1/16
	HLYIPLHPSHPS	2/16
	ENWWRSPAVALA	1/16
	YTPSHLSASIT	5/16

Tables 6, 7, and 8 show the determined sequences for the phage adhesons. While sequences such as HTDNAPRMYDFQ and PKHGEVG showed up more than once from the 16 set of 12-mer phage clone DNA samples, there were no visible residues or sequence motifs in the phage adhesons. It was found that series of linear 12-mer peptides that were isolated from using ultra high molecular weight PE tape was determined from DuPont and found the sequences shown in table 9, but there are no sequences that are identical to our screen against the Imperial Oil PE samples using the 12-mer phage library despite both the tape and the resins being composed of PE. It is likely that the forms of PE are different. It was interesting to note that an 11-mer adheson (YTPSHLSASIT) was determined from the panning of HDPE with the 12-mer

library. This could mean that during the phage amplification, there may have been a deletion that led to the isolation of the 11-mer. It is also possible that a complication from New England Biolabs during the production of the library clones may have led to the 11-mer peptides being displayed on the pIII.

Table 9: Linear 12-mer peptides isolated from DuPont[117]

Type of PE	Sequence
Ultra-high molecular weight PE tape	HNKSSPLTAALP
	LPPWKHKTSGVA
	LPWWLRDSYLLP
	VPWWKHPPLPVP
	HHKQWHNHPHHA
	HIFSSWHQMWHR
	WPAWKTHPILRM

The sequences reported in the patent from DuPont did not have an apparent consensus sequence either. The amino acid sequences obtained from our phage display experiments were analyzed to determine if there are specific amino acids that occur more frequently in comparison to other amino acids. This analysis could aid in the elucidation of the chemical interactions involved in the peptide-PE binding. Figure 23 indicates the composition of amino acid residues in the sequenced peptides from all three libraries.

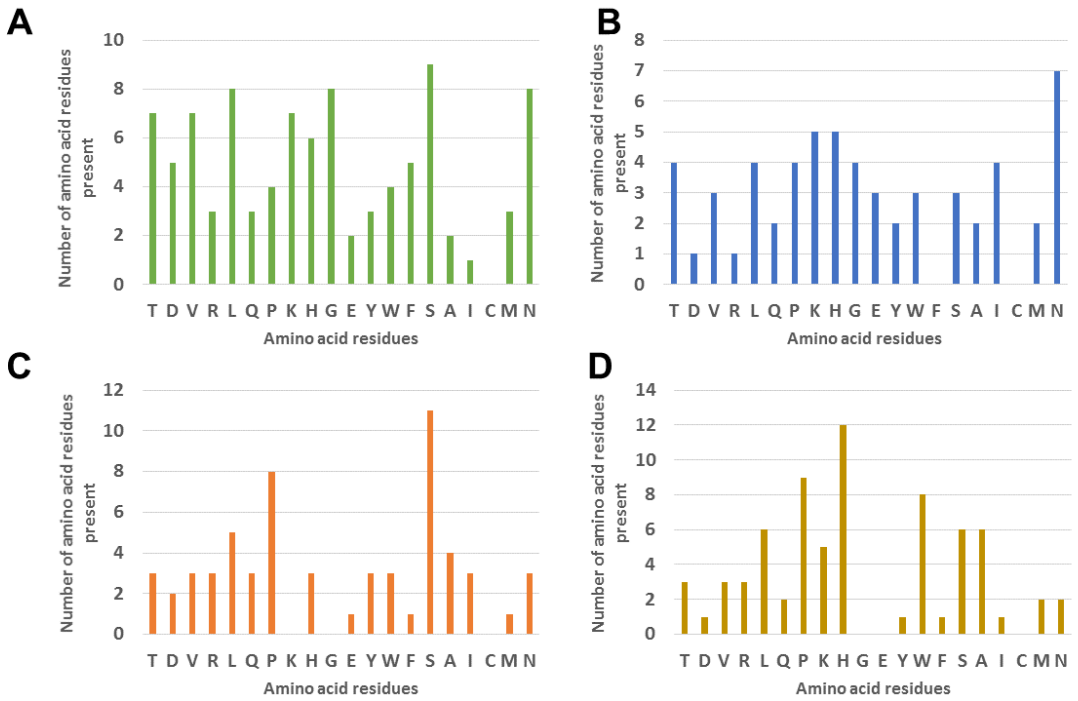

Figure 23: Composition of amino acids in peptide sequences. **A**: linear 7-mer library **B**: disulfide-constrained 7-mer library, **C**: linear 12-mer library, **D**: 12-mer peptides determined from DuPont

One would expect that the resulting adheson should be enriched in hydrophobic amino acids as PE is solely composed of hydrocarbons. From Tables 2, 3, and Figure 23, that appears not to be the case as there are various types of amino acids ranging from charged amino acids to hydrophobic amino acids. It is interesting to note in the linear 7-mer and 12-mer peptides, serine was present more frequently. Peptides isolated by DuPont also show variations in the amino acids residues in a similar manner to the isolated adhesons we obtained. The resulting sequences show that adhesons may interact with residual metals that are on the surface of PE, if metals/ metal ions are present due to the application of metal catalyzed polymerization techniques. It is also possible that the nature of the phage adheson-PE interaction is not purely sequence based, but a mixture of peptide sequence and geometric effects on the surface of PE. The PE surface is

not expected to be a smooth planar surface but likely contains pores that may allow for the binding of phage adhesons to occur. It was reported very recently that 100 wax moths *Galleria mellonella* were able to degrade plastic bags with 92 mg loss that were composed of PE[118]. While the mechanism of PE breakdown by the wax moth is currently unknown, it is possible that wax moths may have exterior structures that consist of sequences from the determined adhesons to bind to PE.

In conclusion, the isolation and determination of the sequences of peptides that exhibit affinity towards PE were successfully accomplished. It was shown that it is indeed possible to isolate bound phage to PE surfaces. While peptide consensus sequence motifs were not found, the isolated phage adhesons can provide some insight into the nature of the non-covalent interactions between the phage adheson and the PE surface and further characterization of the phage adheson and the PE resins themselves are presented in Chapter 3.

Chapter 3: Characterization of Phage Adhesons and PE

3.1 Characterization of Phage Adhesons: Enzyme-linked Immunosorbent Assay

While there are different approaches to the detection of phage binding to a molecule or surface, the enzyme-linked immunosorbent assay (ELISA) is utilized very often in phage display related experiments[110]. ELISA is a technique that allows for the detection and quantification of antigens such as small molecules bound to phage with an enzyme-conjugated antibody that produces a chromogenic product as the attached enzyme reacts with an enzyme substrate. ELISA as a method has found applications in many fields ranging from medical diagnostics to food science[119,120]. ELISA takes advantage of an antibody's specific affinity for its antigen. The method can detect picomolar to femtomolar concentrations of the antigen of interest in a mixture as the absorbance of the chromogenic product is proportional to the amount of the antibody-antigen complex[121].

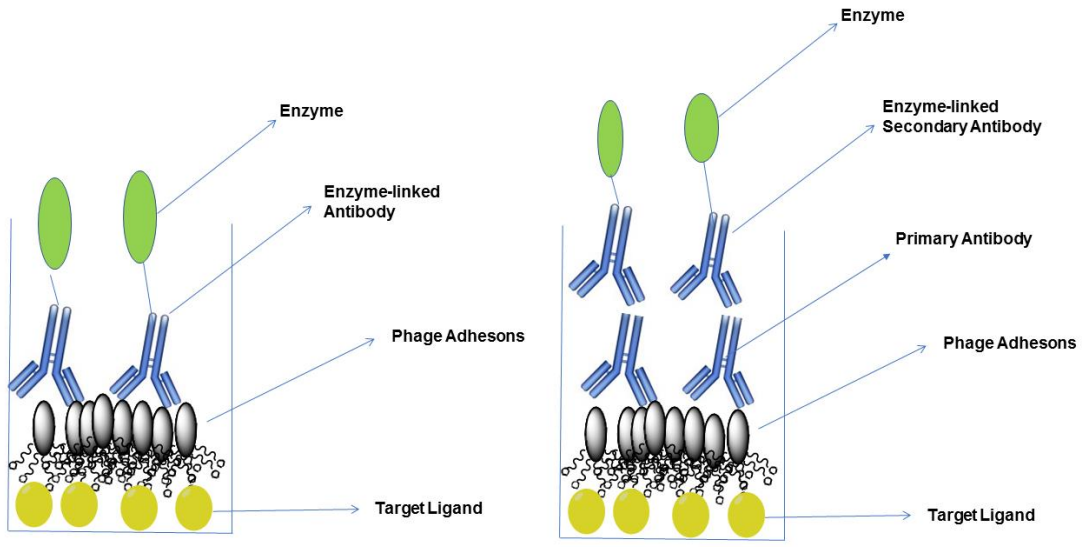

Figure 24: General scheme of direct (left) and indirect (right) ELISA-based assays[122]

In phage-based ELISAs, direct and indirect methods (shown in figure 24) are often done[61,69]. Direct ELISA involves the detection of the antigen (usually a phage coat protein) with an enzyme-conjugated antibody, whereas indirect ELISA involves the detection of a primary antibody that is bound to the antigen (phage coat protein) with an enzyme-conjugated secondary antibody[122]. In addition to the binding studies of the phage adhesons using the ELISA methodology, PE resins themselves were analyzed employing electron microscopy and energy dispersive X-ray spectroscopy.

3.2 Characterization of the PE Structure and Surface: Environmental Scanning Electron Microscopy and Energy Dispersive X-ray Spectroscopy

From the results of the phage biopanning experiments against the various PE samples that were presented in Chapter 2, there were no obvious repeated peptide sequence motifs to be found among the displayed peptides that could lead one to conclude the existence of a common sequence specific for PE binding. The first approach to analyzing the PE surfaces was made by using the technique of scanning electron microscopy (SEM). SEM allows for the visualization of the surface of the material and its topography[123]. Similar to transmission electron microscopy, SEM uses a source of electrons that is scanned across the sample in a raster scan pattern. The images are generated by the detection of secondary electrons, backscattered electrons and Auger electrons produced from the incident electron beam[124]. As PE resins are not conductive, environmental scanning electron microscopy (ESEM) can be used in place of conventional SEM. ESEM differs from conventional SEM in that samples in ESEM can be put under a gaseous environment which dissipates the charge generated from the incident beam on the surface of the

insulating materials. From the resulting phage adheson sequences, it was suspected that residual metals might be present on the surface of some of the PE resins due to the presence of charged amino acids in the adheson sequences which might interact with these surface metals, resulting in a contribution to binding. The technique of energy dispersive X-ray spectroscopy (EDX) was used to detect the presence of metals on the surface of the PE resins. EDX is first done through the generation of x-rays upon colliding with the sample of interest from the beam of electrons or x-rays[125]. As the detected x-rays' energy is directly proportional to the atomic number, it allows for the detection of elements in a sample[126]. The advantage of using EDX is that it allows for both quantitative and qualitative analysis along with the fact that EDX instruments are often coupled to SEMs[126]. The disadvantage comes from the fact that the resolution of the EDX spectrum is dependent on the sample thickness as there are more interactions that lead to a change in the direction of electron path which then broadens the average diameter of the electron beam[126]. EDX is still of interest for surface metal analysis as the signal for carbon should be much lower than any metals that may be present on the surface. Hence a metal should still be detectable despite the thickness of the PE resin. Even though SEM is a powerful technique for visualization of the surface, it does not give any information at the molecular level. For example, it is impossible to determine the effect of α-olefin branches on the PE resin with SEM. Modeling the structure of a theoretical PE surface was investigated using computer molecular modeling to contribute to increasing our understanding of PE surfaces.

3.3 Characterization of the PE Structure and Surface: Computational Modeling

With computers and software becoming more efficient and powerful, computational techniques can serve as valuable assets in the investigation of materials science as they allow for the detailed analysis of systems which can be theoretically assembled and which may be

impossible to investigate in a traditional laboratory setting or through existing instrumentation[127]. The motivation for modeling a material comes from the ability to link theoretical results to the experimental results and to improve current existing materials[127]. Computer modeling has found application in the study of polymers ranging from modeling the crystallization of polymers to the complexities of gold-polymer composite materials[128,129]. A preliminary attempt to model PE structure at a molecular scale was undertaken by modeling a PE cell employing just ethylene homopolymers. Another PE cell was modeled which contained heteropolymers created by computationally polymerizing a α-olefin and ethylene. Previous work on modeling PE to predict melt dynamics and phase transitions have been reported, however we wished to build an amorphous PE cell in order to obtain a simplistic model of a PE surface for our own review which could be manipulated in three dimensions.[130–132]

3.4 Phage-based Fibers and Thin Films

Fibers are utilized in various fields of industry: from the textile industry, with the fabrication of everyday clothing, to the military industry with the fabrication of Kevlar™ for bulletproof vests that are composed of synthetic and natural sources[133]. There has been an intense interest in the fabrication and modification of fibers that possess multiple functionalities from improving the flame retardancy of a textile to incorporating anti-microbial properties onto a textile[134,135] Fibers are composed of synthetic or natural polymers; however, the synthetic and natural polymers often lack reactive functional groups for the modification or fabrication of functional fibers to occur. The fibers are often grafted or reacted with harsh chemicals to incorporate functional groups. The limitations of aforementioned methods could come from the fact that the base synthetic polymer could have trouble reacting upon the introduction of the

chemicals due to its limited reaction selectivity[134]. The motivation for a functional fiber leads to the fabrication of fibers that are entirely composed of M13 units[134,136,137]. Biofibers made from M13 can be advantageous as they have various functional groups that arise from the solvent-exposed region (figure 25) of the major coat protein pVIII.

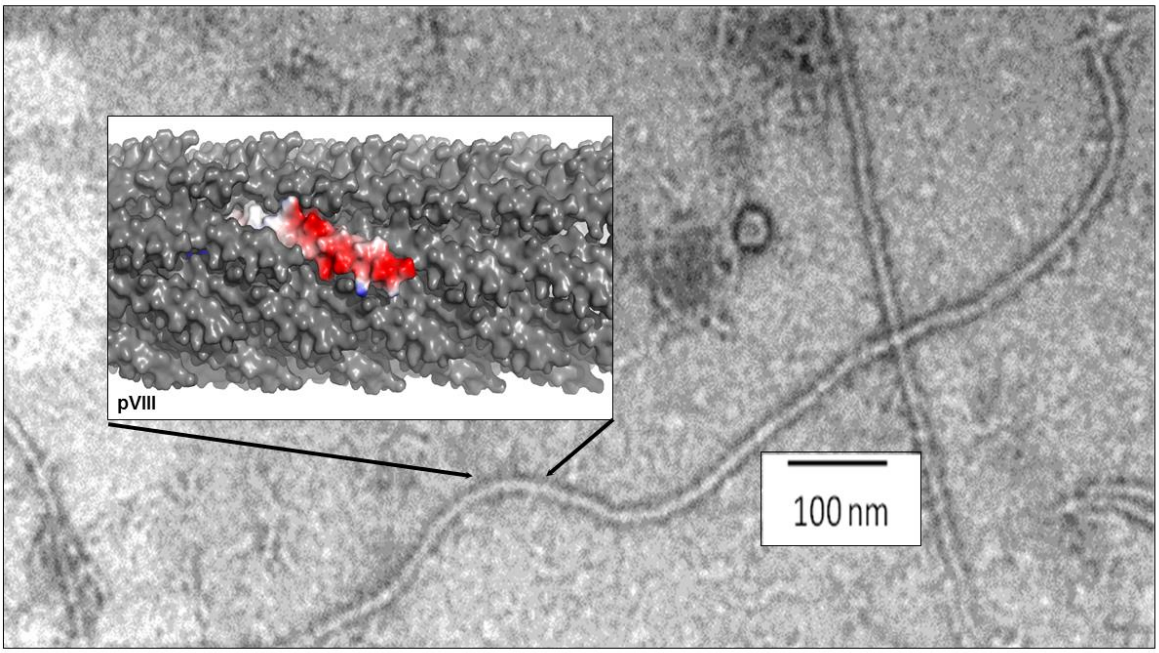

Figure 25: Transmission electron micrograph of M13 (The crystal structure (PDB: 1IFJ in subfigure shows the solvent exposed part of pVIII coat protein). T. Urquhart (Honek laboratory)

M13 phage are also advantageous in that chemical functional groups can be genetically programmed to be expressed on pVIII coat proteins, and they are readily accessible through commercially available chemical reagents[134,137]. The M13 phage fibers were reproduced from the methods of Belcher and her co-workers[134] as a starting point and then we attempted to fabricate M13 phage-based thin films.

3.5 Materials and Methods

3.5.1 Materials

Escherichia coli K12 ER 2738 (New England Biolabs, Ipswich, MA., USA) was used in the preparation of ELISA phage adhesons and large-scale amplification of wild-type M13KE. 96 microplate wells (Greiner Bio-One-VWR, Mississauga, ON., Canada), bovine serum albumin (BioShop Canada, Burlington, ON., Canada), anti-M13 antibody-hrp (Abcam, Cambridge, UK), 2,2'-Azino-bis (3-ethylbenzothiazoline-6-sulfonic acid) diammonium salt (ABTS) (Sigma-Aldrich, Oakville, ON., Canada), H_2O_2 (Sigma-Aldrich, Oakville, ON.), sodium citrate (Spectrum Chemical Mfg. Corp., Gardena, CA.) were used in the direct ELISA. SEM pin stub (Soqulec Ltd., Montreal, QC., Canada) was used in the ESEM.

3.5.2 Preparation of ELISA Phage Adhesons

An overnight culture (5 mL) of *E. coli* K12 ER2738 (New England Biolabs, MA., USA), which had been grown in LB media (10 g/L tryptone,5 g/L NaCl and 5 g/L yeast extract) solution, was diluted to a ratio of 1:100 with LB media solution. Phage supernatant from the replicative form DNA preparation (5 µL) was added to the 20 mL of diluted *E. coli* culture, and the resulting solution was incubated with shaking (200 rpm) for 4.5 hours at 37 °C. The solution was then centrifuged at 12000xg for 10 minutes at 4 °C. The supernatant was precipitated with a solution of 20 % PEG-8000/2.5 M NaCl (4 mL) followed by incubation of the solution overnight at 4 °C. The cloudy solution was centrifuged at 13500xg for 20 minutes 4 °C and the sedimented phage was resuspended in 1 mL of phosphate-buffered saline (PBS) (137 mM NaCl, 2.7 mM KCl, 100 mM Na_2HPO_4, and 1.8 mM KH_2PO_4). The resuspended solution (1 mL) was centrifuged in a benchtop centrifuge at 3834xg for 5 minutes at 4 °C to sediment any residual

cells. The supernatant was transferred to a new Eppendorf tube, and the supernatant was precipitated by the addition of 200 µL of a 20 % PEG-8000 / 2.5 M NaCl solution and the resulting solution was placed on ice and let to stand for one hour. The solution was then centrifuged at 13225xg for 20 minutes at 4 °C. The phage sediment was resuspended in 50 µL of PBS (137 mM NaCl, 2.7 mM KCl, 100 mM Na_2HPO_4, and 1.8 mM KH_2PO_4). The concentrated phage solution was titered as described in Chapter 2 of the thesis. An average of between 5 to 40 plaques at 10^{-12th} dilution were usually observed.

3.5.3 Direct ELISA

To describe the method of the experiment, 96-well microwell plate wells were coated by incubating 320 µL of 5 % bovine serum albumin (BSA) solution in 0.1 M $NaHCO_3$ pH 8.6 into each well used in the assay overnight at 4 °C. The following day, the wells were washed three times with PBS (137 mM NaCl, 2.7 mM KCl, 100 mM Na_2HPO_4, and 1.8 mM KH_2PO_4) with 0.3 % Tween®-20 for the disulfide-constrained phage adhesons and 0.5 % Tween®-20 for linear 12-mer phage adhesons. The wash step in ELISA is done by incubating the wash buffer filled microplate wells for 10 minutes on a benchtop rotator (100 rpm). The phage solutions (initial concentration of [HSDK-1] = 1.6×10^{14} pfu/mL and biopanned and amplified up to 3rd round, [HSDK-2] = 5.0×10^{15} pfu/mL, [HSDK-3] = 5.0×10^{14} pfu/mL and biopanned and amplified up to the 4th round, and [M13KE wild-type] = 4.0×10^{15} pfu/mL) were diluted to $1.0 \times 10^{13} \frac{\text{pfu}}{\text{mL}}$ in 1 mL and two pellets of polyethylene resins were added into the BSA coated wells. Seven droplets of phage solution were added to the corresponding microplate wells by glass Pasteur pipettes. For the blank solution, 200 µL of PBS were dispensed by a micropipette. The phage

solution was removed with glass Pasteur pipettes after incubating the solution for 1 hour, and the wells were washed with 200 μL of PBS and PBST 5 times by incubating the wash solution for 10 minutes on a benchtop rotator for each round of wash. Anti-M13-horseradish peroxidase (HRP) (Abcam, Toronto, ON.) solution (200 μL of 2 μg/mL working solution) was added to each well and incubated for 1 hour at room temperature with shaking in a bench top rotator (100 rpm). The unbound anti-M13-HRP was removed with glass Pasteur pipettes, and each well was washed with 200 μL of PBS and PBST to its corresponding wells five times by incubating the wash solution for 10 minutes on a benchtop rotator (100 rpm) for each round. The substrate solution containing 0.4 mM 2,2'-Azino-bis (3-ethylbenzothiazoline-6-sulfonic acid) diammonium salt (ABTS) and 0.05 % in 50 mM sodium citrate pH 4.0 (200 μL) was added to the microplate wells and incubated for 20 minutes at room temperature with shaking (100 rpm). The PE pellets were removed, and the absorbance at A_{405} was measured using a spectrophotometer (SpectraMax M5, Molecular Devices, Sunnyvale, CA.).

3.5.4 Environmental Scanning Electron Microscopy

PE resins were put onto a carbon tape on an aluminum stand. As a comparison, PE resins were also sputter coated with gold. The environmental SEM (ESEM) (FEI Quanta FEG 250 ESEM, Watlab, Waterloo, ON.) was used in all SEM experiments. The EDX detector (10 mm2 SDD detector X-act) (Oxford Instruments, U.K.) is coupled to the ESEM instrument. The electron gun was set to 10 kV for visualization and 20 kV for EDX analyses. The scanning electron micrographs were taken at a low vacuum condition, and the EDX analyses were done at a high vacuum condition.

3.5.5 Computational Methods for PE Surface Modeling

The program that was used to model a hypothetical surface of PE was Maestro Materials Science Suite (Schrödinger, New York City, NY.). To model the high-density PE surface without branches, ethylene was used as a monomer, and 200 ethylenes were used to create one chain of polyethylene. One hundred chains of PE were used to construct an amorphous cell of PE at a density of 0.9 g/cm^3. To model a PE resin containing a branched structure, the co-monomer 2-butene (figure 26) was chosen with 5 % probability of branching for every ten units of ethylene monomer that were used to create a chain of branched PE for the surface. The number of generation of chains was set to a value of 10.

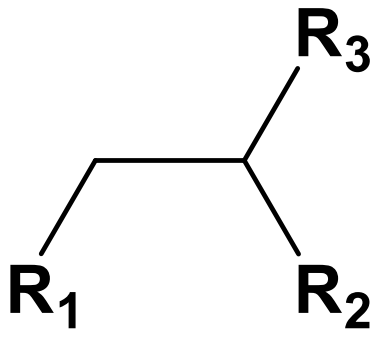

Figure 26: "2-Butene" which was selected as a copolymer. R_1 represents the head group, R_2 represents the tail group, and R_3 represents the branch point of the PE chain. Note: R_1, R_2, and R_3 do not represent alkyl groups, but rather "carbons" to form 2-butane that is required by the software program in its building routine and double bond is assumed to be added by the software.

The amorphous cell for the branched PE was then assembled in a similar manner to the unbranched PE amorphous cell where 100 chains of branched PE were used to form the cell. All other values in the program were set at their default values.

3.5.6 Large-scale Amplification of Wild-type M13KE

An overnight culture of *E. coli* K12 ER 2738 (10 mL) was grown in 1 L of LB media solution containing 45 μmol of tetracycline. It was incubated in a shaker (200 rpm) at 37 ℃ for 2 hours. After 2 hours, M13KE solution (1 mL of 1×10^{11} pfu/mL) was used to infect the culture, and the infected culture was incubated in a shaker (200 rpm) at 37 ℃ overnight. The culture solution was centrifuged at 3000xg for 20 minutes at 10 ℃ and collected 800 mL of the phage-containing supernatant to a sterile flask ensure no residual cell pellets are transferred to the flask. The supernatant was precipitated with 200 mL of 20 % PEG-8000 / 2.5 M NaCl (PEG/NaCl) and let to stand overnight in a fridge. The precipitated solution was centrifuged at 13500xg for 20 minutes at 10 ℃, and the sedimented phage was resuspended in 2.83 mL of PBS (137 mM NaCl, 2.7 mM KCl, 100 mM Na_2HPO_4, and 1.8 mM KH_2PO_4) for each centrifuge bottle used (for 1 L of infected culture, total volume of PBS to use should be 17 mL). The resuspended phage was transferred to a new centrifuge bottle, and it was centrifuged at 12074xg for 15 minutes at 10 ℃ to sediment any residual cells. After collecting the supernatant (17 mL), the solution was precipitated with 4.4 mL PEG/NaCl, and it was left to stand overnight in the fridge. The cloudy solution was centrifuged at 13500xg for 20 minutes at 10 ℃, and the sedimented phage was resuspended with 500 μL PBS (137 mM NaCl, 2.7 mM KCl, 100 mM Na_2HPO_4, and 1.8 mM KH_2PO_4).

3.5.7 Fabrication of M13 Phage Fiber and Thin Film

The concentrated phage solution (500 μL) from the large-scale amplification was centrifuged at 13225xg for 20 minutes at 4 ℃. After removing the supernatant, 10 μL of bis-Tris Propane buffer (10 mM bis-Tris Propane and 137 mM NaCl at pH 9) was added to aid the transfer of the concentrated phage solution into the syringe. Phage solution was transferred to the

syringe by slowly pipetting into the bottom of 100 μL syringe 20 μL at a time. As it is pipetted, the plunger of the syringe is concurrently pulled back slowly to receive the phage. The syringe equipped with a 33 gauge sized needle is submerged into a crosslinking reagent (8 % aqueous glutaraldehyde in 10 mM bis-Tris propane and 137 mM NaCl pH 9), and the plunger is pressed gently. At this point strings of phage should be seen extruding out of the needle to form a fiber. After the extrusion step, the fiber is incubated in the crosslinking reagent for 1 hour to let it fully crosslink. The fibers are transferred to MQ-H_2O for storage. For the fabrication of M13 phage thin film, the syringe filled with the phage solution is extruded dropwise into a droplet of the crosslinking reagent (8 % aqueous glutaraldehyde in 10 mM bis-Tris propane and 137 mM NaCl pH 9). Same sets of the experiment were done, but instead of 8 % aqueous glutaraldehyde, 1 %, and 30 % aqueous glutaraldehyde was also used. The droplet of phage solution is incubated in the droplet of the crosslinking reagent for one hour to have it fully reacted. The thin film was transferred to MQ H_2O for storage.

3.5.8 Characterization of M13 Fiber: Uniaxial Tensile Testing

The fabricated fibers were removed from MQ H_2O to let them dry. The fiber is dry when it shrivels and becomes slightly smaller compared to fibers in solution. The ends of the fiber were glued onto an aluminum alloy plate that was 1 inch in width and 0.5 inches in height with cyanoacrylate glue. Two aluminum alloy plates (Al6061) were glued at the same top and bottom of the fiber to sandwich the ends of the fiber. This allows for the fibers to be held by the grips in the tensile tester (Instron 5548 micro tester, Norwood, MA., USA). The fibers + plates were equipped with the vice grips of the tensile tester, and the sample was run until failure (sample should break in half at failure) with 10 N load cell. As a control, a strand of fishing line (with break strength of 10 lbs) was used.

3.6 Results of ELISA Assays

First, the disulfide-constrained clone of HSDK-1 was analyzed using the ELISA method along with the wild-type M13 phage clones as a control and as a comparison. Several optimizations were made to the assay and included varying the input titer of the phage clones, and changing the use of micropipettes to glass Pasteur pipettes due to problems that ranged from non-specific binding of antibodies/phage to wells in the microplate. The chosen concentration of 0.3 % for HSDK-1 and 0.5 % for linear 12-mer phage adhesons (data not shown) for the Tween®-20 are from the last rounds of biopanning as indicated in chapter 2. The results of these ELISA assays are shown in Figure 27.

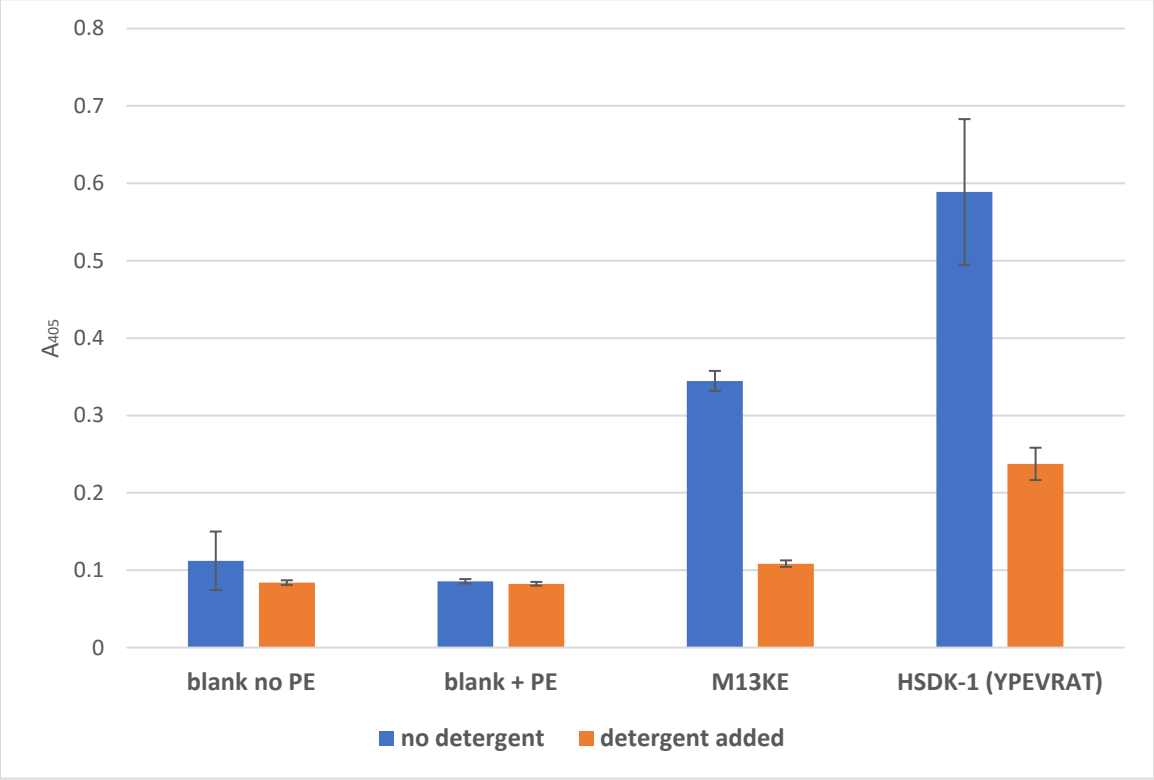

Figure 27: ELISA plot of HSDK-1, where n = 3 for blank + PE and HSDK-1 and n=2 for M13KE and blank no PE. Detergent used in this experiment was 0.3 % Tween®-20

As shown in figure 27, the disulfide-constrained clone exhibits a higher absorbance in the ELISA-based assays when compared to the wild-type and the blank sample, although wild-type M13 does appear to exhibit some non-specific interactions with the PE sample. It is possible that in addition to the adheson-PE interaction, some pVIII coat proteins may show some interaction to PE resins as phage solution is introduced to the PE. This may lead to wild-type M13 exhibiting interaction to PE resins, as evident from figure 27. There were two blank wells in which one well did not contain PE resins and the other well did contain PE. The two blank wells were negative control experiments confirm that the absorbances generated were only from enzyme-conjugated antibody-phage complex formation and not from free antibodies that were non-specifically bound to the PE resins. The wild-type M13 (M13KE) was also run in parallel to the HSDK-1 assays to compare the relative binding affinity between the two phage clones. The assay was done in the absence and the presence of Tween®-20 in the wash buffer. This was the case as previous studies by Hakami and coworkers showed that the use or absence of Tween®-20 could lead to complications[138]. When Tween®-20 is used in the ELISA assay, non-specific background binding was shown when compared to samples lacking Tween®-20. In the absence of Tween®-20 in the ELISA assays, increases in signal-to-noise ratios were observed. The assay was run in the presence and in the absence of Tween®-20 in the wash buffer during the wash step to determine if similar effects were observed in our experiments. Analysis of the results presented in figure 27 indicated that samples washed with Tween®-20 in the wash buffer have lower absorbance signals compared to the samples that were washed with just PBS. The results employing Tween®-20 were expected as Tween®-20 removes phage clones with low-affinity binding from the target of interest. Mean signal-to-noise ratios for Tweenless samples were approximately 10.5. Mean signal-to-noise ratios were calculated as shown in equation 1[139].

Equation 1: Mean signal-to-noise ratio[139]

$$\text{mean SNR (HSDK} - 1) = \frac{MeanA_{405}}{Standard\ Deviation\ of\ A_{405}\ of\ HSDK - 1}$$

When compared to the samples that had Tween®-20 in the wash buffer, the mean signal-to-noise ratio was 15.8. This result is consistent with the thought that the HSDK-1 adheson is binding to PE with little non-specific binding to the microplate well. It is important to note that phage clones that have undergone PEG precipitation can bind to Tween®-20 in the wash buffer which can remove the phage units that are bound to the target[138]. As PEG is hydrophobic, it would be feasible for phage binding to occur with residual PEG in the amplification step. The effect from the PEG precipitation may explain the result shown in figure 27 as samples in the absence of Tween®-20 had a much higher signal compared to the samples that were washed with PBST.

ELISA assays were also undertaken for the isolated 12-mer M13 clones. As shown in figure 28, the results were less clear compared to the data for the HSDK-1 clones. The concentrations in HSDK-1, 2, and 3 were kept constant, although the antibody solution used in HSDK-2 and 3 is from a different supplier (Santa Cruz Biotechnology, Dallas, TX.). Controlling for the different antibody concentrations from different suppliers, abnormal results are seen in figure 28. The abnormal result most likely originated from an excessive nonspecific binding of the antibody as evident from the blank lacking the PE resin well.

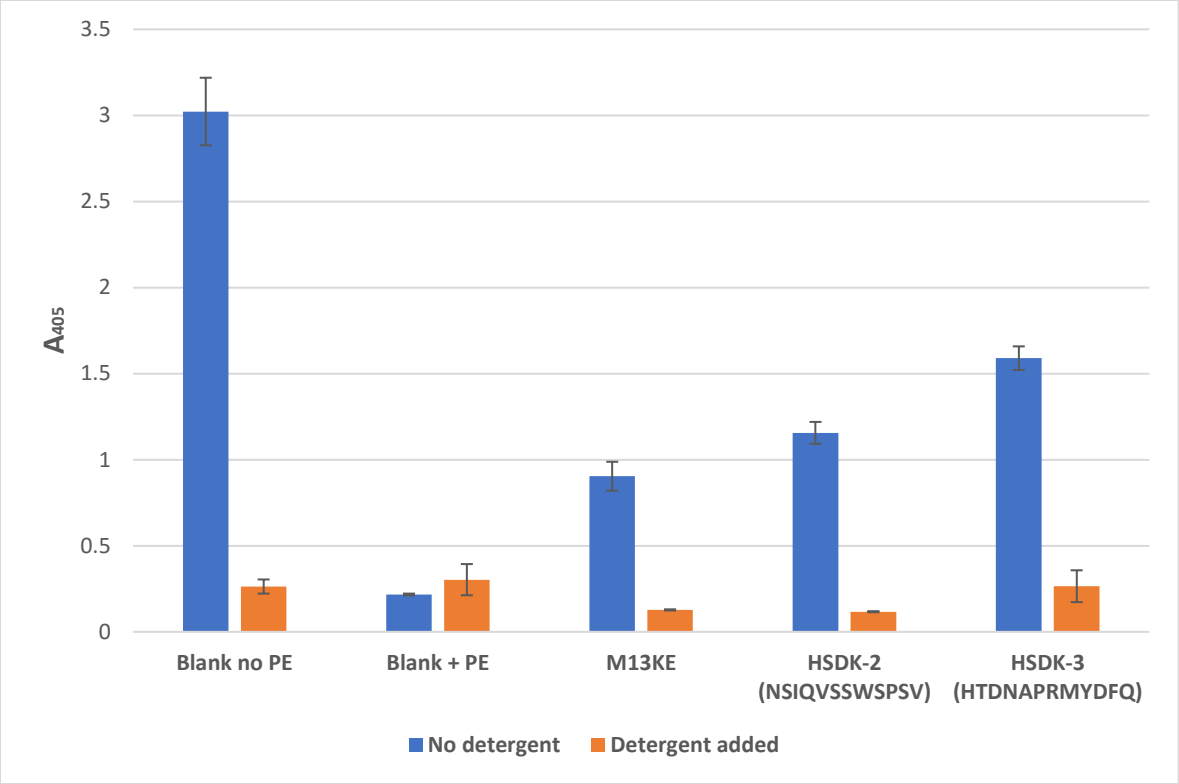

Figure 28: ELISA plot for the 12-mer clones. The detergent was 0.5 % Tween®-20 and n = 2 for all samples in this plot

3.7 Results of Environmental Scanning Electron Microscopy and EDX

The scanning electron micrographs are shown on figure 29. It is noted that at high vacuum it was very difficult to record an image due to the charge build-up effect that arises from a non-conductive sample such as the PE resin as shown in the electron micrograph in EDX spectra (figure 32)[140]

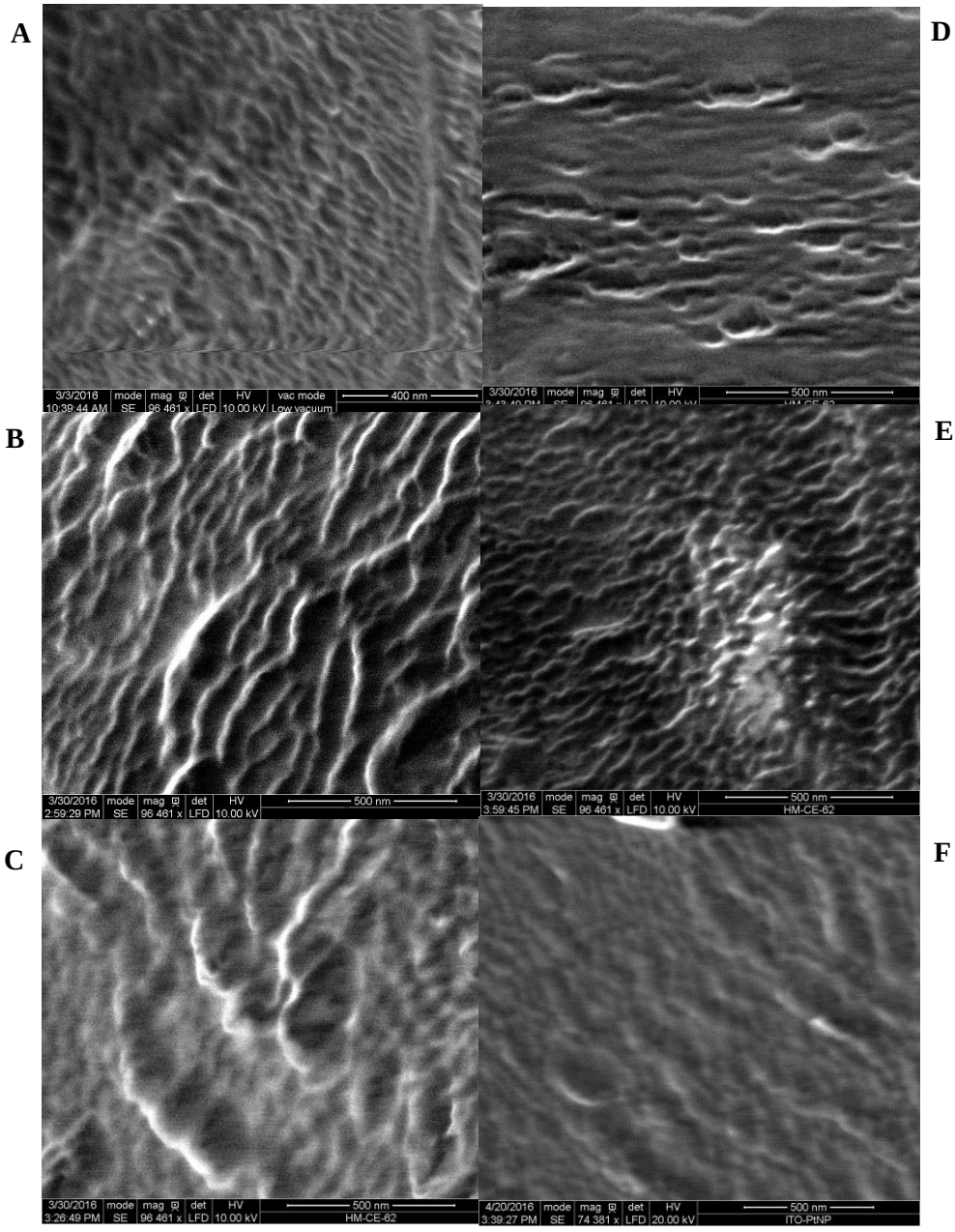

Figure 29: Scanning electron micrograph of PE resin surfaces. A: Ziegler-Natta catalyzed high density PE B: Ziegler-Natta catalyzed linear low density PE C: AD60 D: BA46 E: Exceed 1012KA F: Exceed 1018KA

The surfaces detected for the array of PE samples (figure 29) utilized in this research, are not smooth, but rather have pores, crevices and surface defects. These surface defects may be structures that are important or at least contribute to phage-PE binding affinity interactions. The approximate diameter of the pores in the six PE resins that were studied varied from 56 nm to 194 nm. Even though the depths of the pores are currently unknown, the pores and defects on the surface could still contribute to the binding of the phage adheson as the diameter of the pores is large enough to fit the phage adheson vertically. PE resins that were sputter coated with gold showed that the surface did not show any pores but cracks that could have formed from the gold covering the crevices. A comparison of naked PE surface and the gold-covered surface is shown in figure 30.

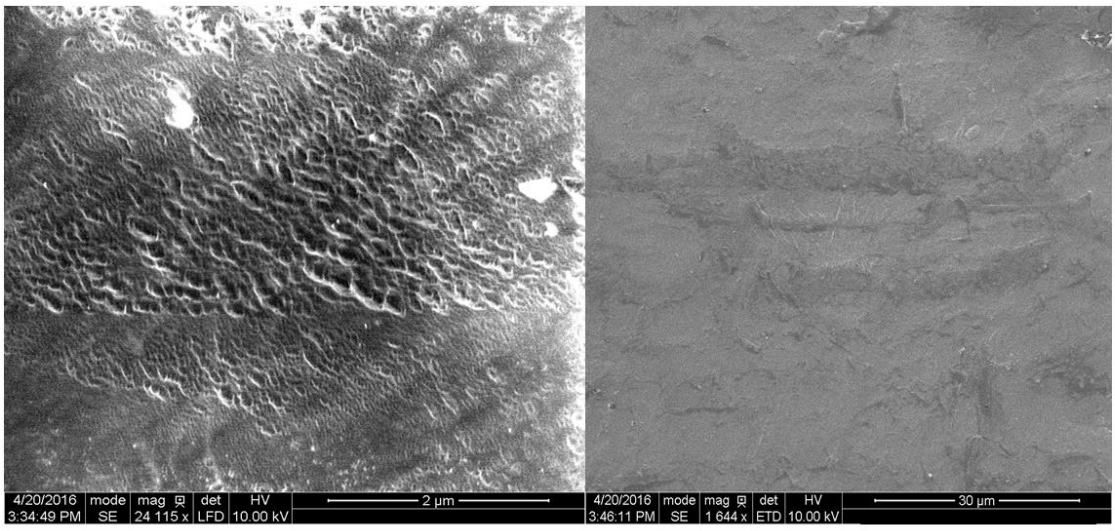

Figure 30: Comparison of naked PE surface (on left) and gold-covered PE surface (on right)

A comparison was made to ensure the pores and crevices are indeed from the production of the PE resin, not from the electron gun of the SEM. From the EDX results shown in figure 31, trace amounts of zinc were shown in a Ziegler-Natta catalyzed HDPE and aluminum is shown in Ziegler-Natta catalyzed LLDPE, BA46, and 1018KA resins.

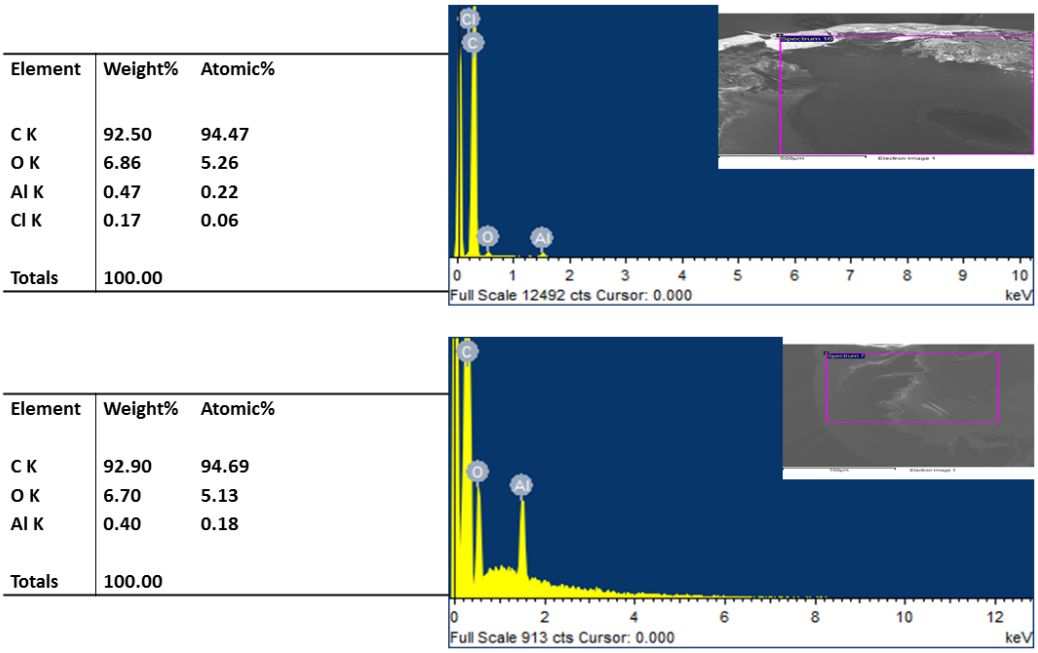

Figure 31: EDX spectra of metallocene 1018KA PE and Ziegler-Natta catalyzed LLDPE

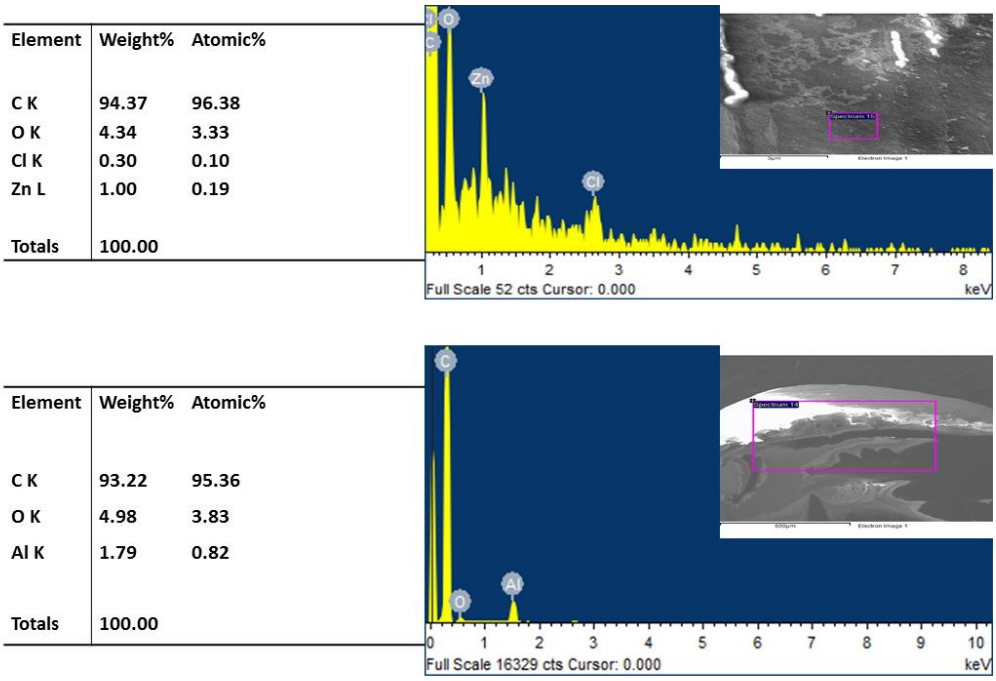

Figure 32: EDX spectra of Ziegler-Natta catalyzed HDPE and chromium catalyzed BA46 PE

After running additional EDX experiments on a different set of PE resins, it was concluded that metals were absent on the surfaces, which may indicate that only one or two resins out of a batch of PEs contain a meager amount of metals that is insignificant to the binding of phage adhesons as shown in figure 32, 33, and 34.

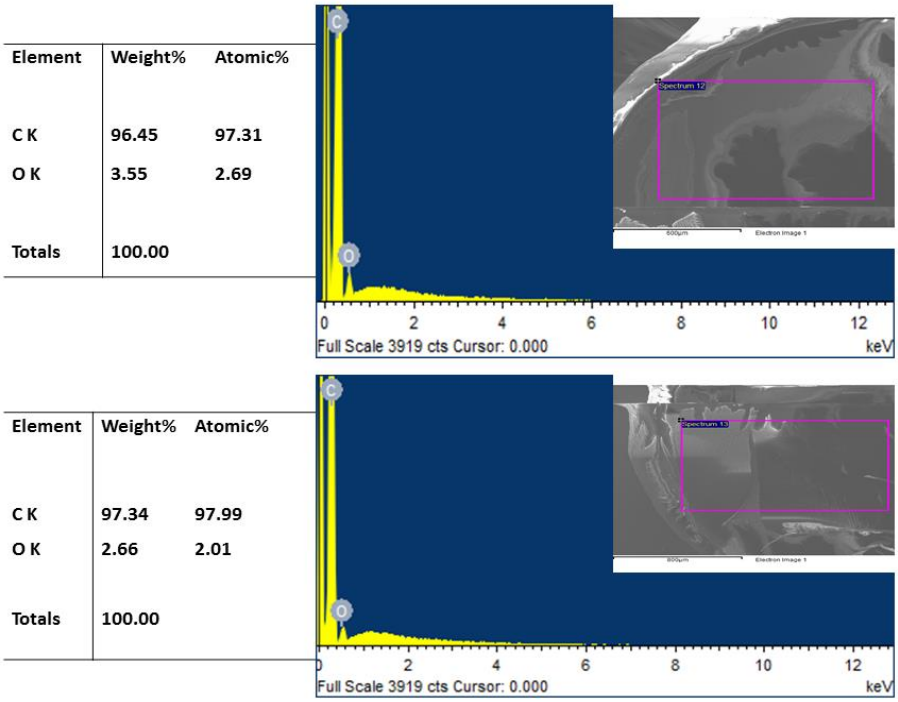

Figure 33: EDX spectra of chromium catalyzed BA46 resin at 2 different regions. No metals are present

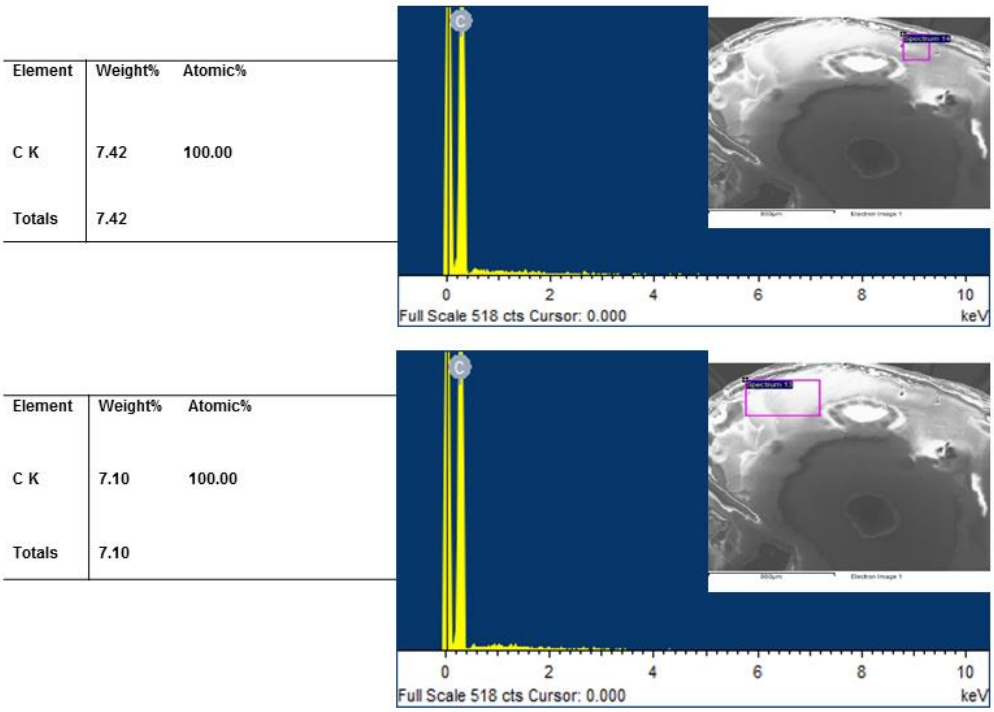

Figure 34: EDX spectra of Ziegler-Natta catalyzed HDPE resin at 2 different regions. No metals are present

It is also possible that PE resins that had an apparent metal present are a contaminant from the SEM stand and the signal for metal did not come from the resins. From the SEM results, insufficient information was given to the effect of branching on the geometric shape of the surface as both Ziegler-Natta catalyzed LLDPE and Ziegler-Natta catalyzed HDPE were structurally similar to each other. To further elucidate the effect of branching at the atomic and molecular level, computational modeling of the PE surface was attempted.

3.8 Preliminary PE Structure Modeling

An amorphous PE cell without any branches was successfully generated using the Schrödinger software alogrithms. Two hundred ethylene monomers were used to construct a chain that led to the assembly of a cell containing 100 chains, each chain containing 200 ethylene units as shown in figure 35 and 36. The PE resins from Imperial Oil are a copolymer of ethylene and hexene, which led to investigating the effect of branching on the PE structure.

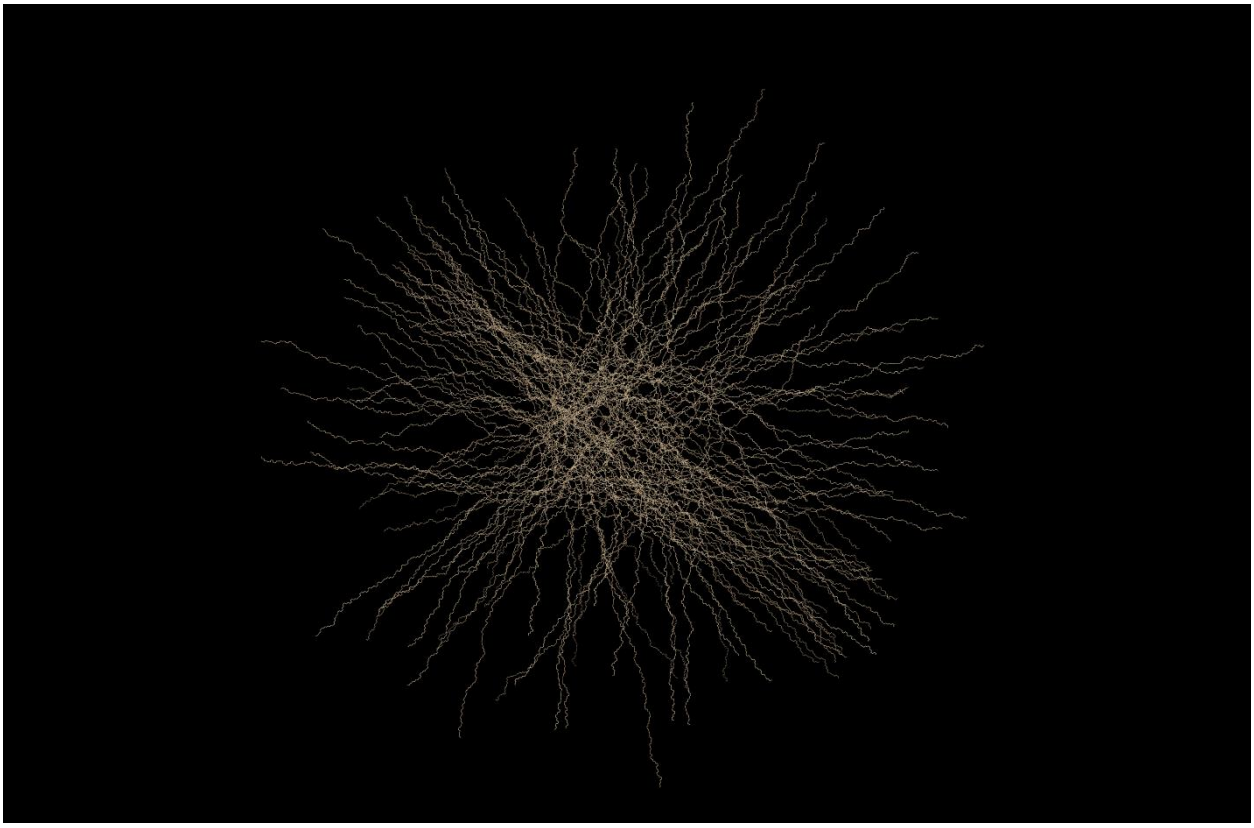

Figure 35: Branchless PE model

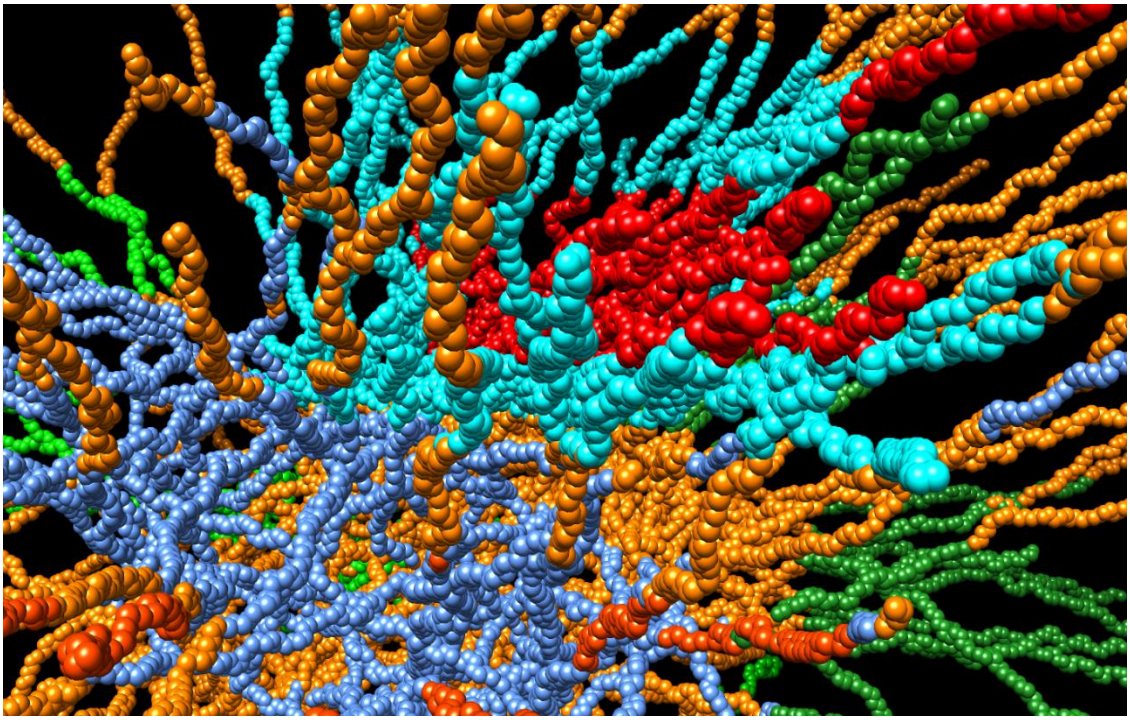

Figure 36: Branchless PE zoomed in to show the interweaved networks of PE chains

It is interesting to compare the results of molecular modeling with the model representation of the PE (figure 12) as the structure of the PE amorphous cell is not ordered in a specific arrangement. Branched PE cell was also successfully modeled using the Schrödinger software algorithms (figure 37). Similar to the branchless PE, interweaved networks of PE chains were shown (figure 37 and 38). The results from the molecular modeling of PE show that molecular representation of PE is a very complex process and that representation of PE such as the model shown in figure 12 is not the most likely representative of PE at a molecular level.

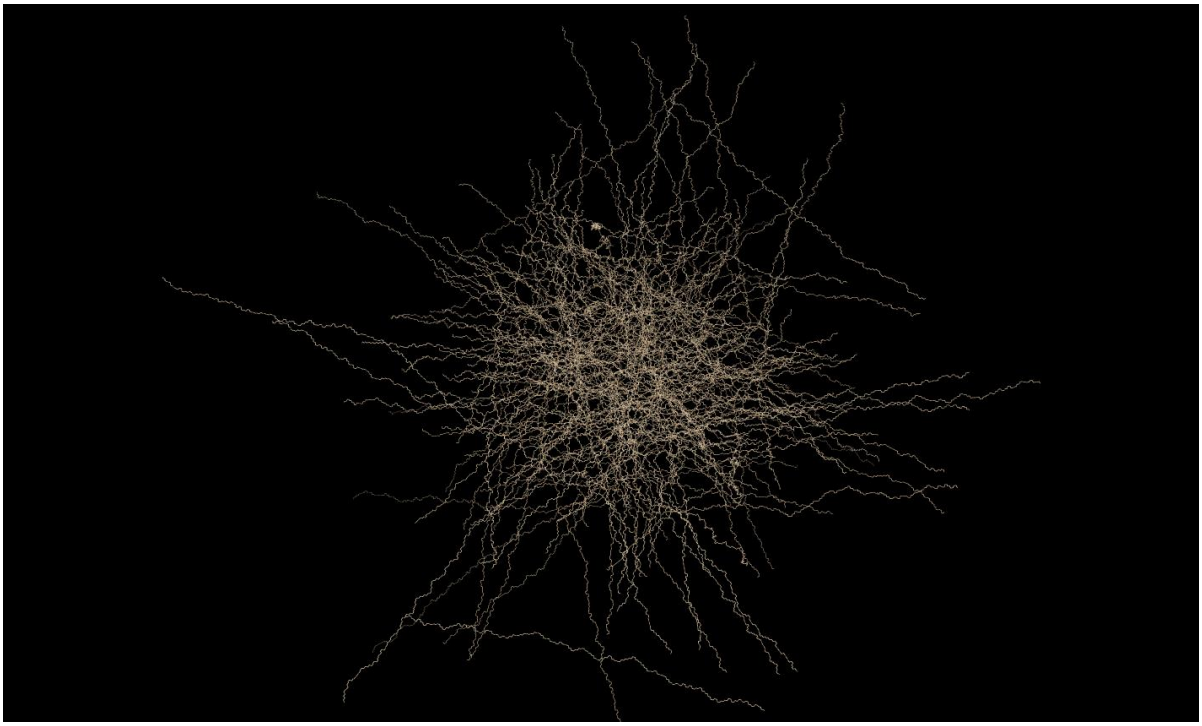

Figure 37: Branched PE model

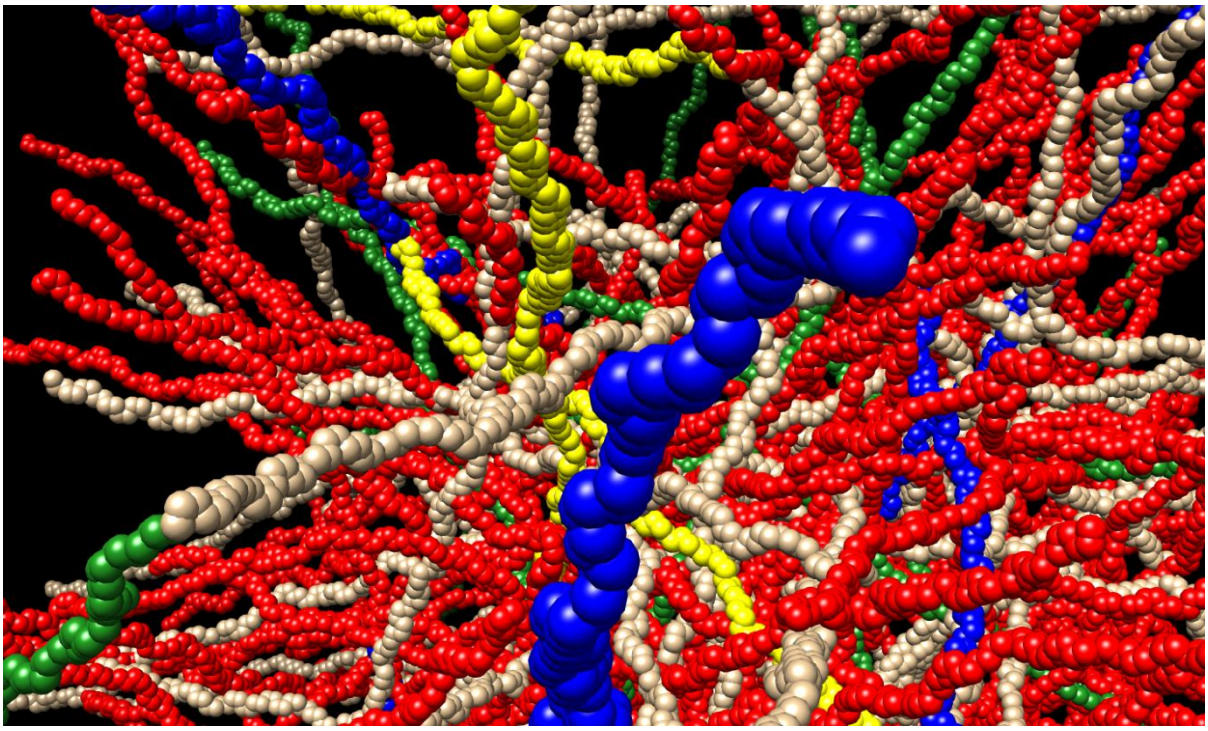

Figure 38: Branched PE model to show the interweaved network of PE chains

3.9 Result of M13 Phage Fibers and Thin Films

M13 phage fibers were successfully reproduced as shown in the top two images in figure 37. To see if varying the concentration of the crosslinking reagent led to a change in fiber strength, fibers were fabricated in three different concentrations as mentioned in materials and methods. The fibers at 1 %, 8 %, and 30 % aqueous glutaraldehyde behaved similar in which upon drying, all three fibers became smaller. They were also susceptible to fragmentation as they were being handled, showing that the concentration of the crosslinking reagent was not critical. The buffer of choice in making the crosslinking reagent was determined to be Bis-Tris propane (pH 9) to produce a solution pH which would increase the nucleophilicity of the lysine side chain on the M13. M13 phage is stable at pH 9 as the pH stability range for M13 is from pH 6 to 9[141]. An important aspect of the crosslinking success is that at high concentrations, phage particles form an ordered configuration[142] which likely assists in the reaction between the phage and the crosslinking reagent.

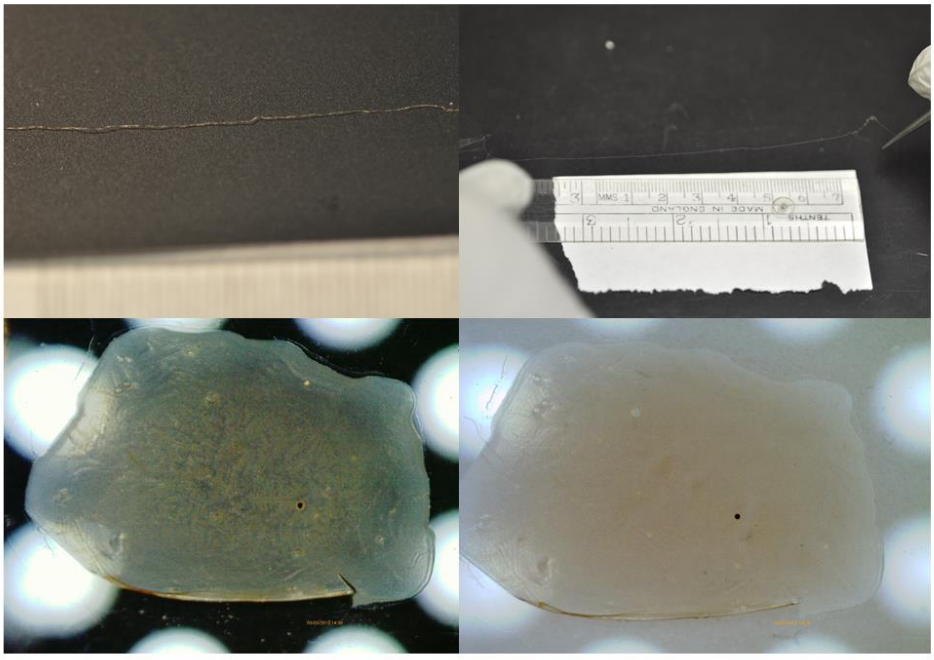

Figure 39: M13 phage fiber at the top and thin film at the bottom

3.9 Preliminary Result of the Tensile Strength Test

M13 phage thin films also behaved similar in which the concentration of the crosslinking was not critical in their behaviour. Uniaxial tensile testing was investigated for M13 phage fibers to measure the elastic modulus. There were some complications which arose from the preparation of the phage samples. The phage fibers have the tendency to fragment even upon handling with gentle care. This led to the fiber being shortened to the point where it was very difficult to equip the fiber + plate onto the tensile tester. The stress-strain curve for the fishing line and M13 fiber are shown in figure 38.

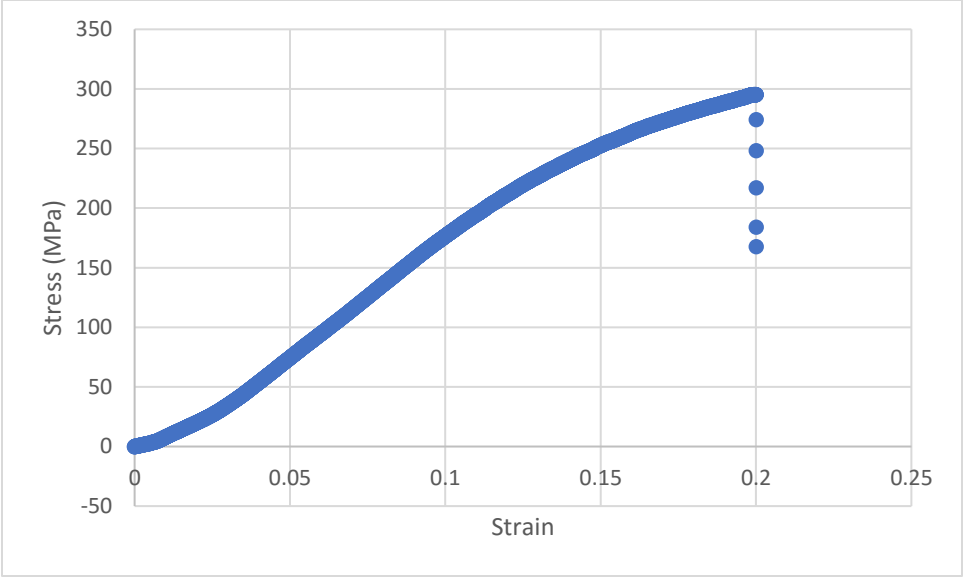

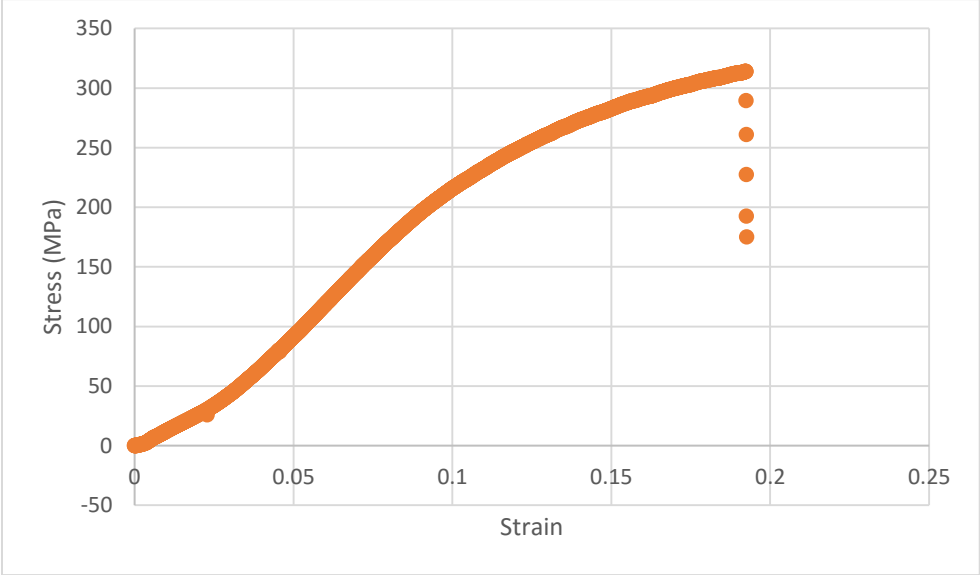

Figure 40: Stress-strain curve of fishing line (top in blue) and M13 fiber (bottom in orange)

As shown in figure 38, both fishing line and M13 fiber showed a similar result in which the estimate elastic modulus from the stress-strain curve was 2.51 GPa for M13 fiber and 2.07 GPa for the fishing line. While the elastic modulus comparables favourably to previously made M13 fibers[137], it was difficult to estimate the elastic modulus due to the unexpected non-linear-

like plot. The mechanical strength of M13 fiber has been determined in preliminary published studies to be similar to the mechanical strength of synthetic polymers such as Nylon[137].

Chapter 4: Summary and Future

4.1 Summary of Project

The objective of this project has been to determine if peptides exist that exhibit affinity towards the important industrial polymer polyethylene (PE). This work was to utilize commercially important PE types produced by a variety of catalytic methods. To date, the current thesis research has identified, through phage display techniques, various peptide sequences that exhibit affinity towards a variety of PE resins. The sequences of adhesons from the linear 7-mer library, while having some consensus sequences, were spread out on the amino acid residues that make up the adhesons. The sequences were a mixture of hydrophobic and polar amino acids. Similar results were seen with disulfide-constrained 7-mer and linear 12-mer libraries on the composition of the amino acids in the adhesion sequences. DuPont has previously reported the identification of a series of peptides that exhibit affinity towards ultra-high molecular weight PE tape[117]. No consensus sequences were identified within their own study nor were any of the DuPont sequences isolated in this current thesis research. This may be due to the different types of PE that were employed in these two studies.

The isolated phage adhesons, disulfide-constrained clone, HSDK-1, and linear 12-mer clones HSDK-2 and 3, were analyzed by enzyme-linked immunosorbent assays (ELISA) to determine their binding affinity to the targeted PE. It was determined by Hakami and coworkers that the use of Tween®-20 may alter the binding interactions as measured by ELISA, at least in their studies[138]. After accounting for the presence of Tween®-20 in our own experiments by running the experiments in the absence and presence of Tween®-20 in the wash buffer during the wash step, its presence was shown to have the opposite effect on affinity binding in our own

research compared to the work reported by Hakami and coworkers. Samples in the presence of Tween®-20 led to a lower signal than samples that were washed with PBS (no Tween®-20). It was also reported[138] that PEG might bind to M13 phage during the amplification step which could then lead to the phage being washed off their target when Tween®-20 is added to the wash buffer. While it is possible that some of the phage adhesons that bind with high affinity have washed off, the signals for HSDK-1 were higher than the wild-type M13 phage (M13KE), indicating that the adheson attached to the phage are truly bound tighter than the wild-type M13. HSDK-2 and 3 had some anomaly likely due to a combination of nonspecific binding of antibodies in both blank wells (with and without PE resins) and the same Tween®-20 effects that may have affected the HSDK-1 clone.

The surfaces of some of the PE samples were first investigated utilizing SEM-EDX to visualize the surface of the resins, which could aid in our understanding of PE surfaces, the target of our peptide binders. Analysis of the data indicated that the surfaces were covered with holes and pores along with the presence of a few crevices, which could trap the phage adhesons within them. EDX was also employed to analyze the PE surfaces to check for any residual metals on the surfaces which might interact with charged or metal chelating amino acids in the adhesons. A trace amount of zinc and aluminum were detected; however, most PE resins did not have any detectable surface metal(s), which would be consistent with the idea that these trace metals were likely present due to low level environmental contamination.

Computer modeling of a theoretical surface of PE was attempted to analyze the structure of PE at an atomistic scale. Analyses of the unbranched and branched PE models showed the presence of empty spaces and zones that possibly contribute to the macroscopic pores in the electron micrographs in chapter 3.

While there is preliminary evidence that some peptides exhibit affinity towards polymeric materials such as PE, there are some experiments that should either be investigated or optimized in the case of the ELISA assays.

A very high concentration of phage (10^{15} to 10^{16} pfu/mL) solution is used to prepare M13 fibers by extruding the phage solution into an aqueous crosslinking reagent with a syringe[134]. Phage thin films were also prepared with a very high concentration of phage at the same concentration as the fiber by introducing small drops of the phage solution to droplets of crosslinking reagent. The concentration of the crosslinking agent was not as critical as expected as crosslinking with 1%, 8 %, and 30 % glutaraldehyde all resulted in fiber fabrication. The mechanical properties of M13 fibers were characterized by employing a uniaxial tensile tester. The stress-strain curve, while it did not exhibit a proper linear region for determination of elastic modulus, was still estimated to have a similar value as reported in literature[137].

4.2 Future Work

With regard the ELISA assays utilized to quantitate the phage binding, it is important that the antibody concentration is optimized to properly analyze the remaining 12-mer phage adhesons isolated from our experiments which would allow for the ranking of the phage adhesons with respect to their relative binding affinities. Subsequently, the use of atomic force microscope (AFM) should be investigated to visualize the surface of the PE resins and determine the depth of the pores found in the resin. If possible, visualizing phage adheson binding to PE could be investigated through a combination of SEM as there are reports on the visualization of phage through the use of environmental SEM[143]. Sample preparation for tensile testing should be optimized to ensure the results are more reliable and reproducible.

Another future experiment would be to investigate the production of phage fibers and thin films that are displaying the identified PE adhesons to provide PE affinity fibers and thin films as a potential modifier of the PE surface. It is also possible that these composites could act as new types of PE adhesives, allowing for the attachment of other types of molecules to the PE surface.

References

(1) Borchers, K.; Genov, S.; Gruber-Traub, C.; Niedergall, K.; Plankalayil, J.; Pufky-Heinrich, D.; Riegler, J.; Schreiber, T.; Tovar, G. E. M.; Weber, A.; Wojciukiewicz, D. In *Cellular and Biomolecular Recognition*; Jelinek, R., Ed.; Wiley-VCH Verlag GmbH & Co. KGaA: Weinheim, Germany, 2009; pp 31–67.

(2) Abergel, R. J.; Clifton, M. C.; Pizarro, J. C.; Warner, J. A.; Shuh, D. K.; Strong, R. K.; Raymond, K. N. *J. Am. Chem. Soc.* **2008**, *130* (10), 11524–11534.

(3) Richter, A.; Eggenstein, E.; Skerra, A. *FEBS Lett.* **2014**, *588* (2), 213–218.

(4) Sawada, T.; Mihara, H.; Serizawa, T. *Chem. Rec.* **2013**, *13* (2), 172–186.

(5) Tamerler, C.; Sarikaya, M. *Acta Biomater.* **2007**, *3* (3 SPEC. ISS.), 289–299.

(6) Peppas, N. A.; Huang, Y. *Pharm. Res.* **2002**, *19* (5), 578–587.

(7) Jaworski, J. In *Biomimetic Approaches for Biomaterials Development*; Mano, J. F., Ed.; Wiley-VCH Verlag GmbH & Co. KGaA: Weinheim, Germany, 2012; pp 117–156.

(8) So, H. M.; Won, K.; Kim, Y. H.; Kim, B. K.; Ryu, B. H.; Na, P. S.; Kim, H.; Lee, J. O. *J. Am. Chem. Soc.* **2005**, *127* (34), 11906–11907.

(9) O'Sullivan, C. K. *Anal. Bioanal. Chem.* **2002**, *372* (1), 44–48.

(10) Liang, H.; Zhang, X. B.; Lv, Y.; Gong, L.; Wang, R.; Zhu, X.; Yang, R.; Tan, W. *Acc. Chem. Res.* **2014**, *47* (6), 1891–1901.

(11) Zheng, D.; Seferos, D. S.; Giljohann, D. A.; Patel, P. C.; Mirkin, C. A. *Nano Lett.* **2009**, *9* (9), 3258–3261.

(12) Fosgerau, K.; Hoffmann, T. *Drug Discov. Today* **2015**, *20* (1), 122–128.

(13) Chow, D.; Nunalee, M. L.; Woo, L. D.; Simnick, A. J.; Chilkoti, A. *Mater. Sci. Eng. R*

Reports **2008**, *62* (4), 125–155.

(14) Eisenberg, D.; Jucker, M. *Cell* **2012**, *148* (6), 1188–1203.

(15) Sarikaya, M.; Tamerler, C.; Jen, A. K.; Schulten, K.; Baneyx, F. *Nat. Mater.* **2003**, *2* (9), 577–585.

(16) Moores, A.; Goettmann, F. *New J. Chem.* **2006**, *30* (8), 1121–1132.

(17) Li, J.; Zhao, T.; Chen, T.; Liu, Y.; Ong, C. N.; Xie, J. *Nanoscale* **2015**, *7* (17), 7502–7519.

(18) Eustis, S.; el-Sayed, M. a. *Chem. Soc. Rev.* **2006**, *35* (3), 209–217.

(19) Brown, S. *Nat. Biotechnol.* **1997**, *15* (3), 269–272.

(20) Kim, J.; Rheem, Y.; Yoo, B.; Chong, Y.; Bozhilov, K. N.; Kim, D.; Sadowsky, M. J.; Hur, H. G.; Myung, N. V. *Acta Biomater.* **2010**, *6* (7), 2681–2689.

(21) Slocik, J. M.; Stone, M. O.; Naik, R. R. *Small* **2005**, *1* (11), 1048–1052.

(22) Hnilova, M.; Oren, E. E.; Seker, U. O. S.; Wilson, B. R.; Collino, S.; Evans, J. S.; Tamerler, C.; Sarikaya, M. *Langmuir* **2008**, *24* (21), 12440–12445.

(23) Naik, R. R.; Stringer, S. J.; Agarwal, G.; Jones, S. E.; Stone, M. O. *Nat. Mater.* **2002**, *1* (3), 169–172.

(24) Božič Abram, S.; Aupič, J.; Dražić, G.; Gradišar, H.; Jerala, R. *Biochem. Biophys. Res. Commun.* **2016**, *472* (3), 566–571.

(25) Seker, U. O. S.; Wilson, B.; Dincer, S.; Kim, I. W.; Oren, E. E.; Evans, J. S.; Tamerler, C.; Sarikaya, M. *Langmuir* **2007**, *23* (15), 7895–7900.

(26) Sarikaya, M.; Tamerler, C.; Schwartz, D. T.; Baneyx, F. *Annu. Rev. Mater. Res.* **2004**, *34* (1), 373–408.

(27) Chiu, C.-Y.; Li, Y.; Ruan, L.; Ye, X.; Murray, C. B.; Huang, Y. *Nat. Chem.* **2011**, *3* (5), 393–399.

(28) Brown, S.; Sarikaya, M.; Johnson, E. *J. Mol. Biol.* **2000**, *299* (3), 725–735.

(29) Lee, E.; Kim, D. H.; Woo, Y.; Hur, H. G.; Lim, Y. *Biochem. Biophys. Res. Commun.* **2008**, *376* (3), 595–598.

(30) Song, C.; Blaber, M. G.; Zhao, G.; Zhang, P.; Fry, H. C.; Schatz, G. C.; Rosi, N. L. *Nano Lett.* **2013**, *13* (7), 3256–3261.

(31) Merg, A. D.; Boatz, J. C.; Mandal, A.; Zhao, G.; Mokashi-Punekar, S.; Liu, C.; Wang, X.; Zhang, P.; van der Wel, P. C. A.; Rosi, N. L. *J. Am. Chem. Soc.* **2016**, *138* (41), 13655–13663.

(32) Kim, J.; Kim, D. H.; Lee, S. J.; Rheem, Y.; Myung, N. V; Hur, H. G. *Biosci. Biotechnol. Biochem.* **2016**, *80* (8), 1478–1483.

(33) Dai, L.; Chang, D. W.; Baek, J.-B.; Lu, W. *Small* **2012**, *8* (8), 1130–1166.

(34) Su, Z.; Leung, T.; Honek, J. F. *J. Phys. Chem. B* **2006**, *110* (47), 23623–23627.

(35) Wang, S.; Humphreys, E. S.; Chung, S. Y.; Delduco, D. F.; Lustig, S. R.; Wang, H.; Parker, K. N.; Rizzo, N. W.; Subramoney, S.; Chiang, Y. M.; Jagota, A. *Nat. Mater.* **2003**, *2* (3), 196–200.

(36) Lipson, H.; Stokes, A. R. *Nature* **1942**, *149*, 328.

(37) So, C. R.; Hayamizu, Y.; Yazici, H.; Gresswell, C.; Khatayevich, D.; Tamerler, C.; Sarikaya, M. *ACS Nano* **2012**, *6* (2), 1648–1656.

(38) Penna, M. J.; Mijajlovic, M.; Tamerler, C.; Biggs, M. J. *Soft Matter* **2015**, *11* (26), 5192–5203.

(39) Wanamo, S.; Song, R.; Wang, L.; Jin, W.; Ding, D.; Wang, Z.; Zhang, R.-Q. *J. Mater. Chem.* **2012**, *22* (44), 23380–23386.

(40) Katoch, J.; Kim, S. N.; Kuang, Z. F.; Farmer, B. L.; Nalk, R. R.; Tatulian, S. A.; Ishigami,

M. *Nano Lett.* **2012**, *12* (5), 2342–2346.

(41) Cui, Y.; Kim, S. N.; Jones, S. E.; Wissler, L. L.; Naik, R. R.; McAlpine, M. C. *Nano Lett.* **2010**, *10* (11), 4559–4565.

(42) Kim, S. N.; Kuang, Z. F.; Slocik, J. M.; Jones, S. E.; Cui, Y.; Farmer, B. L.; McAlpine, M. C.; Naik, R. R. *J. Am. Chem. Soc.* **2011**, *133* (37), 14480–14483.

(43) Tomasio, S. M.; Walsh, T. R. *J. Phys. Chem. C* **2009**, *113* (20), 8778–8785.

(44) Coyle, B. L.; Rolandi, M.; Baneyx, F. *Langmuir* **2013**, *29* (15), 4839–4846.

(45) Gu, Z.; Yang, Z.; Wang, L.; Zhou, H.; Jimenez-Cruz, C. A.; Zhou, R. *Sci. Rep.* **2015**, *5*, 1–11.

(46) Xiao, D.; Sun, W.; Dai, H.; Zhang, Y.; Qin, X.; Li, L.; Wei, Z.; Chen, X. *J. Phys. Chem. C* **2014**, *118* (35), 20694–20701.

(47) Rajesh, C.; Majumder, C.; Mizuseki, H.; Kawazoe, Y. *J. Chem. Phys.* **2009**, *130* (12), 1–6.

(48) Hughes, Z. E.; Tomasio, S. M.; Walsh, T. R. *Nanoscale* **2014**, *6* (10), 5438–5448.

(49) Hughes, Z. E.; Walsh, T. R. *J. Mater. Chem. B* **2015**, *3* (16), 3211–3221.

(50) Camden, A. N.; Barr, S. A.; Berry, R. J. *J. Phys. Chem. B* **2013**, *117* (37), 10691–10697.

(51) Kim, S. S.; Kuang, Z. F.; Ngo, Y. H.; Farmer, B. L.; Naik, R. R. *ACS Appl. Mater. Interfaces* **2015**, *7* (36), 20447–20453.

(52) Braden, B. C.; Goldbaum, F. A.; Chen, B. X.; Kirschner, A. N.; Wilson, S. R.; Erlanger, B. F. *Proc. Natl. Acad. Sci. U. S. A.* **2000**, *97* (22), 12193–12197.

(53) Morita, Y.; Ohsugi, T.; Iwasa, Y.; Tamiya, E. *J. Mol. Catal. B-Enzymatic* **2004**, *28* (4–6), 185–190.

(54) Marken, F.; Gerrard, M. L.; Mellor, I. M.; Mortimer, R. J.; Madden, C. E.; Fletcher, S.; Holt, K.; Foord, J. S.; Dahm, R. H.; Page, F. *Electrochem. commun.* **2001**, *3* (4), 177–180.

(55) Murphy, M. A.; Wilcox, G. D.; Dahm, R. H.; Marken, F. *Indian J. Chem. Sect. A- Inorg. Bio-inorganic Phys. Theor. Anal. Chem.* **2005**, *44* (5), 924–931.

(56) Niedziolka, J.; Murphy, M. A.; Marken, F.; Opallo, M. *Electrochim. Acta* **2006**, *51* (26), 5897–5903.

(57) Hacker, V.; Wallnofer, E.; Baumgartner, W.; Schaffer, T.; Besenhard, J. O.; Schrottner, H.; Schmied, M. *Electrochem. commun.* **2005**, *7* (4), 377–382.

(58) Li, W.; Yang, Z.; Cheng, J.; Zhong, X.; Gu, L.; Yu, Y. *Nanoscale* **2014**, *6* (9), 4532–4537.

(59) Wang, K.; Wang, Y.; Wang, Y.; Hosono, E.; Zhou, H. *J. Phys. Chem. C* **2009**, *113* (3), 1093–1097.

(60) Szot-Karpinska, K.; Golec, P.; Lesniewski, A.; Palys, B.; Marken, F.; Niedziolka-Jonsson, J.; Wegrzyn, G.; Los, M. *Bioconjug. Chem.* **2016**, *27* (12), 2900–2910.

(61) Gabryelczyk, B.; Szilvay, G. R.; Salomäki, M.; Laaksonen, P.; Linder, M. B. *Colloids Surfaces B Biointerfaces* **2013**, *110*, 66–73.

(62) Gabryelczyk, B.; Szilvay, G. R.; Singh, V. K.; Mikkila, J.; Kostiainen, M. A.; Koskinen, J.; Linder, M. B. *Biomacromolecules* **2015**, *16* (2), 476–482.

(63) Swaminathan, S.; Cui, Y. *Rsc Adv.* **2016**, *6* (54), 49127–49129.

(64) Yamaguchi, A.; Isozaki, K.; Nakamura, M.; Takaya, H.; Watanabe, T. *Sci. Rep.* **2016**, *6*, 1–11.

(65) Serizawa, T.; Techawanitchai, P.; Matsuno, H. *Chembiochem* **2007**, *8* (9), 989–993.

(66) Sanghvi, A. B.; Miller, K. P.-H.; Belcher, A. M.; Schmidt, C. E. *Nat. Mater.* **2005**, *4* (6), 496–502.

(67) Fukusaki, E.; Ogawa, K.; Okazawa, A.; Kajiyama, S. I.; Kobayashi, A. *J. Mol. Catal. B Enzym.* **2004**, *28* (4–6), 181–184.

(68) Serizawa, T.; Iida, K.; Matsuno, H.; Kurita, K. *Chem. Lett.* **2007**, *36* (8), 988–989.

(69) Khoushab, F.; Jaruseranee, N.; Tanthanuch, W.; Yamabhai, M. *Int. J. Biol. Macromol.* **2012**, *50* (5), 1267–1274.

(70) Serizawa, T.; Sawada, T.; Matsuno, H.; Matsubara, T.; Sato, T. *J. Am. Chem. Soc.* **2005**, *127* (40), 13780–13781.

(71) Vodnik, M.; Strukelj, B.; Lunder, M. *Anal. Biochem.* **2012**, *424* (2), 83–86.

(72) Hu, Y. F.; Gao, X. C.; Xu, T. Q.; Dun, Z.; Yu, X. L. *Comb. Chem. High Throughput Screen.* **2016**, *19* (4), 283–289.

(73) Kogot, J. M.; Sarkes, D. A.; Val-Addo, I.; Pellegrino, P. M.; Stratis-Cullum, D. N. *Biotechniques* **2012**, *52* (2), 95–101.

(74) Ejima, H.; Matsuno, H.; Serizawa, T. *Langmuir* **2010**, *26* (22), 17278–17285.

(75) Nomura, Y.; Sharma, V.; Yamamura, A.; Yokobayashi, Y. *Biotechnol. Lett.* **2011**, *33* (5), 1069–1073.

(76) Lee R. Lynd, Paul J. Weimer, Willem H. van Zyl, I. S. P. *Microbiol. Mol. Biol. Rev.* **2002**, *66* (3), 506–577.

(77) Habibi, Y.; Lucia, L. A.; Rojas, O. J. *Chem. Rev.* **2010**, *110* (6), 3479–3500.

(78) Boufi, S.; González, I.; Delgado-Aguilar, M.; Tarrès, Q.; Pèlach, M. À.; Mutjé, P. *Carbohydr. Polym.* **2016**, *154*, 151–166.

(79) Chandel, A. K.; Chandrasekhar, G.; Silva, M. B.; Silvério da Silva, S. *Crit. Rev. Biotechnol.* **2012**, *32* (3), 187–202.

(80) Fontes, C. M. G. A.; Gilbert, H. J. *Annu. Rev. Biochem.* **2010**, *79* (1), 655–681.

(81) Guo, J.; Catchmark, J. M.; Mohamed, M. N. A.; Benesi, A. J.; Tien, M.; Kao, T. H.; Watts, H. D.; Kubicki, J. D. *Biomacromolecules* **2013**, *14* (6), 1795–1805.

(82) Zeng, Y.; Zhao, S.; Yang, S.; Ding, S. Y. *Curr. Opin. Biotechnol.* **2014**, *27*, 98–45.

(83) Reddy, S. N.; Nanda, S.; Dalai, A. K.; Kozinski, J. A. *Int. J. Hydrogen Energy* **2014**, *39* (13), 6912–6926.

(84) Nguyen, J. D.; Matsuura, B. S.; Stephenson, C. R. J. *J. Am. Chem. Soc.* **2014**, *136* (4), 1218–1221.

(85) Xu, C.; Arneil, R.; Arancon, D.; Labidi, J.; Luque, R. *Chem. Soc. Rev.* **2014**, *43* (43), 7485–7500.

(86) Adey, N. B.; Mataragnon, A. H.; Rider, J. E.; Carter, J. M.; Kay, B. K. *Gene* **1995**, *156* (1), 27–31.

(87) Kumada, Y.; Tokunaga, Y.; Imanaka, H.; Imamura, K.; Sakiyama, T.; Katoh, S.; Nakanishi, K. *Biotechnol. Prog.* **2006**, *22* (2), 401–405.

(88) Andrady, A. L.; Neal, M. A. *Philos. Trans. R. Soc. Lond. B. Biol. Sci.* **2009**, *364* (1526), 1977–1984.

(89) Kissin, Y. V. *Polyethylene: End use and their physical meaning*; Carl Hanser Verlag: Munich, Germany, 2012.

(90) Malpass, D. B. *Introduction to Industrial Polyethylene: Properties, Catalysts, Processes*; Scrivener Publishing LLC.: Salem, MA., USA, 2010.

(91) Shamiri, A.; Chakrabarti, M. H.; Jahan, S.; Hussain, M. A.; Kaminsky, W.; Aravind, P. V.; Yehye, W. A. *Materials (Basel).* **2014**, *7* (7), 5069–5108.

(92) Kim, S. H.; Somorjai, G. A. *Proc. Natl. Acad. Sci. U. S. A.* **2006**, *103* (42), 15289–15294.

(93) Desai, S. M.; Singh, R. P. In *Long Term Properties of Polyolefins*; Albertsson Ann-Christine, Ed.; Springer-Verlag Berlin Heidelberg: Heidelberg, Germany, 2004; Vol. 169, pp 231–294.

(94) Smith, G. P. *Science (80-.).* **1985**, *228* (4705), 1315–1317.

(95) Parmley, S. F.; Smith, G. P. *Gene* **1988**, *73* (2), 305–318.

(96) Rakonjac, J.; Bennett, N. J.; Spagnuolo, J.; Gagic, D.; Russel, M. *Curr. Issues Mol. Biol.* **2011**, *13* (2), 51–76.

(97) Cwirla, S. E.; Peters, E. a; Barrett, R. W.; Dower, W. J. *Proc. Natl. Acad. Sci. U. S. A.* **1990**, *87* (August), 6378–6382.

(98) Zwick, M. B.; Shen, J.; Scott, J. K. *Curr. Opin. Biotechnol.* **1998**, *9* (4), 427–436.

(99) Dammers, C.; Yolcu, D.; Kukuk, L.; Willbold, D.; Pickhardt, M.; Mandelkow, E.; Horn, A. H. C.; Sticht, H.; Malhis, M. N.; Will, N.; Schuster, J.; Funke, S. A. *PLoS One* **2016**, *11* (12), e0167432.

(100) Bellotto, S.; Chen, S.; Rentero Rebollo, I.; Wegner, H. A.; Heinis, C. *J. Am. Chem. Soc.* **2014**, *136* (16), 5880–5883.

(101) Yu, T.; Gong, Y.; Chen, Y.; Liao, K. *RSC Adv.* **2010**, *2*, 1466–1476.

(102) Golec, P.; Karczewska-Golec, J.; Los, M.; Wegrzyn, G. *J. Nanoparticle Res.* **2012**, *14* (11), 1218.

(103) Rahbarnia, L.; Farajnia, S.; Babaei, H.; Majidi, J.; Veisi, K.; Ahmadzadeh, V.; Akbari, B. *J. Drug Target.* **2016**, *0* (0), 1–33.

(104) Seker, U. O. S.; Demir, H. V. *Molecules* **2011**, *16* (2), 1426–1451.

(105) Rothenstein, D.; Claasen, B.; Omiecienski, B.; Lammel, P.; Bill, J. *J Am Chem Soc* **2012**, *134* (30), 12547–12556.

(106) Günay, K. A.; Klok, H. *Bioconjug. Chem.* **2015**, *26* (10), 2002–2015.

(107) Estephan, E.; Saab, M. B.; Agarwal, V.; Cuisinier, F. J. G.; Larroque, C.; Gergely, C. *Adv. Funct. Mater.* **2011**, *21* (11), 2003–2011.

(108) Grosse, S.; Wilke, P.; Borner, H. G. *Angew. Chemie-International Ed.* **2016**.

(109) Schwemmer, T.; Baumgartner, J.; Faivre, D.; Borner, H. G. *J. Am. Chem. Soc.* **2012**, *134* (4), 2385–2391.

(110) Smith, G. P.; Petrenko, V. a. *Chem. Rev.* **1997**, *97* (96), 391–410.

(111) Lubkowki, J.; Hennecke, F.; Pluckthun, A.; Wlodawer, A. *Nat. Struct. Biol.* **1998**, *5* (2), 140–147.

(112) Marvin, D. A.; Hale, R. D.; Nave, C.; Citterich, M. H. *J. Mol. Biol.* **1994**, *235* (1), 260–286.

(113) Russel, M.; Lowman, H. B.; Clackson, T. In *Phage Display*; Clackson, T., Lowman, H. B., Eds.; Oxford University Press Inc.: New York, New York, USA, 2004; pp 1–26.

(114) Matochko, W. L.; Cory Li, S.; Tang, S. K.; Derda, R. *Nucleic Acids Res.* **2014**, *42* (3), 1784–1798.

(115) Matochko, W. L.; Chu, K.; Jin, B.; Lee, S. W.; Whitesides, G. M.; Derda, R. *Methods* **2012**, *58* (1), 47–55.

(116) Bakhshinejad, B.; Zade, H. M.; Shekarabi, H. S. Z.; Neman, S. *Amino Acids* **2016**, *48* (12), 2699–2716.

(117) Cunningham, S. D.; Lowe, D. J.; O'Brien, J. P.; Wang, H.; Wilkins, A. E. Polyethylene Binding Peptides and Methods of Use. US 7906617 B2, 2009.

(118) Bombelli, P.; Howe, C. J.; Bertocchini, F. *Curr. Biol.* **2017**, *27* (8), R292–R293.

(119) Amagai, M.; Komai, A.; Hashimoto, T.; Shirakata, Y.; Hashimoto, K.; Yamada, T.; Kitajima, Y.; Ohya, K.; Iwanami, H.; Nishikawa, T. *Br. J. Dermatol.* **1999**, *140* (2), 351–357.

(120) Asensio, L.; González, I.; García, T.; Martín, R. *Food Control* **2008**, *19* (1), 1–8.

(121) Anderson, G. L.; McNellis, L. A. *J. Chem. Educ.* **1998**, *75* (10), 1275.

(122) Gan, S. D.; Patel, K. R. *J. Invest. Dermatol.* **2013**, *133* (9), e12.

(123) Vernon-Parry, K. D. *III-Vs Rev.* **2000**, *13* (4), 40–44.

(124) Schatten, H. In *Scanning Electron Microscopy for the Life Sciences*; Schatten, H., Ed.; Cambridge University Press: Cambridge, UK, 2013; pp 1–16.

(125) Newbury, D. E.; Ritchie, N. W. M. *J. Anal. At. Spectrom.* **2013**, *28* (7), 973–988.

(126) Schneider, R. In *Surface and Thin Film Analysis*; Friedbacher, G., Bubert, H., Eds.; Wiley-VCH Verlag GmbH & Co. KGaA: Weinheim, Germany, 2011; pp 293–310.

(127) Lee, J. G. *Computational Materials Science: An Introduction*, Second Edi.; Taylor & Francis Group, LLC: Boca Raton, Florida, 2017.

(128) Yamamoto, T. *Polymer (Guildf).* **2009**, *50* (9), 1975–1985.

(129) Bargmann, S.; Soyarslan, C.; Husser, E.; Konchakova, N. *Mech. Mater.* **2016**, *94*, 53–65.

(130) Haghighatpanah, S.; Bolton, K. *Front. Chem.* **2014**, *2*, 1–10.

(131) Gedde, U. W.; Mattozzi, A. In *Long Term Properties of Polyolefins*; Albertsson, A.-C., Ed.; Springer Berlin Heidelberg: Heidelberg, Germany, 2004; pp 29–74.

(132) Ramos, J.; Vega, J. F.; Martínez-Salazar, J. *Macromolecules* **2015**, *48* (14), 5016–5027.

(133) Singh, T. J.; Samanta, S. *Mater. Today Proc.* **2015**, *2* (4–5), 1381–1387.

(134) Mao, J. Y.; Belcher, A. M.; Van Vliet, K. J. *Adv. Funct. Mater.* **2010**, *20* (2), 209–214.

(135) Horrocks, A. R. *Polym. Degrad. Stab.* **2011**, *96* (3), 377–392.

(136) Lee, S. W.; Belcher, A. M. *Nano Lett.* **2004**, *4* (3), 387–390.

(137) Chiang, C. Y.; Mello, C. M.; Gu, J.; Silva, E. C. C. M.; Van Vliet, K. J.; Belcher, A. M. *Adv. Mater.* **2007**, *19* (6), 826–832.

(138) Hakami, A. R.; Ball, J. K.; Tarr, A. W. *J. Virol. Methods* **2015**, *221*, 1–8.

(139) Magnotta, V. A.; Friedman, L. *J. Digit. Imaging* **2006**, *19* (2), 140–147.

(140) Sim, K. S.; Tan, Y. Y.; Lai, M. A.; Tso, C. P.; Lim, W. K. *J. Microsc.* **2010**, *238* (1), 44–56.

(141) Jończyk, E.; Kłak, M.; Międzybrodzki, R.; Górski, A. *Folia Microbiol* **2011**, *56*, 191–200.

(142) Zeltins, A. In *Viral Nanotechnology*; Khudyakov, Y., Pumpens, P., Eds.; Taylor & Francis Group, LLC: Boca Raton, Florida, 2016; pp 93–121.

(143) Wild, P.; Kaech, A.; Lucas, M. S. In *Scanning Electron Microscopy for the Life Sciences*; Schatten, H., Ed.; Cambridge University Press: Cambridge, UK, 2013; pp 99–115.

(144) Darmostuk, M.; Rimpelova, S.; Gbelcova, H.; Ruml, T. *Biotechnol. Adv.* **2014**, *33* (6), 1141–1161.

Appendix A: Primary Data of Adheson Sequences

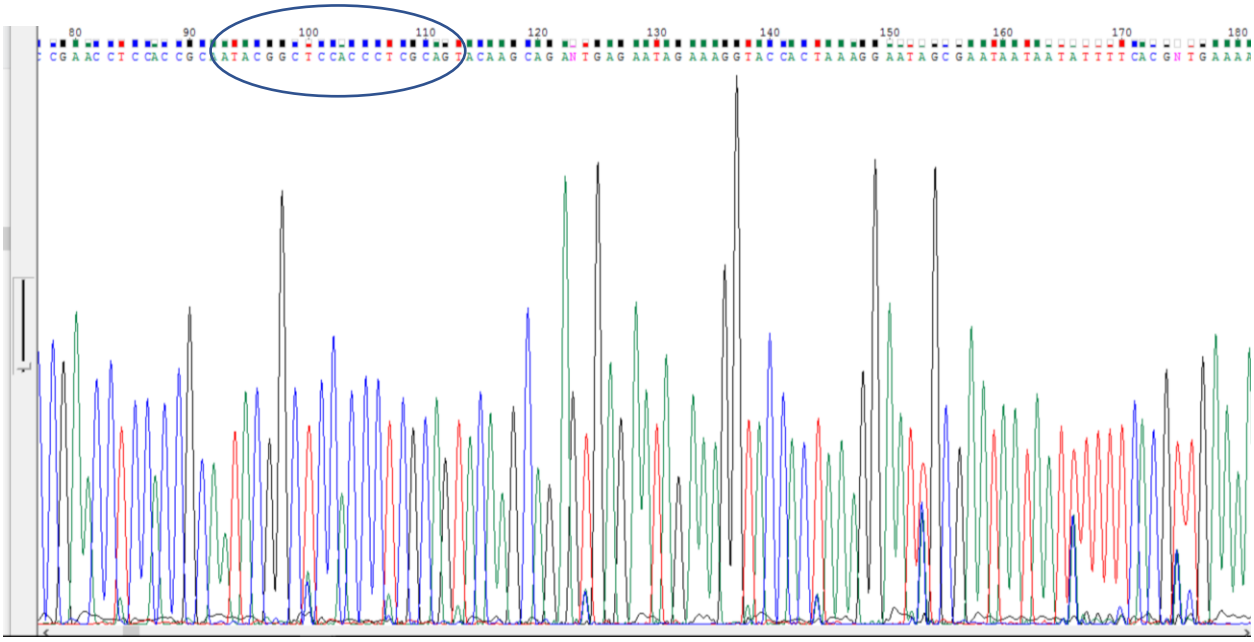

Appendix A 1: HSDK-1 (YPEVRAT) DNA sequence (circled)

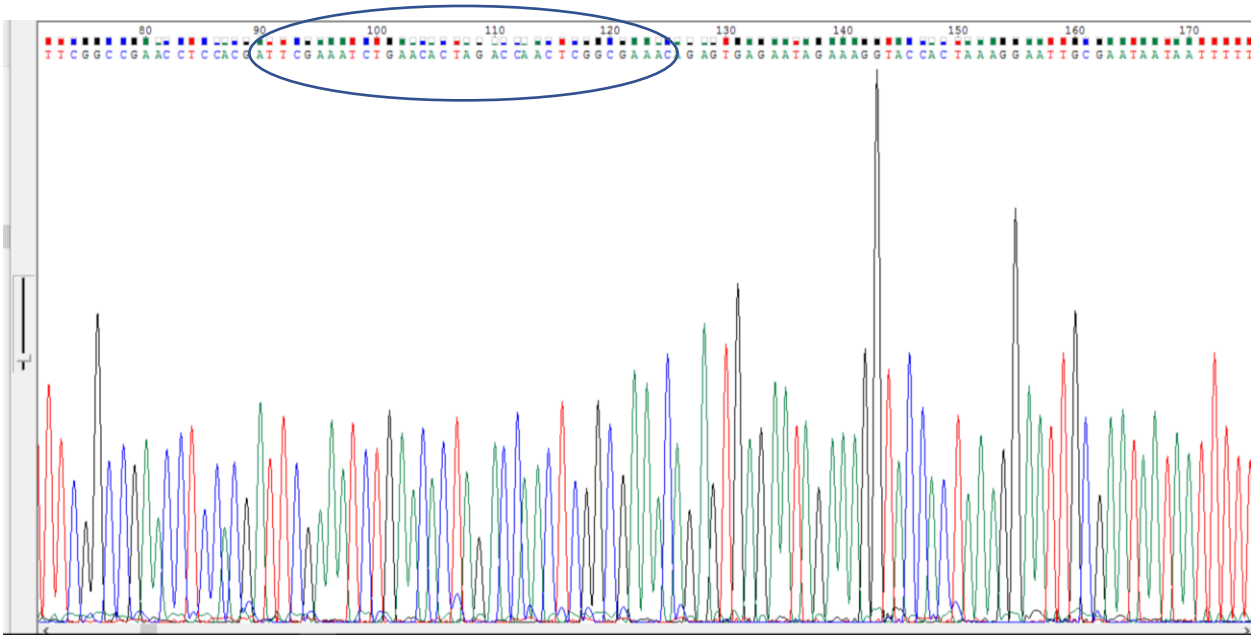

Appendix A 2: HSDK-2 (NSIQVSSWSPSV) DNA sequence (circled)

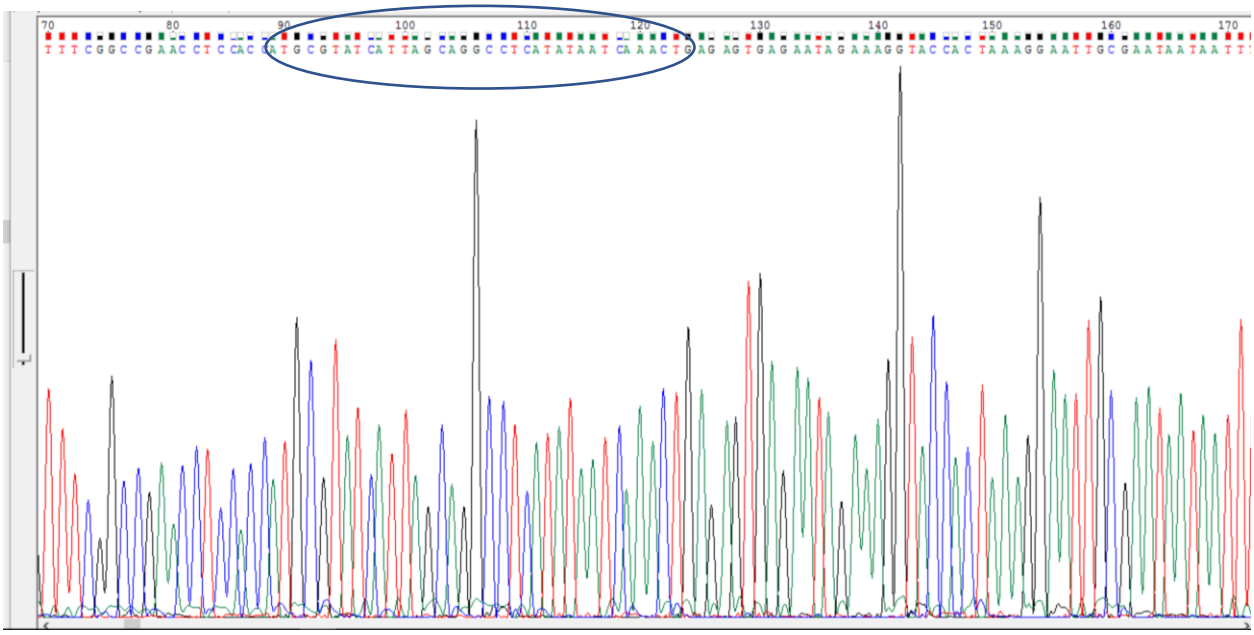

Appendix A 3: HSDK-3 (HTDNAPRMYDFQ) DNA sequence (circled)

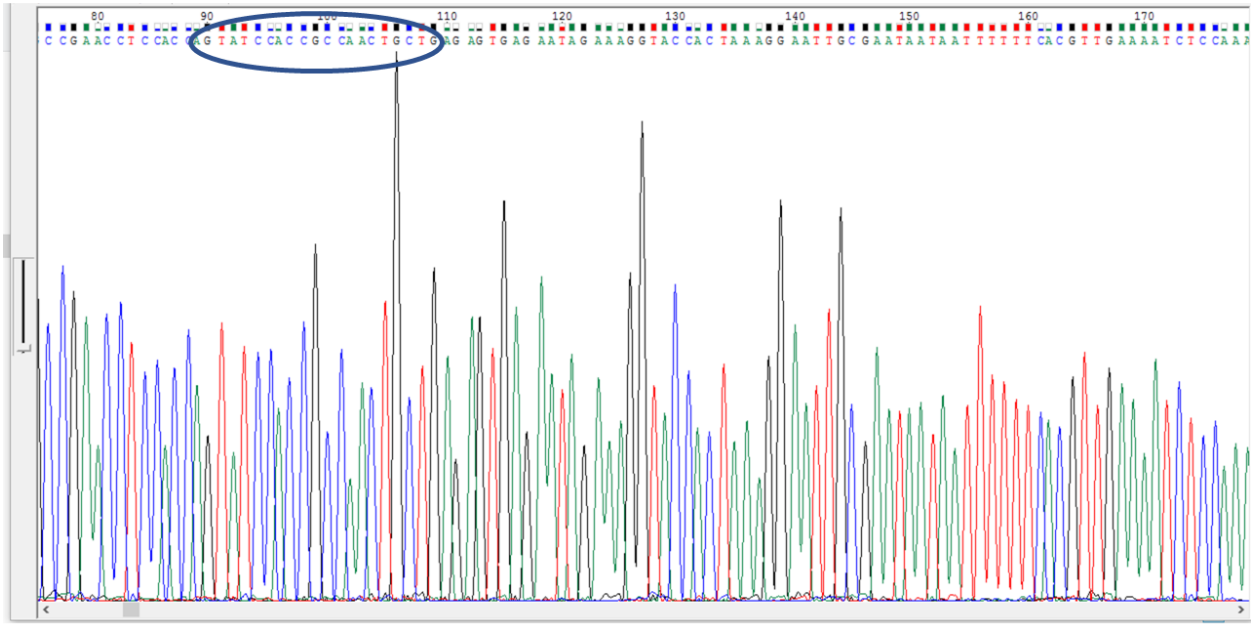

Appendix A 4: TDVLQQS DNA sequence circled

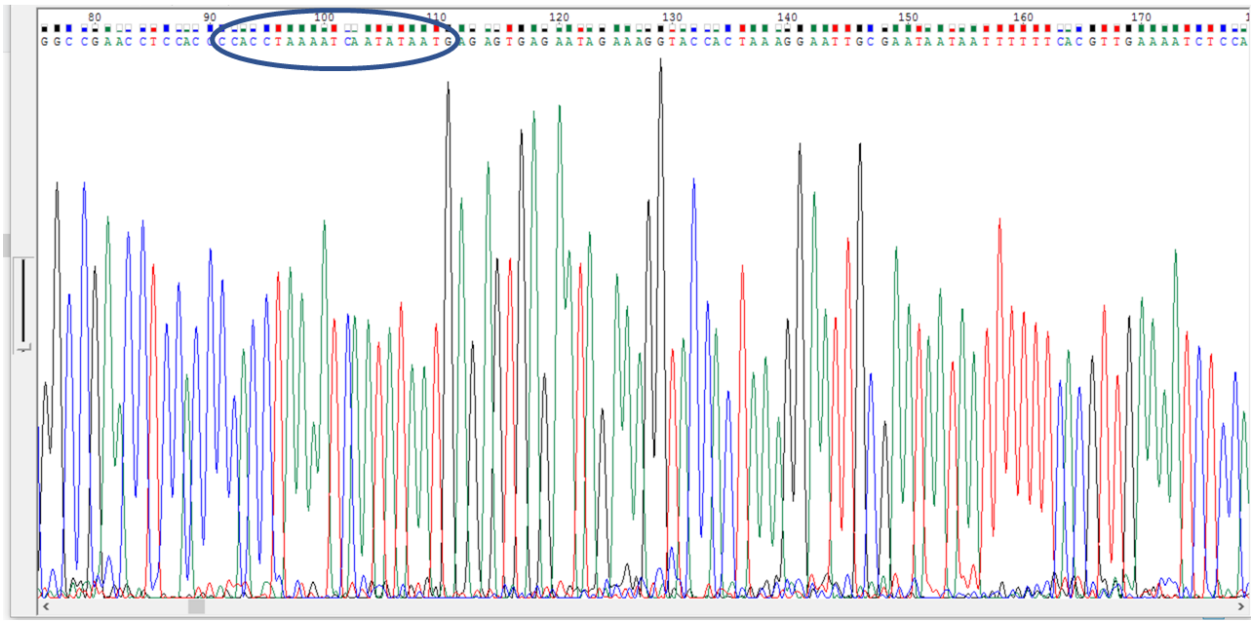

Appendix A 5: WRFDIYH DNA sequence circled

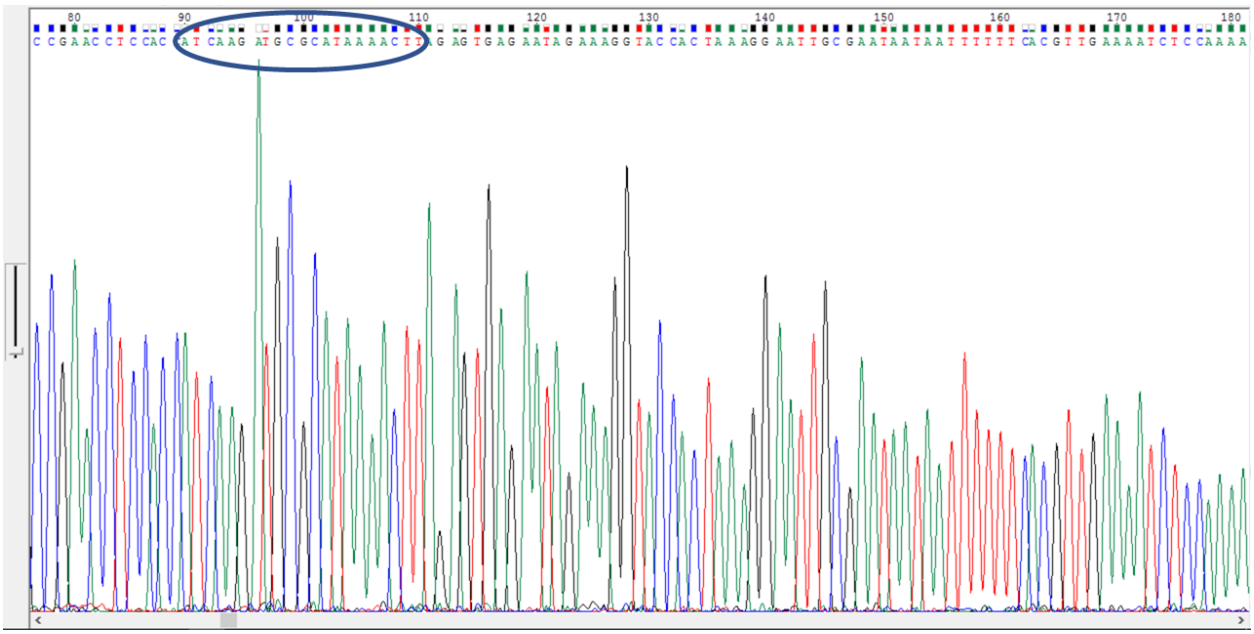

Appendix A 6:DLHAYFK DNA sequence circled

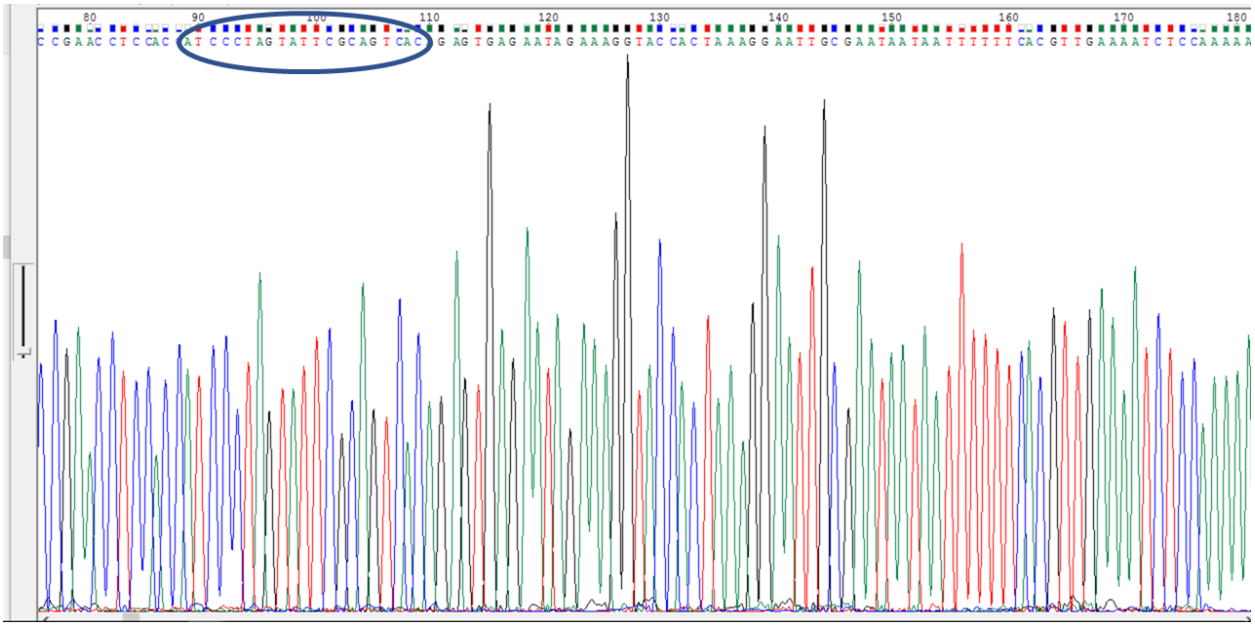

Appendix A 7:DRTNATV DNA sequence circled

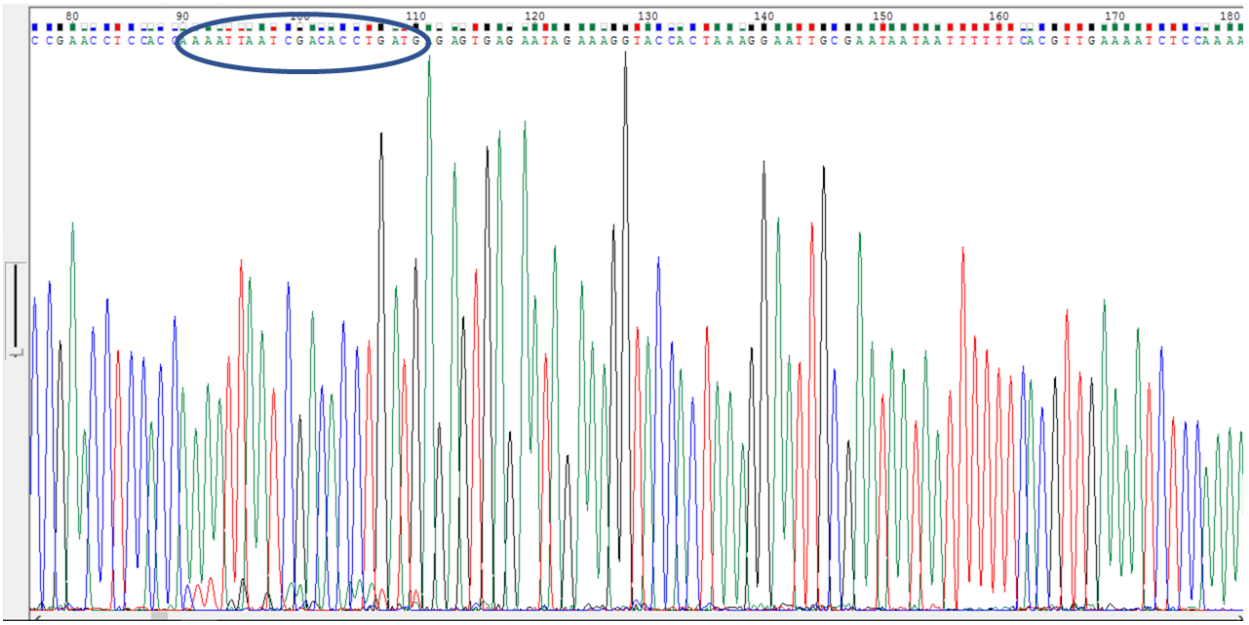

Appendix A 8: FNISVQH DNA sequence circled

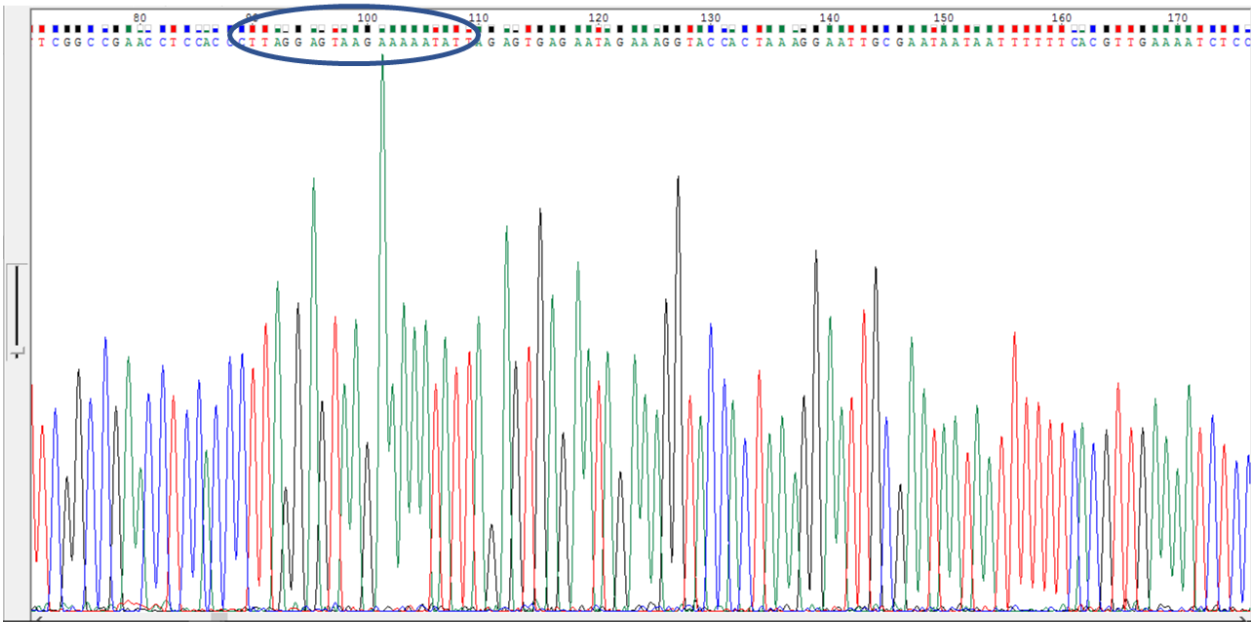

Appendix A 9: KPTLFIN DNA sequence circled

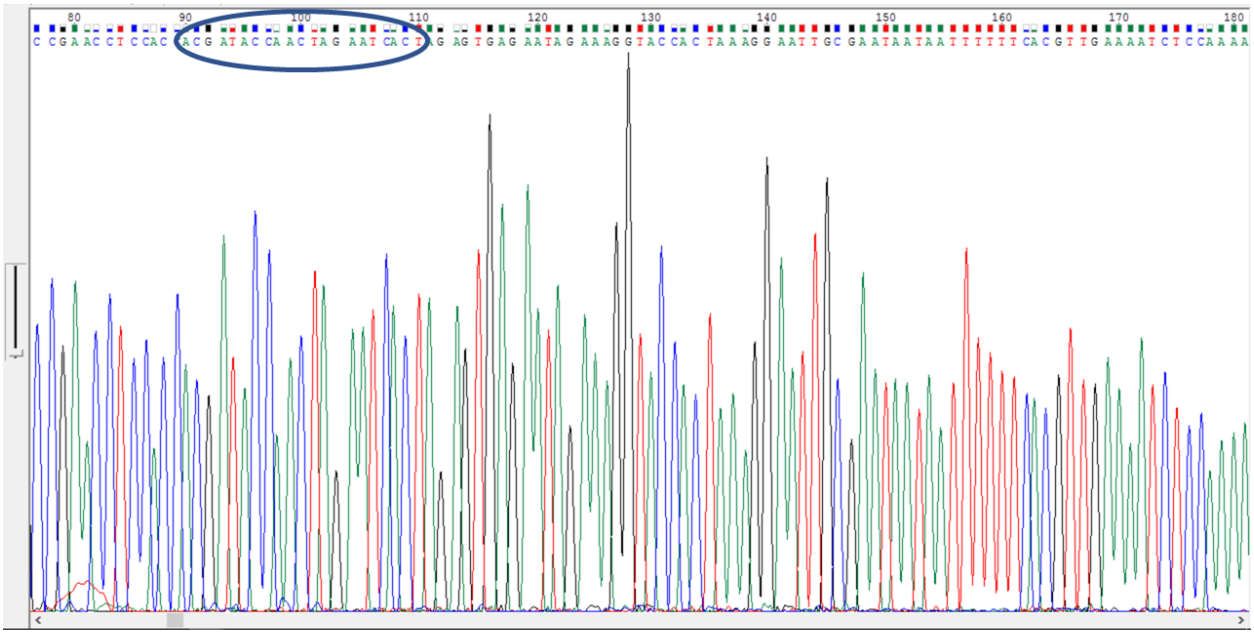

Appendix A 10: RYWSSDS DNA sequence circled

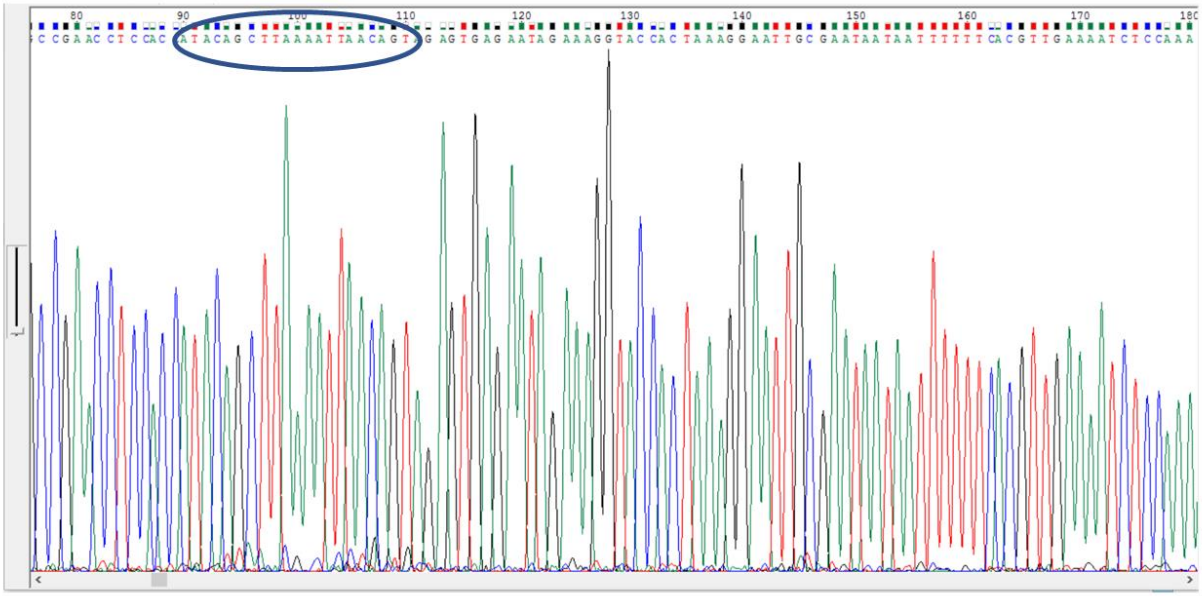

Appendix A 11: YLKFNVT DNA sequence circled (for both HDPE and LLDPE linear 7-mer)

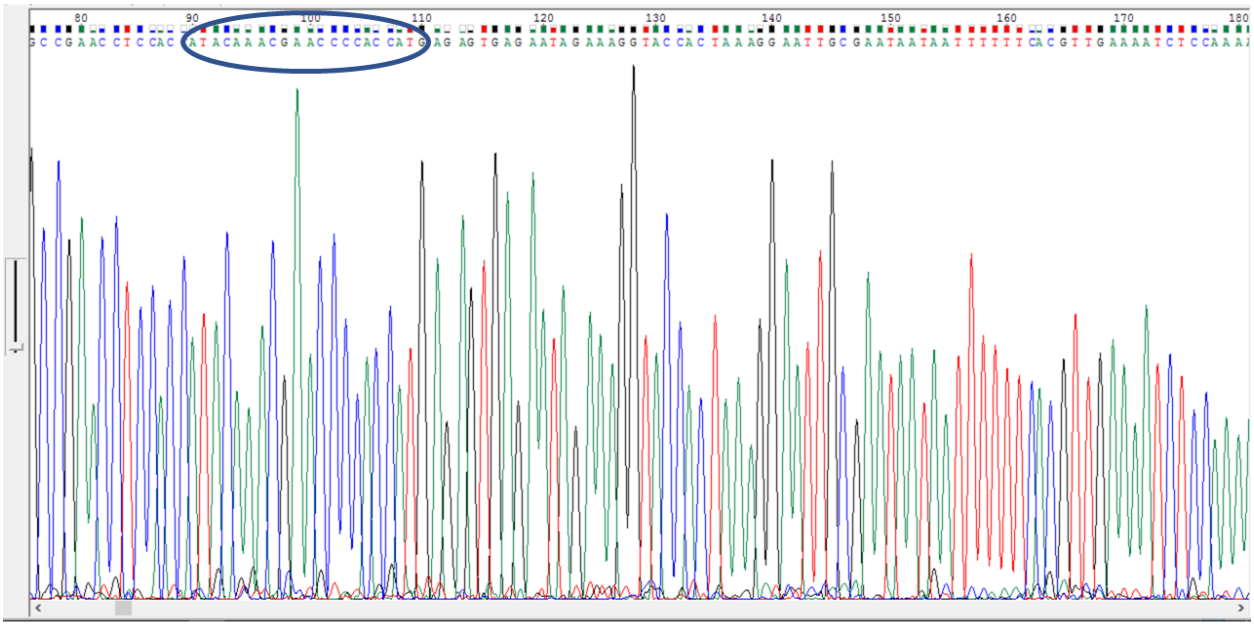

Appendix A 12: YLRVGGH DNA sequence circled

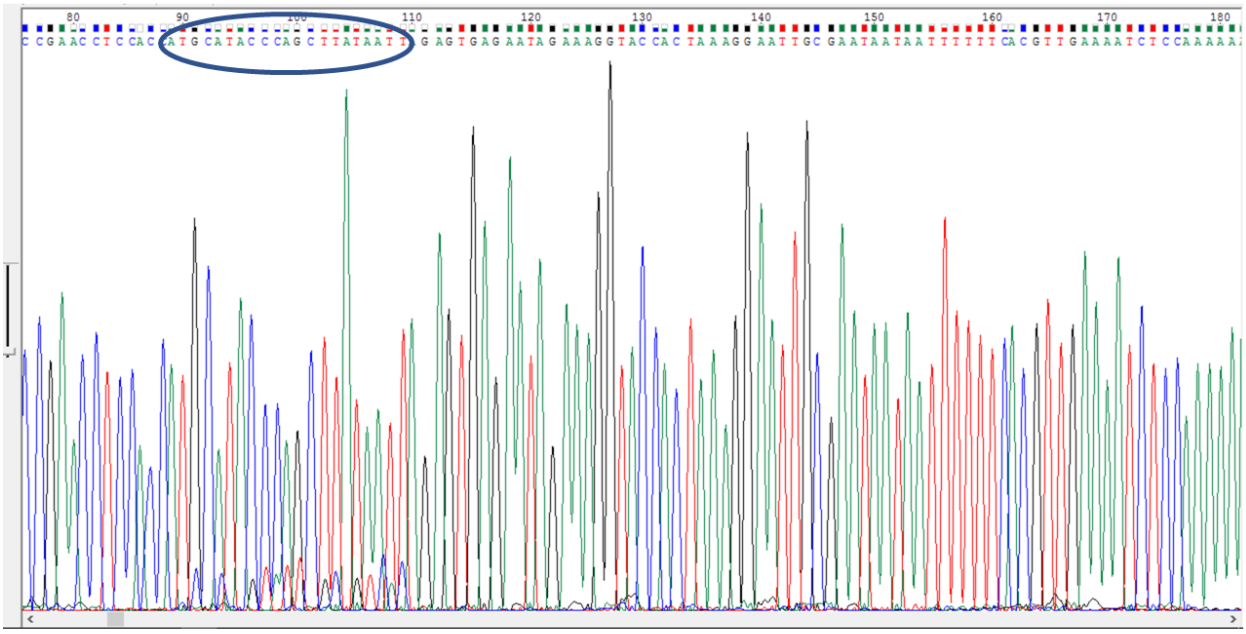

Appendix A 13: HMGLNYN DNA sequence circled

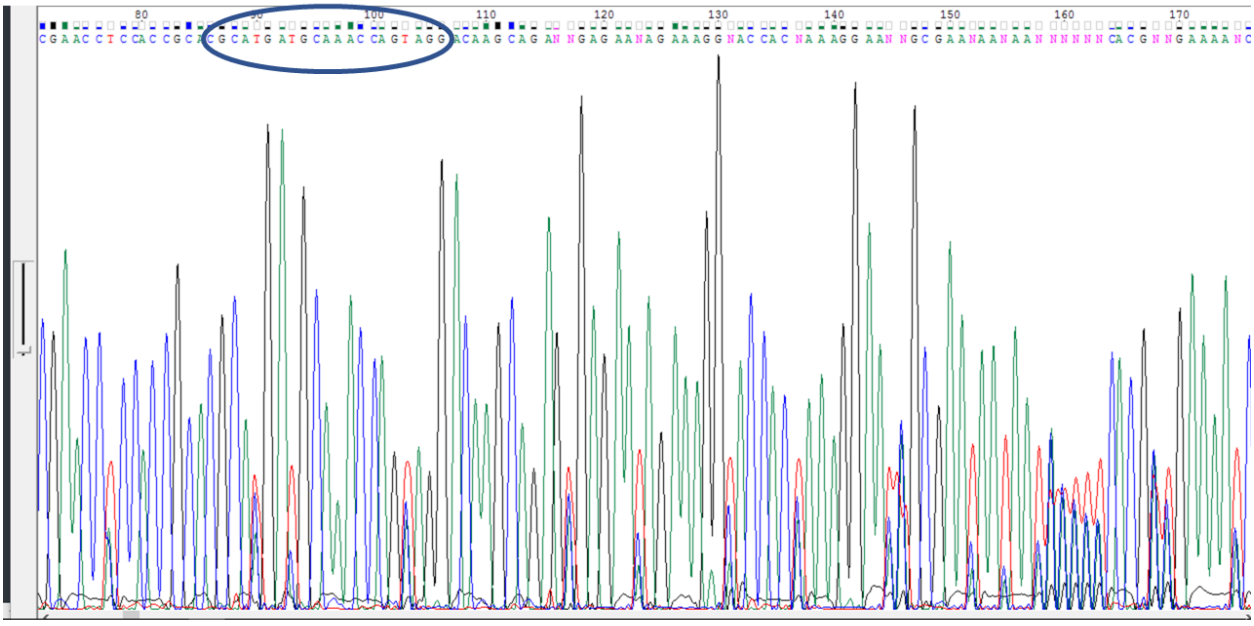

Appendix A 14: AHHWGTP DNA sequence circled

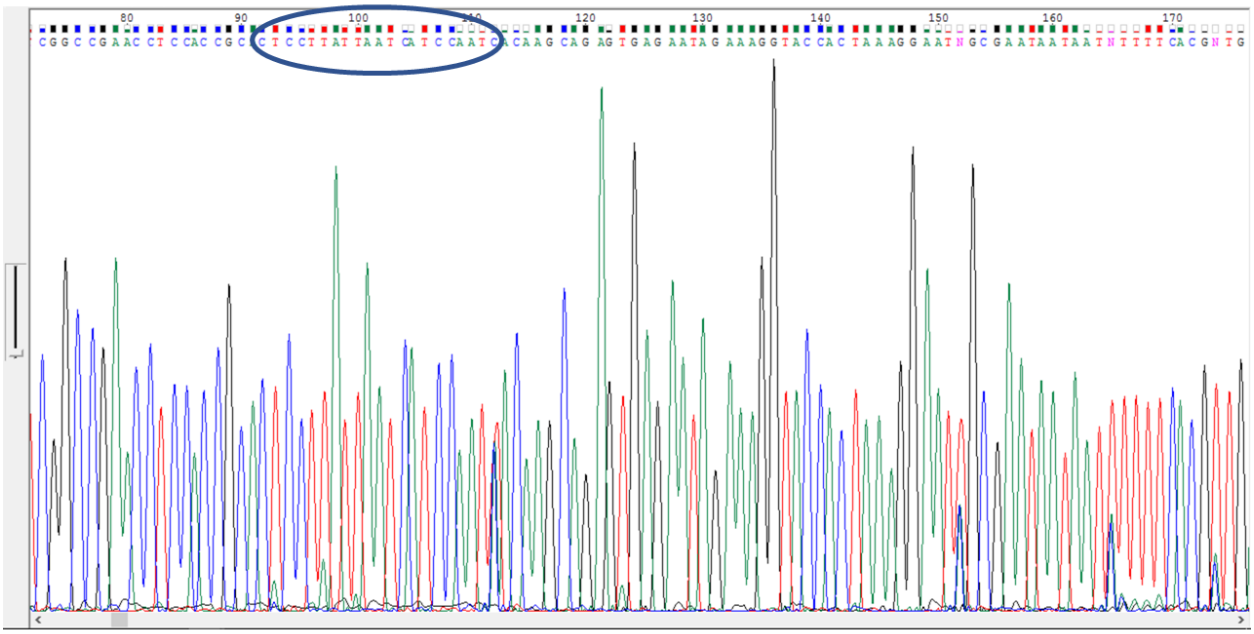

Appendix A 15: EKNIMWD DNA sequence circled

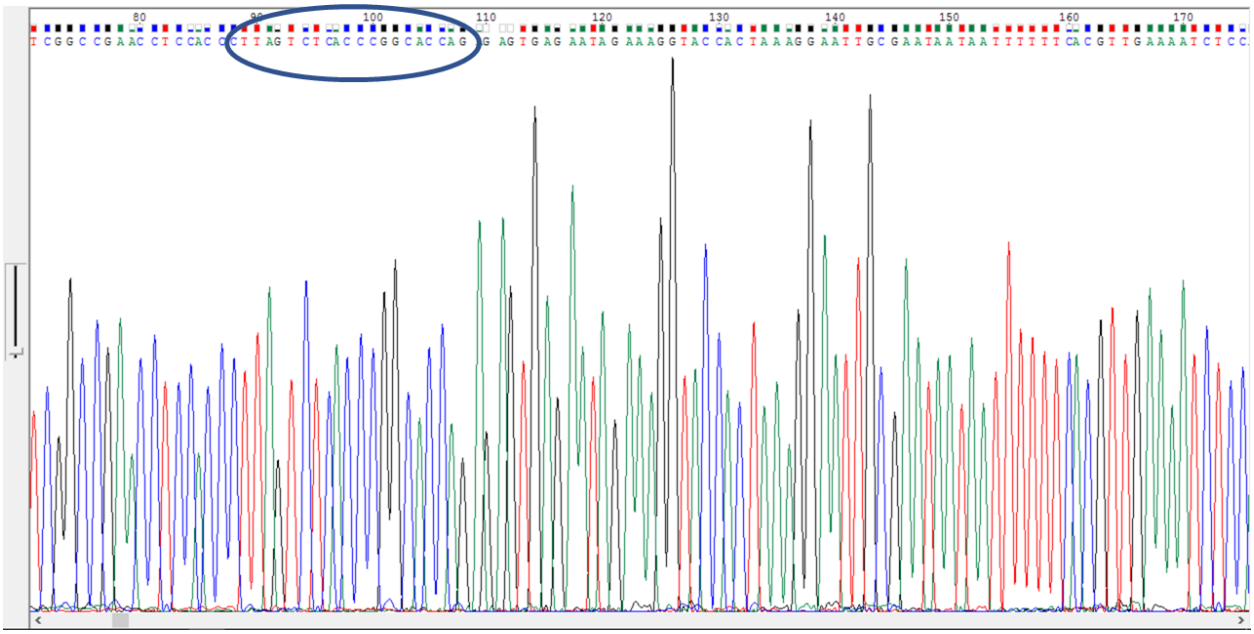

Appendix A 16: KTEGPVL DNA sequence circled

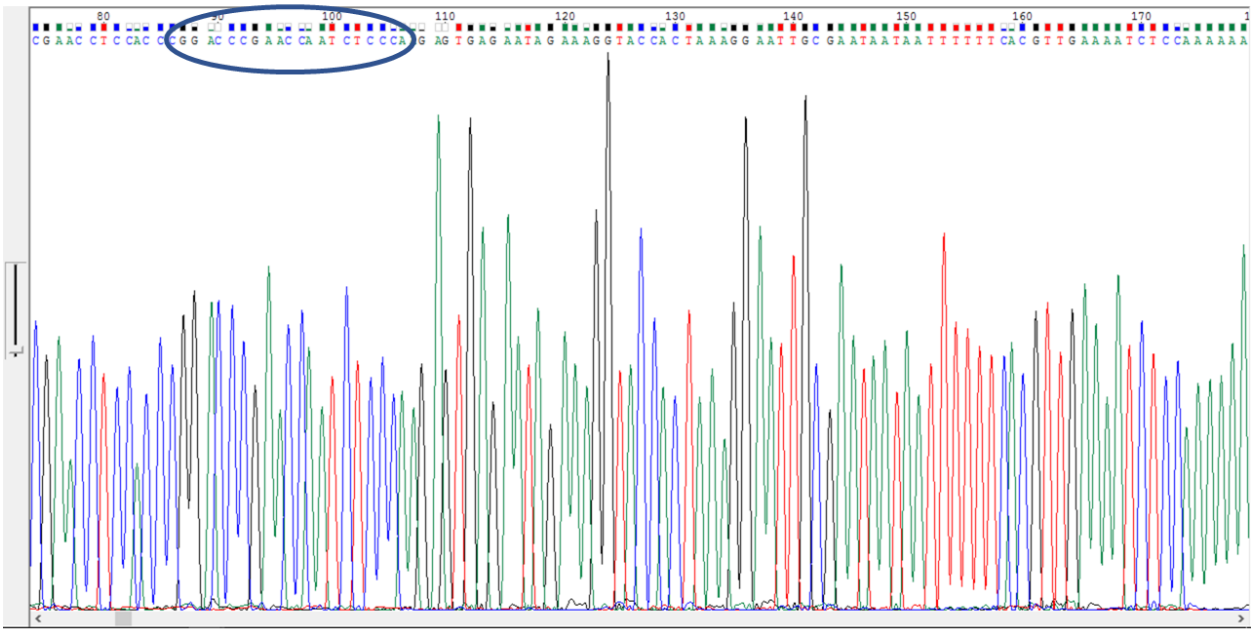

Appendix A 17: PGSGIEW DNA sequence circled

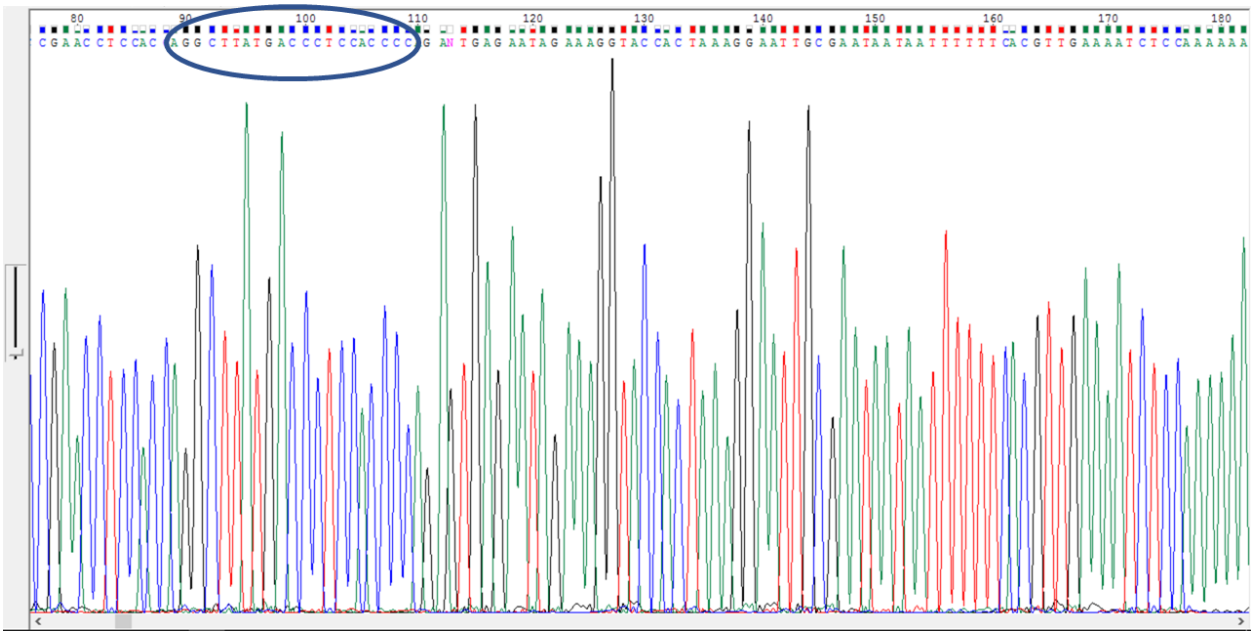

Appendix A 18: PKHGEVG DNA sequence circled

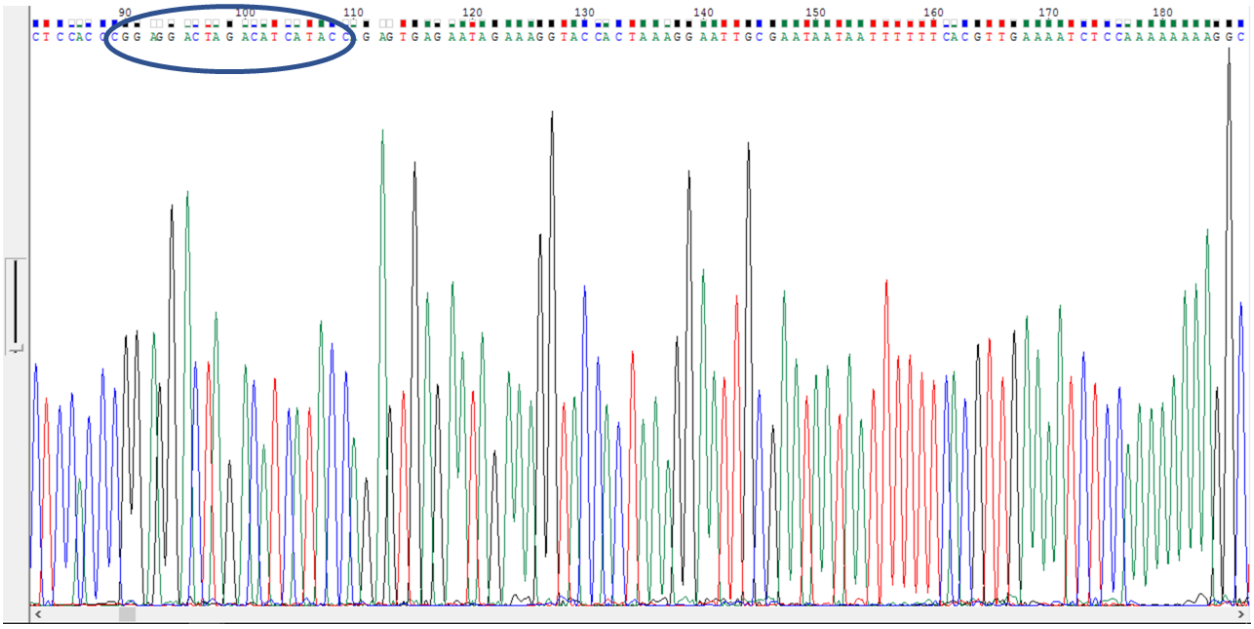

Appendix A 19: PPSSMMG DNA sequence circled

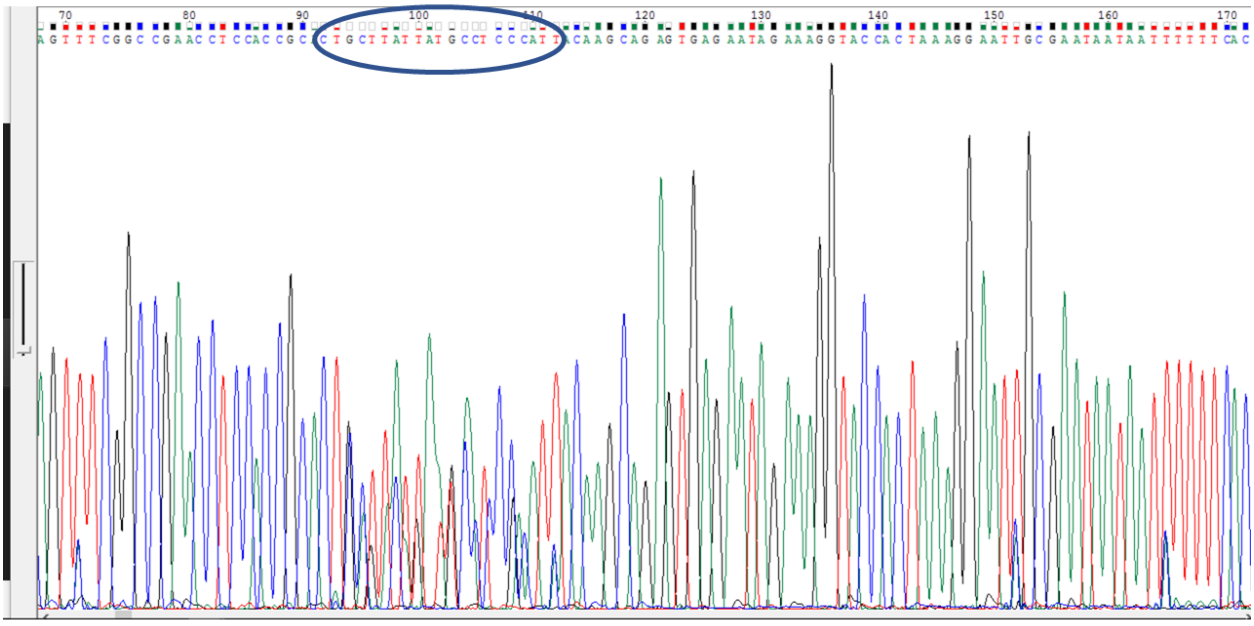

Appendix A 20: QKNHRGN DNA sequence circled

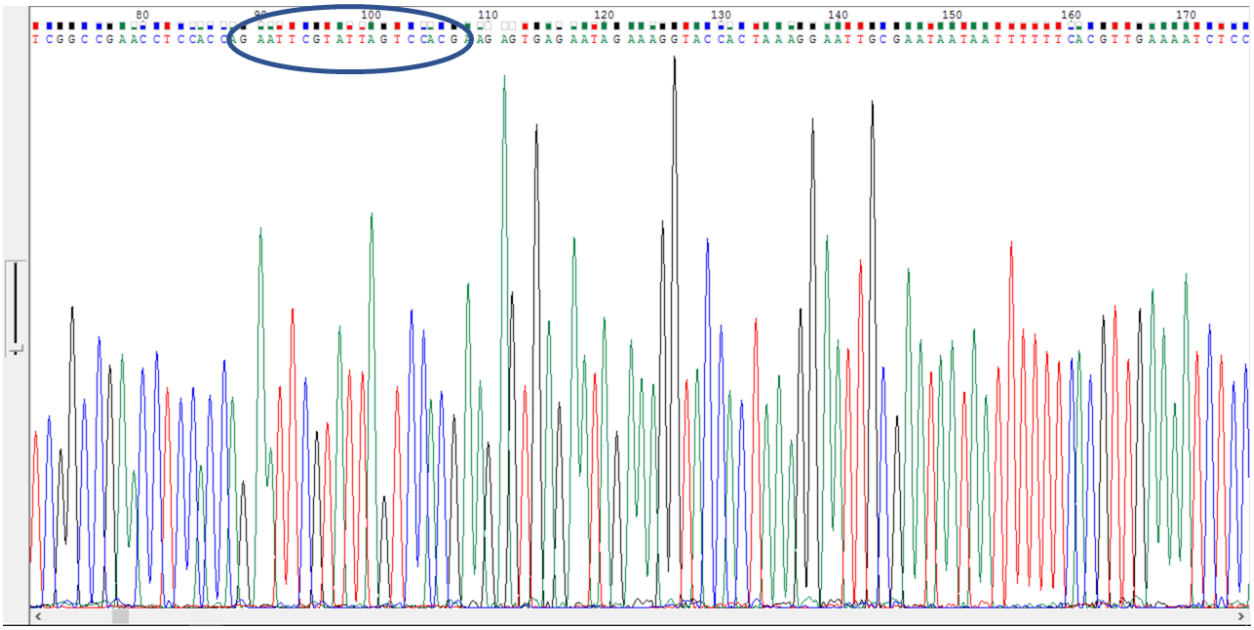

Appendix A 21: SNTNTWS DNA sequence circled

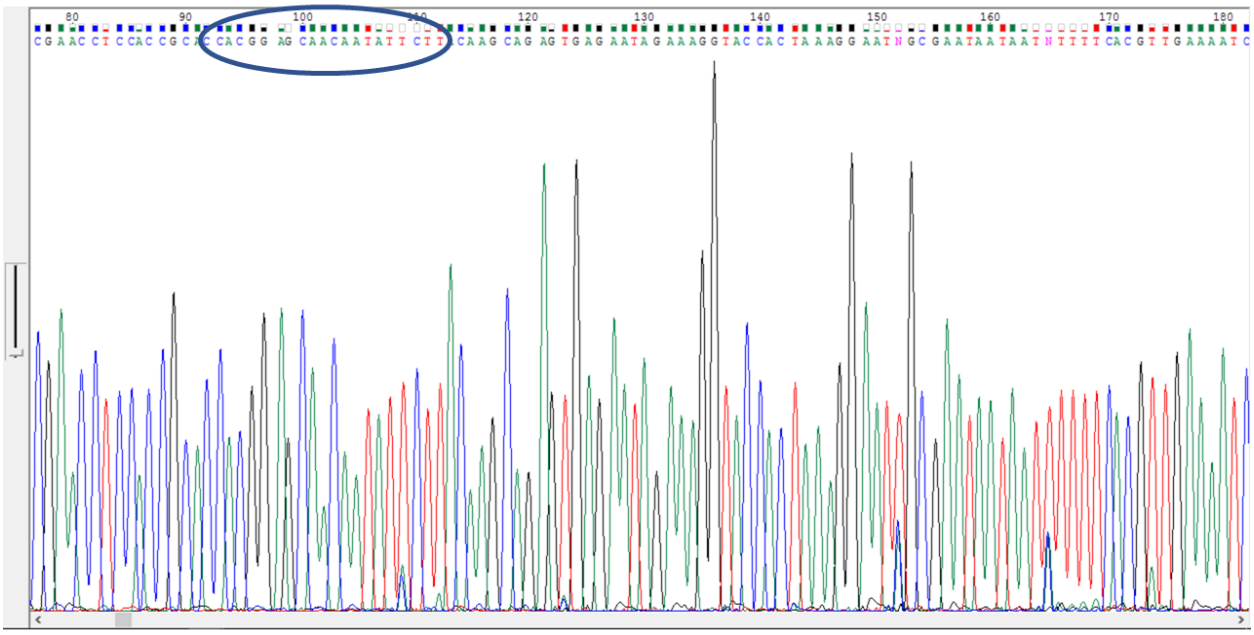

Appendix A 22: WPVVINK DNA sequence circled

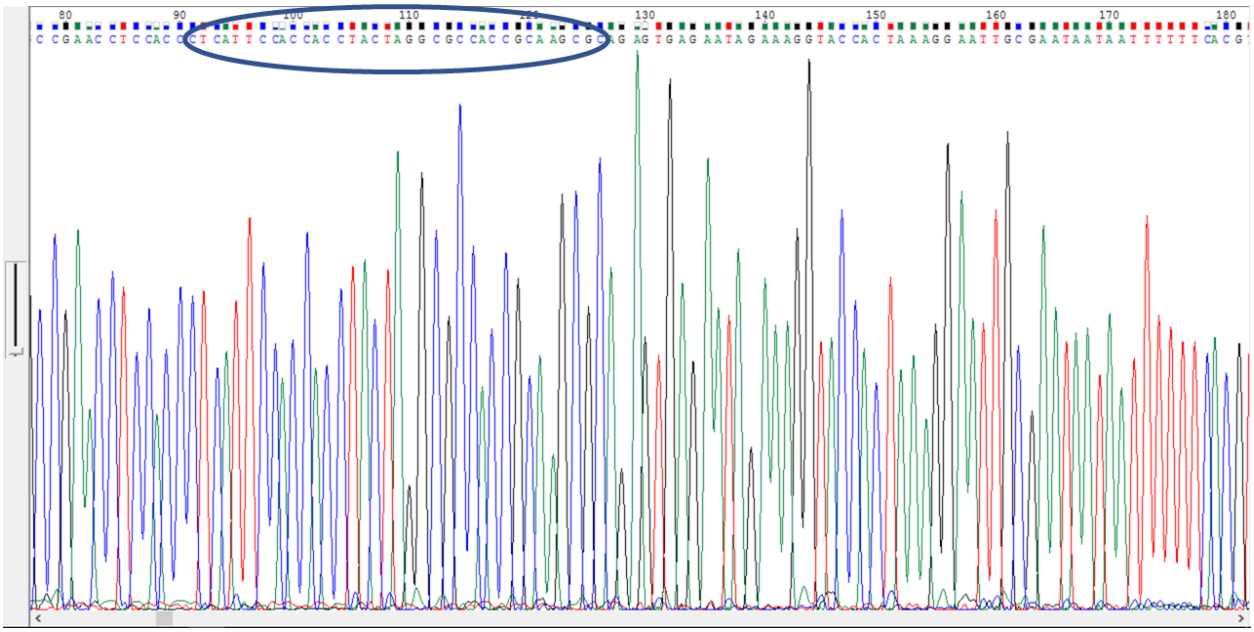

Appendix A 23: ENWWRSPAVALA DNA sequence circled

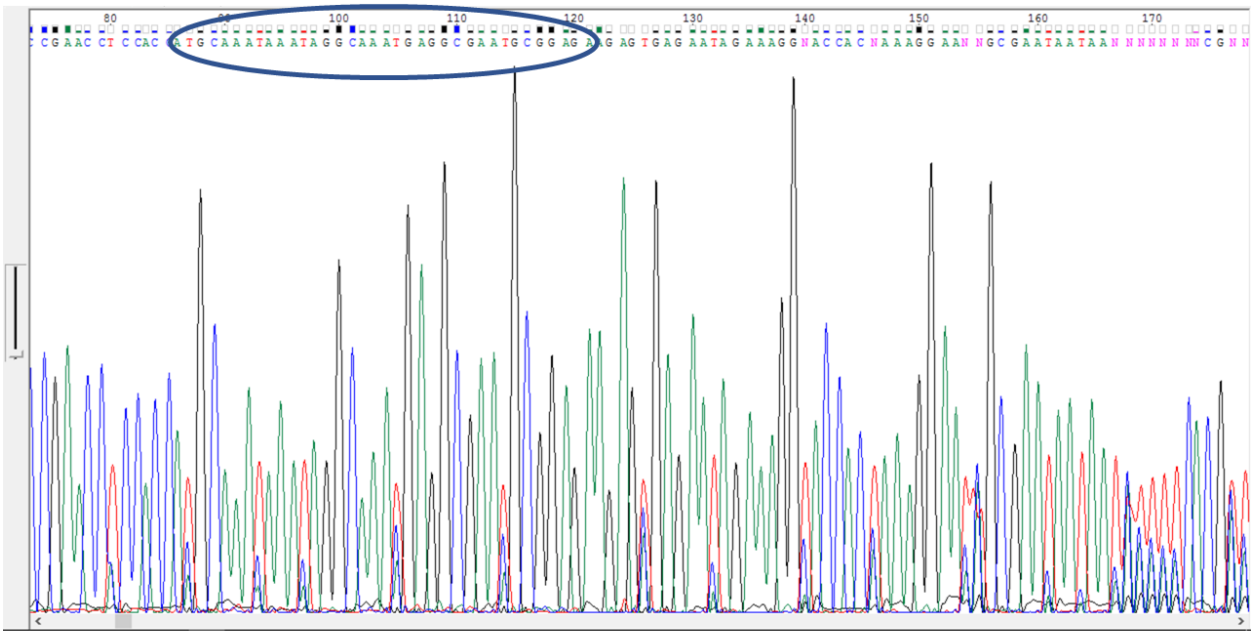

Appendix A 24: HLYIPLHPSHPS DNA sequence circled

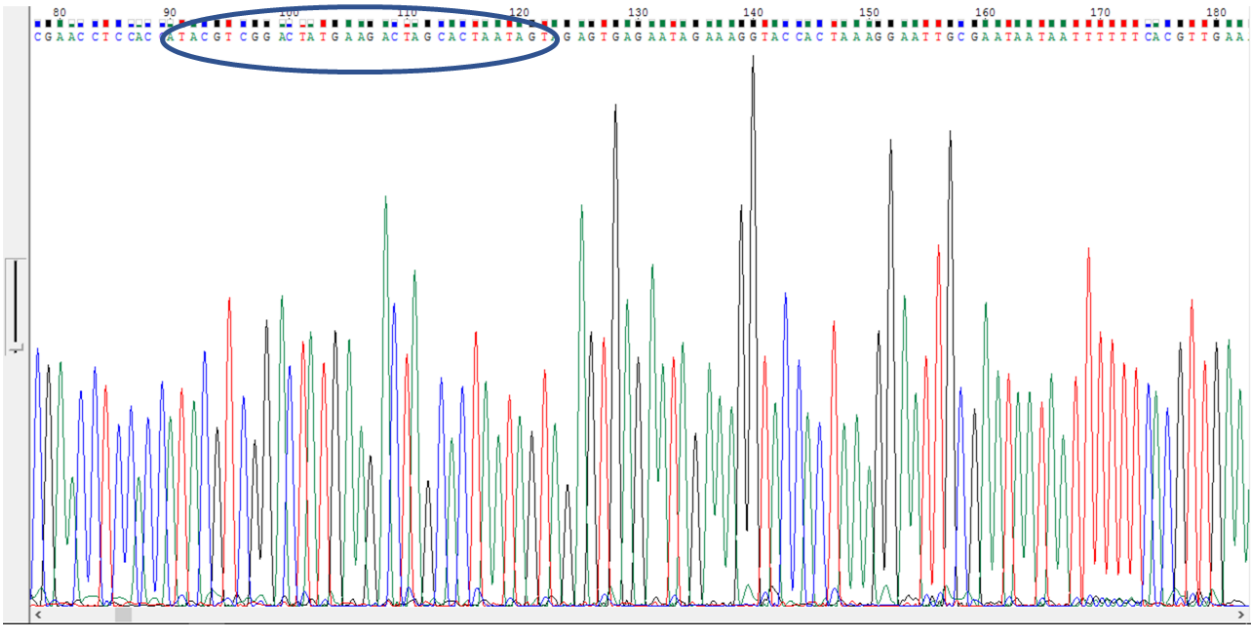

Appendix A 25: YTPSHLSASIT DNA sequence circled

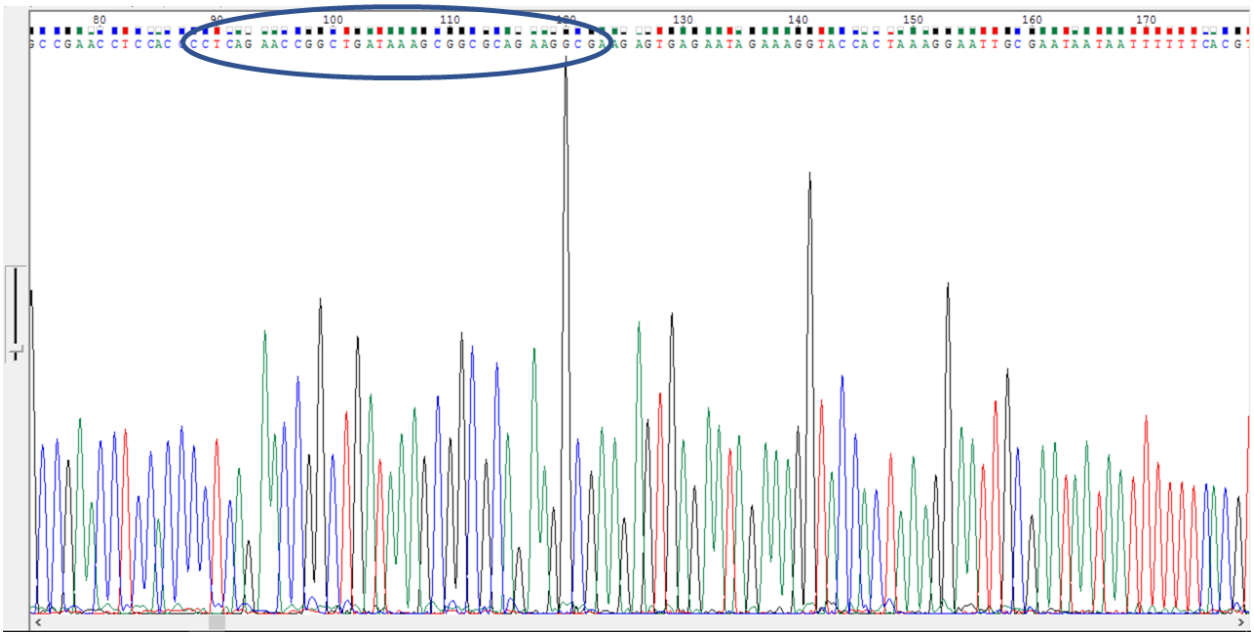

Appendix A 26: RLVPQYLPASPS DNA sequence circled